Thermal Turbulence in Variable Property Channel Flows

DNS and RANS

A.M. Hasan

Master of Science Thesis

TU Delft Delft University of Technology

Energy, Flow and Process Technology

Thermal Turbulence in Variable Property Channel Flows
DNS and RANS

Master of Science Thesis

For the degree of Master of Science in Energy, Flow and Process Technology at Delft University of Technology

A.M. Hasan

June 11, 2021

Faculty of Mechanical, Maritime and Materials Engineering (3mE) · Delft University of Technology

Copyright © Process and Energy
All rights reserved.

Delft University of Technology
Department of
Process and Energy

The undersigned hereby certify that they have read and recommend to the Faculty of Mechanical, Maritime and Materials Engineering (3mE) for acceptance of the thesis entitled

Thermal Turbulence in Variable Property Channel Flows

by

A.M. Hasan

in partial fulfillment of the requirements for the degree of

Master of Science Energy, Flow and Process Technology

Dated: June 11, 2021

Supervisor(s):

Dr. R. Pecnik

Ir. S. Silvestri

Ir. S.H.H.J. Smit

Reader(s):

Prof.dr.ir. B.J. Boersma

Prof.dr. D.J.E.M. Roekaerts

Prof.dr. S. Hickel

Abstract

Over the past decades, engineers have focused on a common goal - to reduce emissions by making industrial processes more efficient and by utilizing renewable energy sources. One possibility to reach this goal can be achieved by employing processes with non-ideal fluids, such as fluids at supercritical conditions in refrigeration, heat pump cycles and power cycles. Most of the flows in industry are turbulent and hence the need to study turbulence in non-ideal fluids arose. Turbulence in non-ideal fluids is extremely challenging since there are many complex effects at play. One such effect is caused by variations in properties, which also occurs in compressible flows, flows with high concentration gradients, or flows in heat exchangers.

This thesis presents a review of the existing theory on semi-local scaling for variable property flows with the aim to take it one step further and apply it to turbulent heat flux modeling. Two types of variable property cases are analysed in this thesis; (1) low-Mach number flows with uniform pseudo-heating sources, (2) high-Mach number flows with non-uniform viscous heating. For the former, a Direct Numerical Simulation (DNS) data-base, already available at TU Delft, has been post-processed with the main goal to investigate if the semi-local theory can also be applied to thermal turbulence and its modeling. For the latter, additional DNS simulations of high-Mach number channel flows have been performed to investigate how the viscous heating and its correlations can be accounted for in the semi-local scaling framework.

Using a 2-equation heat flux model, we find that modeling thermal turbulence in semi-local scales considerably improves the results for low-Mach number flows. However, for high-Mach number flows, additional unknown (closure) terms arise due to fluctuations in the viscous heating source. A model for the source term in the enthalpy variance equation is successfully proposed. In addition, the DNS study of two high-Mach number flows with constant semi-local Reynolds number (Re^*_τ) profiles shed light on the importance of a newly defined parameter (modified Eckert number) and also unveils one of the most important conditions in which semi-local theory can be compromised, e.g. extreme density gradients.

Table of Contents

List of Figures

List of Tables

Preface

This document is a part of my Master of Science graduation thesis. When I came to TU Delft, I was of the opinion that I want to pursue my career in the field of system modeling. I was interested in modeling of heat pumps and gas turbines which is why I chose to do my internship on heat pump modeling. I was not-very motivated to study turbulence which is why I decided to not take the elective course on turbulence, however, in September 2020 I became extremely curios to try a topic that is challenging and to move out of my comfort zone of system modeling. This is why I started considering topics on combustion, CFD modeling, and others. Among a lot of topics that I discussed with different professors, the topic of my thesis was something that I looked upon as a challenge. A challenge to learn turbulence, a challenge to move out of comfort zone, a challenge to try something new. With this thought I pursued the topic of this thesis and I liked it so much that now I will continue in this domain for my PhD.

Acknowledgements

I would like to thank my supervisor Dr. R. Pecnik for his assistance during the entire tenure of this thesis. His passion for research motivates me to stay in the research field for my future career. The meetings that were scheduled for an hour usually got extended because of his curious nature and capability to make discussions like a peer-to-peer discussion more than a student-supervisor discussion. This attitude helped me to push my limits of thinking further. I would also like to thank him for helping me in running the DNS cases. I would like to thank my daily supervisors Ir. S. Silvestri and Ir. S.H.H.J. Smit for being available for a Skype call/ discussion during any time of the day. Ir. S.H.H.J. Smit helped me to learn the art of communicating difficult things in a simple and interesting manner. I admire Ir. S. Silvestri for his coding skills and it helped me to improve mine as well during the course of the thesis.

I am thankful to Dr. Andrew Trettel and Dr. Johan Larsson for helping me to understand their data on supersonic channel flow simulations. I am also thankful to Prof.dr. K. Hanjalic for the enlightening discussions on turbulence modeling. I express sincere gratitude to the committee of this thesis, Prof.dr.ir. B.J. Boersma , Prof.dr. D.J.E.M. Roekaerts and Prof.dr. S. Hickel for reading and evaluating my thesis.

I am thankful to TATA Foundation for selecting me as one of their scholars and providing me with two scholarships, which helped me to get some relaxation with regards to financing my education.

I want to thank my family for standing rock solid behind me no matter what the situation. They were the ones who motivated me to pursue higher education abroad despite having a well paid job in one of the most successful companies in India.

Last, but not the least, I want to thank all my friends here in Delft and in India for being there for me during my happy and not so happy moments.

Delft, University of Technology A.M. Hasan
June 11, 2021

"Imagination is more important than knowledge. Knowledge is limited. Imagination encircles the world"

— *Albert Einstein*

Chapter 1

Introduction

Climate at a global level is deteriorating every passing day mainly due to emissions from the industrial processes in the past decades. Efforts to reduce the emissions and to make the industrial processes more efficient are required now, more than ever. Research over a large range of domains is performed to achieve this objective. One of the ways this can be achieved is by exploiting renewable energy sources to produce electricity in the power industry and chemical products in the process industry. However, due to the inherent intermittent nature of renewable energy sources, more options need to be explored. Recently, several research institutions are evaluating the possibility to use supercritical power cycles not only for converting various heat sources into electricity, but also to use supercritical fluids in process industries. For example, supercritical water-cooled reactors (SCWR), which have been accepted as one of the six most promising nuclear reactor concepts recommended by Generation IV International Forum (DoE, 2002), are expected to increase the thermal efficiency of nuclear power plants from 34-36% currently to >44%. Supercritical fluids are also expected to be widely used in extraction processes. High diffusion coefficients, low surface tension, and low viscosity make supercritical fluids an important extracting solvent.

Most of the wall-bounded industrial flows are turbulent. Understanding turbulent heat and momentum transport is of utmost importance for designing engineering components. This becomes more challenging if there are extreme gradients in properties. High variations in fluid properties alter turbulence. The characterization laws (like law-of-the-wall) developed considering constant properties in the domain, fail for variable property flows.

In general, variable property flows are those in which there are extreme gradients in fluid properties in the flow domain due to highly non-ideal fluids, high gradients in temperature, concentration, etc. An important class of variable property flows are those involving supercritical fluids. Supercritical fluids undergo extreme variations in properties near the pseudo-critical point. The fluid is said to undergo a continuous transition from a liquid-like to a gas-like state near the pseudo-critical temperature, as we increase the temperature at constant pressure. This causes a tremendous change in certain properties, like specific heat capacity c_p, thermal conductivity λ, density ρ, viscosity μ, and others. This effect is prominent at supercritical temperatures and pressures near the liquid-vapor critical point. Apart

Low Mach Cases	High Mach Cases
• Low Mach approximation. Incompressible flow but with variable properties.	• Compressible flow.
• No pure-compressibility effects.	• Negligible pure-compressibility effects (Mach < 5).
• Temperature gradients are created with volumetric heat sources that are user-specified and are uniform in the domain.	• Temperature gradients are created as a result of viscous dissipation of kinetic energy.

Figure 1-1: Types of variable property cases analysed in this thesis.

from applications employing supercritical fluids, variations in properties are also found in heat exchanger flows with extreme heat flux, rocket propulsion systems, combustion, and all applications involving compressible flows as compressible flows are inherently variable property flows.

In this thesis, the main focus is on variable property fully developed channel flows with variation in properties due to temperature gradients. There is a strong coupling between energy and momentum equations as the energy equation governs the temperature, which influences the properties, thus affecting the momentum equation.

We will analyse thermal turbulence in two types of variable property flows as described in figure 1-1.

In the next section we will introduce semi-local scaling which is an important tool to characterize variable property flows.

1-1 Semi-Local Scaling

For variable property flows, the scaling laws developed for constant property flows (classical scaling) fail and thus, the need to explore a different scaling methodology arose. Semi-local scaling is a methodology in which the variables are scaled with quantities based on local properties. Patel et al. (2015) developed a mathematical framework to support the use of semi-local scaling that has been initially proposed by Huang et al. (1995). Patel et al. first hypothesized that, just like constant property flows are characterized by wall-normal distance y/h_c and friction Reynolds number Re_τ, variable property flows can be characterized by wall-normal distance y/h_c and semi-local Reynolds number Re^*_τ. h_c is the channel half-width (sub-script "c" is intentionally added in this thesis to distinguish from enthalpy h). This hypothesis was verified using a Direct Numerical Simulation (DNS) study for a fully developed channel flow based on different fluid types with different combinations of property profiles. In the end, turbulent structures were analysed in detail for different variable property cases and it was found that in semi-local scales, near the wall (semi-local wall-normal distance, $y^* = y/h_c Re^*_\tau < 10$), there was turbulent structure modulation with respect to constant property flows due to gradients in Re^*_τ profile, but away from the wall ($y^* > 10$), when viewed

in semi-local scales, there was no modulation. This analysis gave a strong hint towards the similarities between semi-locally scaled variable property flows and classically scaled constant property flows.

In constant property turbulent channel flows, there exists a universal law of the wall (Pope, 2001): classically scaled mean velocity collapses, independent of Re_τ, as a function of y^+ over the entire inner layer (inner layer comprises of viscous sublayer, buffer layer and log-law layer, mathematically $y/h_c < 0.1$). It was noted, that the van Driest transformed velocity collapses for quasi-similar Re^*_τ profiles (Patel et al., 2015) but a universal velocity transformation was missing for variable property flows. Patel et al. (2016) used a similar DNS database as used for Patel et al. (2015) and noticed that the collapse of semi-locally scaled viscous stress over the entire inner layer is independent of Re^*_τ profiles. Using this collapse, an extended van Driest transformation was derived, that collapses velocity profiles independent of Re^*_τ profiles.

Trettel and Larsson (2016) arrived at the same extended van Driest velocity transformation as was obtained by Patel et al. (2016), but using a different approach. They proposed transformation kernels that transformed the compressible variable property flow at hand into an incompressible flow field of friction Reynolds number (Re_τ) computed using properties at the channel centre in the untransformed case. A few assumptions in their analysis, are: (1) the slope of the velocity profile in the log-law region is the same in the untransformed and transformed states, the slope being given by the von-Karman constant κ; (2) the turbulent and viscous shear stresses are equal in the transformed and untransformed states, over the entire inner layer. More details about the transformation can be found in the PhD dissertation, Trettel (2019).

Pecnik and Patel (2017) derived the semi-locally scaled form of the turbulent kinetic energy (TKE, k) equation. They analysed the budget of the semi-local TKE and found the property dependent terms to be very small. Thus, what was left for a fully developed channel flow, were terms that were governed by just one parameter, i.e. Re^*_τ. This led to the conclusion that the leading-order effect of variable properties on turbulence is characterized by Re^*_τ. They solved the turbulence model equations in their semi-locally scaled form and found the results to be exceptionally improved with respect to solving the equations in their conventional form. This was a major breakthrough in using the theory developed on semi-local scaling, for modeling.

Otero Rodriguez et al. (2018) built on the work of Pecnik and Patel (2017) but now they compared the results for different turbulence models (Cess (1958), Spalart and Allmaras (1992), Myong and Kasagi (1990), Menter (1993) and Durbin (1995)). They solved the turbulence model equations in their semi-local form but the variables were written in the classically scaled form. This was done to avoid rescaling the variables with updated local properties at every iteration step while solving the model. It was found that semi-local scaling improves the prediction of eddy-viscosity (μ_t) for most of the models. The best improvement of semi-local results, as compared to solving conventional equations, is observed for Myong and Kasagi's $k-\epsilon$ model. Conventional scaling proves to provide poor results for variable property flows for most of the models. Interestingly, Spalart and Allmaras's model provides sufficiently accurate results without any modifications.

The energy equation is also solved by Otero Rodriguez et al. (2018) to obtain the temperature profile. The eddy-conductivity (λ_t) is computed from the eddy-viscosity (μ_t) using a constant turbulent Prandtl number (Pr_t) of unity, as suggested in the analysis of Patel et al. (2017). The results were not as convincing as they were for velocity, especially for the gas-like fluid.

This suggested, that using Pr_t of unity is not the most accurate way of solving for eddy-conductivity (λ_t) for variable property flows and shed light on the need to study different heat flux models in detail. However, a major drive to study heat flux modeling for variable property cases also comes from the fact that constant Pr_t models fail in cases where turbulent heat flux and turbulent shear stress are not strongly correlated, for instance, cases in which buoyancy effects are dominant (So and Speziale, 1999; Patel, 2013). Before proceeding with heat flux modeling in variable property flows, reviewing the literature on turbulent heat transfer in constant property flows is important to create analogies and for a comprehensive understanding.

1-2 DNS of Turbulent Heat Transfer and Heat Flux Modeling for Constant Property Channel Flows

Article	**Boundary Condition**	**Pr**	**Re_τ**
Kim and Moin (1989)	Iso-thermal	0.71	180
Kasagi et al. (1992)	Iso-flux	0.71	150
Kasagi and Ohtsubo (1993)	Iso-flux	0.025	150
Kawamura et al. (1998)	Iso-flux	0.025 - 5	180
Kawamura et al. (1999)	Iso-flux	0.025, 0.2, 0.71	180, 395

Table 1-1: A compilation of the DNS studies performed to study turbulent heat transfer in channel flows

Various DNS studies have been performed over the years to study more about the turbulent heat transfer physics. Kawamura et al. (1998) concluded that for $Pr \geq 0.1$, the turbulent Prandtl number Pr_t is independent of molecular Prandtl number Pr. Kawamura et al. (1999) studied effects of Reynolds and Prandtl number on thermal statistics and it was found that the turbulent Prandtl number is independent of friction Reynolds number and molecular Prandtl number for fluids with $Pr \geq 0.2$. Kasagi and Ohtsubo (1993) presented instantaneous thermal structures for a low Prandtl number fluid ($Pr = 0.025$), and substantial difference was noted compared to the structures obtained for a fluid with $Pr = 0.71$. Kawamura et al. (1999) also presented instantaneous thermal structures for a high and a low Prandtl number fluid at two different Reynolds numbers.

Heat flux modeling: Research on heat flux models has been limited as compared to the research on turbulent stress models. This is understandable, as turbulent stresses have a direct implication on the equations required to solve for mean temperature, and an indirect implication through their influence on mean velocity (Launder, 1976). Thus, development of turbulent stress models precedes development of heat flux models. Constant turbulent Prandtl number model with the value of Pr_t near unity is widely used for heat transfer calculations and has an implicit assumption of a strong analogy between heat and momentum transport. However, with the advent of computational power and the need for accurate results, research to develop heat flux models gained importance. Also, it is known that constant Pr_t models fail for flows with strong buoyancy effects (So and Speziale, 1999).

Launder (1976) was one of the pioneering researches in heat flux modeling. Launder discussed about closures for the heat flux transport equation. Transport equation of the temperature fluctuation $\overline{\theta'^2}$ (analogous to turbulent kinetic energy equation), which was originally presented by Corrsin (1952), is also discussed. The turbulent diffusion term in that equation is closed using a gradient type representation. Another term that needs to be modeled so as to construct a time scale (alongwith $\overline{\theta'^2}$) was the dissipation of thermal fluctuation (ϵ_θ) term. The usual way of modeling this term, using the definition of time scale ratio (R), is not accurate, as it demands specification of the time scale ratio beforehand. Beguier et al. (1978) suggests the ratio to be constant at 0.5 for pipe flows. However, the heated grid experiments of Warhaft and Lumley (1978) suggested that the decay exponent of the thermal fluctuations depend on the heat flux input and is not a constant. The DNS data of Kawamura et al. (1998) shows a clear Prandtl number Pr dependence of the time scale ratio for channel flows. The non-uniqueness of R suggests that using it for computing dissipation of thermal fluctuations is not the right way as was also concluded by Launder (1976). This necessitates solving a transport equation for ϵ_θ. Launder (1976) extensively discusses modeling of dissipation and generation terms in the ϵ_θ transport equation, and also mentions the challenge in modeling these terms due to the availability of twice as many parameters as were there for modeling of velocity fluctuation dissipation (ϵ). For example, two time scales (k/ϵ and $\overline{\theta'^2}/\epsilon_\theta$) and two dimensionless measures of generation rates (P/ϵ and P_θ/ϵ_θ). k denotes the turbulent kinetic energy and P, P_θ denotes the rate of production of turbulent kinetic energy k and thermal variance $\overline{\theta'^2}$ respectively.

An extensive review of turbulent heat transfer modeling was presented by So and Speziale (1999). The authors reviewed different high-Re heat flux models and classified them appropriately (0,1,2-equation models, etc.). Near wall models are also presented in which the near wall effects are incorporated by modifying the model equations, such that they are valid in the entire domain all the way up to the wall. Boundary condition of thermal fluctuations, $\overline{\theta'^2} = 0$, is a valid approximation for both, iso-thermal and iso-flux boundary conditions, for engineering applications as long as $Pr > 0.1$. This was concluded based on the analysis of the effect of $\overline{\theta'^2} = 0$ boundary condition on the mean temperature and associated integral quantities, done by Sommer et al. (1994). Near wall behaviour of turbulent thermal quantities like turbulent heat flux ($\overline{v'\theta'}$), thermal fluctuations ($\overline{\theta'^2}$) and dissipation (ϵ_θ) exhibit a Pr dependency and, as per the authors, very few models are able to capture this dependency.

In this thesis, we shall use a 2-equation heat flux model. The 2-equation class of heat flux models obtain their name because they solve transport equations of two thermal quantities, thermal variance ($\overline{\theta'^2}$) and its dissipation (ϵ_θ). These two quantities are used to construct a time scale called the thermal time scale ($\tau_t = (\overline{\theta'^2}/2)/\epsilon_\theta$). This time scale along with the velocity time scale $\tau_u = k/\epsilon$, is used to construct a composite (hybrid) time scale (τ_m) for heat transfer. This hybrid time scale is then used to estimate the eddy conductivity λ_t.

Deng et al. (2001) and Nagano and Kim (1988) approximated this hybrid time scale as $\sqrt{\tau_u \tau_t}$, whereas, Abe et al. (1995) checked for multiple formulations of the hybrid time scale. One of the formulations is the one by Zeman and Lumley (1976) which models the hybrid time scale as the harmonic average of the thermal and velocity time scales. This implies that the lower one of τ_u and τ_t will have more importance on the estimation of τ_m. Nagano and Shimada (1996) also used the harmonic average formulation of the time scale.

Near wall effects are incorporated in the model using suitable damping functions or using

additional terms. Deng et al. (2001) used a damping function to model the near wall effects on eddy conductivity λ_t but without incorporation of Prandtl number dependency. Nagano and Kim (1988) used a formulation of damping function with incorporation of Prandtl number effects on the near wall behaviour. Abe et al. (1995); Nagano and Shimada (1996) modeled the near wall effects on eddy conductivity in more detail. They proposed an additional time scale dependent on the dissipative eddy time scale based on the motivation that near the wall, the relevant dynamics are governed by the dissipative time scale. Also, these models took care of the Prandtl number effects on λ_t.

Deng et al. (2001) incorporated the near wall effects on the model equations ($\overline{\theta'^2}/2, \epsilon_\theta$) using damping functions to modify the model constants in the ϵ_θ equation. Nagano and Kim (1988) did not use any damping function in the model equations. However, they incorporated the near wall behaviour by modeling an extra term. Hanjalić and Launder (1976) found that modeling an analogous term to what Nagano and Kim (1988) modeled, proves to be very beneficial to incorporate the near wall effects on TKE dissipation ϵ. Abe et al. (1995) used damping functions and Nagano and Shimada (1996) used both the damping functions and also modeled the extra term that Nagano and Kim (1988) modeled. Nagano and Shimada (1996) attempted to incorporate Prandtl number effects also in the model equations which other models don't. This is why the Nagano and Shimada model works well for a range of Prandtl numbers.

Nagano and Kim (1988) and Nagano and Shimada (1996) did not solve for the actual thermal variance dissipation but for its isotropic part such that it goes to zero at the wall. Doing so is found to be computationally very stable. Jones and Launder (1973) solved for the isotropic part of TKE dissipation in their $k - \epsilon$ model with the motivation of computational stability.

Due to the dependency of heat flux models on turbulent stress models and not vice versa, So and Speziale (1999) suggested to use turbulent stress models belonging to the same or higher hierarchy than what is used for heat flux modeling. For example, if a two equation model is used for heat flux then the turbulent stress model should be either two equation or of higher hierarchy and not one equation or lower.

1-3 Turbulent Heat Transfer in Variable Property Channel Flows

DNS studies mentioned in section 1-2 treated temperature as a passive scalar which means that the temperature field will not have any effect on turbulent motions. For cases with very high heat flux or for fluids with strong temperature dependency of properties, property variations due to temperature are severe and temperature does not remain a passive scalar anymore (Patel et al., 2017). It influences fluid properties that modify turbulence. Effect of variable properties on turbulence in a fully developed low-Mach number channel flow has been extensively studied (Patel et al., 2015, 2016; Pecnik and Patel, 2017). Effect of variable properties on scalar transport has been studied by Patel et al. (2017).

Patel et al. (2017) performed DNS of low-Mach number fully developed channel flows for a set of fluids with different variations in properties, leading to a variety of profiles of semi-local Reynolds number Re^*_τ and semi-local Prandtl number Pr^*. Unlike the collapse of viscous and turbulent shear stresses observed in Patel et al. (2016), neither the semi-locally scaled conductive heat flux nor the semi-locally scaled turbulent heat flux have a universal profile in

the entire inner layer when plotted against the semi-local co-ordinate y^*. Thus, the technique which Patel et al. (2016) used to derive a universal transformation for velocity, will not work to derive a universal transformation for temperature. However, the authors came up with an extended van Driest temperature transformation using the collapse of semi-locally scaled turbulent heat flux in the log-law layer. The extended transformation collapses for cases with quasi-similar Pr^* profiles independent of Re_τ^* profiles.The fluids with quasi-similar Re_τ^* and Pr^* profiles have thermal statistics that almost collapse, hinting towards the characterization of heat transfer in variable property flows by Re_τ^* and Pr^* profiles. For all the cases, the turbulent Prandtl number was found to be near unity, which inspired Otero Rodriguez et al. (2018) to use unity turbulent Prandtl number in their analysis.

Lee et al. (2014) studied the effect of variable viscosity in a thermal turbulent boundary layer on thermal statistics. They modified the original Kader's relation which computed the van Driest temperature ($\overline{\theta^{vD}}$) based on the Prandtl number of fluids. Lee et al. assumed that the effect of variable Prandtl number on $\overline{\theta^{vD}}$ can be captured by using semi-local Prandtl number Pr^* in the equation and by modifying the elevation of the edge of log-law region. The modifications proved to work well with the cases proposed in Lee et al. (2014). However, Patel et al. (2017) tested the modifications for their cases, and the modified equation proved to fail. Patel et al. (2017) reasoned this failure due to the fact that the modifications do not capture the effect of Re_τ^* gradients on the slope of the log-law profile.

Earlier studies on scalar transport in variable property flows (Patel et al., 2017; Lee et al., 2014) used DNS in their research to draw out important conclusions. However, an extensive research on heat flux modeling of variable property flows needs to be carried out. Using a constant turbulent Prandtl number of unity for heat flux modeling is not the right way as it results in high errors, especially for the gas-like fluids, as can be seen in the results of Otero Rodriguez et al. (2018). Also, to achieve the final goal of predicting heat transfer in supercritical fluids, capturing of additional physics (due to buoyancy and acceleration) is required, and a constant Pr_t model would be insufficient to capture these effects. Therefore, an extensive study of heat flux modeling for variable property turbulent channel flows is needed.

1-4 Compressible Channel Flows

Compressible flows are an important class of flows with variable properties. These flows are different than the constant property incompressible turbulent flows because of two main reasons; they have variation in properties and they have "pure compressibility" effects. Coleman et al. (1995) performed DNS simulations of compressible channel flows up to bulk Mach number of 3. They observed that near the wall, fluctuations in density and temperature are mainly caused due to solenoidal passive mixing and hence is an outcome of mean gradient in temperature and density. These fluctuations are not of acoustic nature and this is clarified using joint probability density functions studied. To isolate the pure compressibility effects from the effects arising due to mean gradients in properties, they constructed a case with fictitious heating source which balances the viscous heating such that the net heat source is zero. This implies constant temperature and properties in the domain. The study showed that the case with fictitious heat source is identical to incompressible flows with constant properties and thus, reinforced the fact that pure compressibility effects are small.

Huang et al. (1995) was the first study that introduced semi-locally scaled wall-normal coordinate (y^*). In this study, differences between Reynolds and Favre averaging is studied using DNS simulations of supersonic channel flows. The difference between Reynolds and Favre averaged streamwise velocity is found to be small and limited to the near wall region. This supports Markovin's hypothesis in the sense that effects of density fluctuations are negligible. The budget of TKE was plotted and it is found that the terms due to "pure compressibility", for instance, pressure-dilatation correlation, are small.

These studies and numerous others have the same broad conclusion: pure compressibility effects in supersonic channel flows (bulk Mach number < 5) are small (for more details about pure-compressibility effects on turbulence, refer Lele (1994)). The variable property cases analysed in Patel et al. (2015, 2016, 2017) are "low-Mach number" cases. The low-Mach number approximation implies that these flows are similar to incompressible flows, but with variable properties. All compressibility effects are neglected in this approximation. The fact that pure compressibility effects are small in supersonic channel flows motivates us to treat them like low-Mach number variable property flows.

Morinishi et al. (2004) discussed about the difference in low-Mach number flows with "uniform heating" and high-Mach number flows with "viscous heating". They showed that for high-Mach number cases, due to the dissipation term, there exists no log-law region in the temperature profile (normalized by friction temperature). The budget of mean internal energy, for the compressible and low-Mach number cases, are presented and a clear distinction between the two type of flows is visible. A more detailed discussion on the contents of Morinishi et al. (2004) can be found in the PhD dissertation by Tamano (2002).

In high-Mach number flows, fluctuations in dissipation and in temperature can correlate to form a source/sink term in the temperature variance budget equation. Plate (1971) neglected this correlation for atmospheric boundary layers. It was neglected based on the assumption that dissipation is dominant in high frequency range of the velocity spectrum (small scales) whereas temperature fluctuations are small in this frequency range. However, Antonia et al. (1980) claimed that even though the correlation term is negligible in the thermal variance budget for atmospheric surface layers, the correlation coefficient is not negligible. It will be interesting to study this correlation for high-Mach number channel flows, especially near the wall where dissipation is very high.

1-5 Research Objectives, Scope and Goal

In this thesis, two different but related research objectives will be achieved.

Research Objective 1:

> *To analyse the governing parameters for thermal turbulence in low-Mach number variable property flows with uniform volumetric heating and to explore if semi-locally scaled heat flux models capture variable inertia effects better than conventionally scaled models.*

PhD work of Patel (2017) is a major contribution towards the study of variable property turbulence in channel flows. However, an extensive analysis of heat flux modeling still needs

to be done for variable property flows. A constant turbulent Prandtl number model is not the most robust solution as it fails in cases with strong buoyancy or in cases where the similarity between heat and momentum transport does not hold. Thus, an accurate 2-equation heat flux model for variable property flows has to be developed.

Research Objective 2:

> *To study the physics and importance of viscous heating for high-Mach number channel flows, using correlation coefficients and budgets of thermal quantities. To analyse the governing parameters for thermal turbulence and to solve RANS (Reynolds Averaged Navier Stokes) equations using a 2-equation heat flux model in high-Mach number flows.*

A detailed study of 2-equation heat flux modeling is needed for compressible flows in situations where the assumption of a constant turbulent Prandtl number or the validity of Reynolds analogies fail. Fluctuations in dissipation of kinetic energy (viscous heating) can add source/sink terms in the model equations. An analysis is thus required to develop and implement proper models for capturing these flows physics. If semi-local scaling is capable to capture (to a certain extent) the variable inertia effects in thermal turbulence, then a semi-locally scaled heat flux model can be used to isolate and analyse the effect of viscous heating on the model equations. This is why, this objective is combined with the first one.

The **Goal** of this thesis to extend the existing constant-property heat flux models for variable property flows. The research in this thesis can be applied further to build robust heat flux models for supercritical flows to finally be able to predict the heat transfer deterioration (HTD) and heat transfer enhancement (HTE) phenomena. The target of the research is not only limited to RANS modeling but can also be extended to wall-modeled Large Eddy Simulations (LES).

The **Scope** of this thesis is limited to calorifically perfect fluids in a fully developed channel flow with extreme variations in properties (ρ, μ, λ), but with negligible buoyancy effects. The high-Mach number cases analysed will be supersonic and the low-Mach number cases will be the ones with uniform heating.

- In chapter 2, a background on governing equations and basics of modeling is provided.
- Chapter 3 describes the motivation behind modeling in semi-local scales. It also coherently presents the mathematics associated with semi-local scaling. The equations that are previously derived in literature and the equations that will be derived in this thesis are presented.
- In Chapter 4, variable property cases analysed in this thesis are presented. They include the low-Mach number cases of Patel et al. (2017), high-Mach number cases of Trettel and Larsson (2016) and the constant Re^*_τ cases that are simulated (DNS) in this thesis using the in-house FORTRAN code.
- Chapter 5 is related to research objective 1. The enthalpy variance equation presented in chapter 3 is simplified for low-Mach number cases by developing a FORTRAN post-processing code to post-process existing DNS data. The governing parameters for thermal turbulence are analysed. The 2-equation heat flux model of Nagano and Shimada

(1996) is solved on MATLAB in semi-locally scaled form and compared with the results from solving it in conventional form.

- Chapter 6 is related to research objective 2. The viscous heating cases are compared with the low-Mach number uniform heating cases. The physics behind fluctuations in dissipation is discussed using correlation coefficients, that are computed using a post-processing FORTRAN code. The effects of viscous heating on mean enthalpy, enthalpy variance and turbulent heat flux equations are presented. Using the constant Re_τ^* high-Mach number cases simulated in this thesis, the importance of the modified Eckert number ($Ec_{\theta_\tau^*}$) is isolated and discussed. In the end we describe the effects of viscous heating on the 2-equation heat flux models and also propose a model for viscous heating source term in enthalpy variance equation, motivated from near-wall physics.
- In chapter 7, we discuss on one of the main criteria under which semi-local scaling can be compromised - extreme density gradients.

Chapter 2

Governing Equations

In this chapter, the governing equations in the instantaneous form are presented. Then, the equations are averaged using Reynolds and Favre decompositions to obtain the Reynolds Averaged Navier Stokes (RANS) equations. In the end, ways to model the unclosed terms in RANS equations are briefly discussed.

2-1 Governing Equations: Instantaneous Form

The Navier-Stokes equation in dimensional form are presented in this section.

- **Continuity equation**

$$\frac{\partial \rho}{\partial t} + \frac{\partial \rho u_i}{\partial x_i} = 0, \tag{2-1}$$

where u_i is the instantaneous velocity. The sub-script i defines the direction. For example, u_2 corresponds to velocity v in the x_2 direction, i.e. y direction. In this thesis, x_1, x_2, x_3 (or x, y, z) correspond to streamwise, wall-normal and spanwise directions in a channel, respectively.

- **Momentum equation**

$$\rho \frac{\partial u_i}{\partial t} + \rho u_j \frac{\partial u_i}{\partial x_j} = -\frac{\partial P}{\partial x_i} + \frac{\partial \tau_{ij}}{\partial x_j} - \frac{\partial \rho \Psi}{\partial x_i}. \tag{2-2}$$

Defining modified pressure as defined in Pope (2001),

$$p = P + \rho \Psi, \tag{2-3}$$

where Ψ is the gravitational potential. For a Newtonian fluid, the overall stress tensor is defined as,

$$T_{ij} = -P\delta_{ij} + 2\mu S_{ij} + \lambda_v \frac{\partial u_k}{\partial x_k}\delta_{ij}, \tag{2-4}$$

where μ is defined as the first coefficient of viscosity and λ_v is defined as the second coefficient of viscosity. P is the thermodynamic pressure and S_{ij} is the rate of strain tensor defined as,

$$S_{ij} = \frac{1}{2}\left(\frac{\partial u_i}{\partial x_j} + \frac{\partial u_j}{\partial x_i}\right). \tag{2-5}$$

Mechanical pressure is defined as the trace of the stress tensor given by (White, 1974),

$$p_{mech} = -P + \left(\frac{2\mu}{3} + \lambda_v\right)\frac{\partial u_k}{\partial x_k}. \tag{2-6}$$

Thus, the thermodynamic pressure due to vibration of molecules, and mechanical pressure are different by the definition of equation (2-6). However, using Stoke's hypothesis, the bulk viscosity defined as, $k = \frac{2\mu}{3} + \lambda_v$, is zero and thus, the mechanical and thermodynamic pressures are equal.

By incorporating the Stoke's hypothesis, we get,

$$T_{ij} = -P\delta_{ij} + 2\mu S_{ij} - \frac{2}{3}\mu\frac{\partial u_k}{\partial x_k}\delta_{ij}, \tag{2-7}$$

which can be written as,

$$T_{ij} = -P\delta_{ij} + \tau_{ij}. \tag{2-8}$$

For more details on how did we arrive from equation (2-4) to equation (2-8), reader is referred to White (1974), chapter 2.

The anisotropic part of stress tensor, τ_{ij}, is symmetric and is defined as,

$$\tau_{ij} = 2\mu S_{ij} - \frac{2}{3}\mu\frac{\partial u_k}{\partial x_k}\delta_{ij}. \tag{2-9}$$

- **Energy equation**

$$\rho\frac{\partial h}{\partial t} + \rho u_j\frac{\partial h}{\partial x_j} = \frac{\partial p}{\partial t} + u_j\frac{\partial p}{\partial x_j} + \frac{\partial}{\partial x_j}\left(\lambda\frac{\partial T}{\partial x_j}\right) + \Phi, \tag{2-10}$$

where λ is the thermal conductivity, h is the enthalpy of fluid per unit mass, T is the temperature and Φ is the volumetric heat source/sink per unit volume. c_p is defined as,

$$\left.\frac{\partial h}{\partial T}\right|_p = c_p, \tag{2-11}$$

and thus we can write,

$$dh = c_p dT, \tag{2-12}$$

only when the thermodynamic pressure is constant. In general,

$$dh = \left.\frac{\partial h}{\partial T}\right|_p dT + \left.\frac{\partial h}{\partial p}\right|_T dP. \tag{2-13}$$

For ideal gases,

$$\left.\frac{\partial h}{\partial p}\right|_T = 0, \tag{2-14}$$

and thus, equation (2-12) always holds. However, for fluids with a different equation of state, equation (2-12) can be written only under the assumption of small variations in thermodynamic pressure. In this thesis, we will either analyse ideal gases or flows in low-Mach number approximation (thermodynamic pressure = constant) and thus we will use equation (2-12) to replace temperature in the diffusion term of equation (2-10) by enthalpy.

Using,

$$\alpha = \frac{\lambda}{c_p}, \tag{2-15}$$

the final equation becomes,

$$\rho\frac{\partial h}{\partial t} + \rho u_j \frac{\partial h}{\partial x_j} = \frac{\partial p}{\partial t} + u_j\frac{\partial p}{\partial x_j} + \frac{\partial}{\partial x_j}\left(\alpha\frac{\partial h}{\partial x_j}\right) + \Phi. \tag{2-16}$$

Writing an equation in terms of h instead of T will be preferred in this thesis. Here, c_p is the specific heat capacity and α is a form of conductivity. Note that in most of the literature, α is defined as thermal diffusivity, $\alpha = \lambda/(\rho c_p)$. We will use Γ_t to denote thermal diffusivity. In this Master thesis we will deal with calorifically perfect fluids, i.e. c_p will be treated as constant in the domain.

Equations (2-1, 2-2 and 2-16) are instantaneous equations which are solved in a Direct Numerical Simulation (DNS) code for turbulent flows. In DNS, all scales are resolved and thus the mesh needs to be very fine. As useful as this sounds for academic study, performing a DNS simulation for industrial applications is not always practically feasible. For industrial applications, often the averaged form of these equations are solved which are nothing but the RANS equations. They are discussed in the next section.

2-2 Governing Equations: Averaged Form

Osborne Reynolds, in 1895, proposed a decomposition as,

$$\gamma = \langle\gamma\rangle + \gamma', \tag{2-17}$$

where γ is any quantity and $\langle . \rangle$ is the mean operator. Thus, the instantaneous quantity is decomposed into a mean and a fluctuating part such that,

$$\langle\gamma'\rangle = 0. \tag{2-18}$$

For variable density flows, density-weighted averaging is used for velocity u_i and enthalpy h, which helps to keep the form of the governing equations similar to constant property RANS equations. The decomposition using density-weighted mean is called Favre decomposition and is written as,

$$\gamma = \{\gamma\} + \gamma'', \tag{2-19}$$

where, {.} is the Favre-mean operator and,

$$\{\gamma\} = \frac{\langle \rho\gamma \rangle}{\langle \rho \rangle}, \tag{2-20}$$

and,

$$\langle \gamma'' \rangle \neq 0, \tag{2-21}$$

but,

$$\langle \rho\gamma'' \rangle = 0. \tag{2-22}$$

Favre decomposition for velocity and enthalpy (or temperature), and Reynolds decomposition for all other quantities shall be used from now on. To arrive at the RANS set of governing equations from the instantaneous equations, following recipe can be used:

1. Decompose the variables using Reynolds decomposition or Favre decomposition as suitable,
$$\begin{array}{c} u_i = \{u_i\} + u_i'', \quad h = \{h\} + h'', \quad \mu = \langle \mu \rangle + \mu', \quad p = \langle p \rangle + p', \\ \alpha = \langle \alpha \rangle + \alpha', \qquad \rho = \langle \rho \rangle + \rho'. \end{array} \tag{2-23}$$
2. Take Reynolds average $\langle . \rangle$ of the entire equation.
3. Apply rules of averaging and simplify.

- **Continuity equation**

$$\frac{\partial \langle \rho \rangle}{\partial t} + \frac{\partial \langle \rho \rangle \{u_i\}}{\partial x_i} = 0. \tag{2-24}$$

- **Momentum equation**

$$\langle \rho \rangle \frac{\partial \{u_i\}}{\partial t} + \langle \rho \rangle \{u_j\} \frac{\partial \{u_i\}}{\partial x_j} = -\frac{\partial \langle p \rangle}{\partial x_i} + \frac{\partial \langle \tau_{ij} \rangle}{\partial x_j} - \frac{\partial \langle \rho u_i'' u_j'' \rangle}{\partial x_j}, \tag{2-25}$$

where,

$$\langle \tau_{ij} \rangle = \left\langle 2\mu S_{ij} - \frac{2}{3}\mu \frac{\partial u_k}{\partial x_k} \delta_{ij} \right\rangle. \tag{2-26}$$

The additional unclosed term, $\partial \langle \rho u_i'' u_j'' \rangle / \partial x_j$ in equation (2-25), originates from the advection term, but due to its form being very similar to the viscous stress term in the momentum equation, this term is called "Reynolds stress". The Reynolds stress tensor is splitted into an isotropic part and a deviatoric part as,

$$\langle \rho u_i'' u_j'' \rangle = a_{ij} + \frac{2}{3} \langle \rho \rangle \{k\} \delta_{ij}, \tag{2-27}$$

where,

$$k = \frac{u_i'' u_i''}{2}. \tag{2-28}$$

{k} is defined as the turbulent kinetic energy (TKE) and, a_{ij}, is the deviatoric part of the Reynolds stress tensor.

- **Energy equation**

$$\langle\rho\rangle\frac{\partial\{h\}}{\partial t}+\langle\rho\rangle\{u_j\}\frac{\partial\{h\}}{\partial x_j}=\frac{\partial\langle p\rangle}{\partial t}+\left\langle u_j\frac{\partial p}{\partial x_j}\right\rangle+\frac{\partial\langle q_j\rangle}{\partial x_j}-\frac{\partial\langle\rho u_j''h''\rangle}{\partial x_j}+\langle\Phi\rangle, \tag{2-29}$$

where,

$$\langle q_j\rangle=\left\langle\alpha\frac{\partial h}{\partial x_j}\right\rangle. \tag{2-30}$$

The additional term on the right hand side originates from the advection term and it represents transport of enthalpy due to fluctuating motions (eddies). Due to its form being very similar to the conductive heat flux, this term is usually referred to as turbulent heat flux.

As can be seen from equations (2-25, 2-29), averaging the instantaneous equations results in additional unknown terms like the Reynolds stress or the turbulent heat flux that need closure equations. In the section to follow, closures for these quantities will be discussed.

2-3 Turbulence Modeling

In this section, we will discuss various types of models used for modeling the additional terms in equations (2-25) and (2-29).

2-3-1 Reynolds Stress Modeling

2-3-1-1 Turbulent viscosity models

A very well-known way of modeling the Reynolds stresses is by using the turbulent viscosity hypothesis. This hypothesis is written as,

$$a_{ij}=-\mu_t\left[\left(\frac{\partial\{u_i\}}{\partial x_j}+\frac{\partial\{u_j\}}{\partial x_i}\right)-\frac{2}{3}\frac{\partial\{u_k\}}{\partial x_k}\delta_{ij}\right], \tag{2-31}$$

where a_{ij} is defined in equation (2-27).

Deviatoric part of the Reynolds stress tensor is proportional to the deviatoric part of the mean rate of strain tensor and the constant of proportionality is the eddy viscosity (μ_t). This is analogous to the relation of viscous stress in a Newtonian fluid, the difference being in the constant of proportionality.

Equation (2-31) involves an intrinsic assumption and a specific assumption (Pope, 2001). The intrinsic assumption is that the hypothesis defines turbulent stress at a point based on local velocity gradient at that point. Turbulence at a point in the domain is often influenced by the conditions upstream (memory effects) of the point and thus, it is not always a local phenomenon described by local quantities. However, this assumption works for simple shear flows due to the absence of memory effects. A specific assumption is that the hypothesis assumes a linear relation between the turbulent stress and the mean rate of strain tensor with the constant of proportionality μ_t. This is patently incorrect even for the simplest of flows

(Pope, 2001). However, for fully developed channel flows, just one component of the Reynolds stress tensor needs modeling which is,

$$\langle \rho u'' v'' \rangle = -\mu_t \partial\{u\}/\partial y. \tag{2-32}$$

Equation (2-32) can be used as a definition of μ_t and thus no assumptions are involved (Pope, 2001).

For turbulent channel flows, referring equation (2-32), the main task now is to find μ_t. As commonly done in literature, we shall discuss ways to compute ν_t which is related to μ_t as,

$$\nu_t = \mu_t/\langle \rho \rangle. \tag{2-33}$$

The dimension of ν_t is $\mathrm{m}^2\,\mathrm{s}^{-1}$ and is a flow property rather than a fluid property. Writing ν_t in terms of flow quantities,

$$\nu_t \sim u_o l_o, \tag{2-34}$$

where u_o and l_o are large eddy velocity and length scales, as majority of the contribution to momentum transport will be done by large eddies.

Different types of models try to approach the problem of finding a suitable estimation of velocity scale u_o and length scale l_o in different ways. Most of the models solve the transport equations of turbulent quantities like TKE (k), dissipation of TKE (ϵ), etc. to construct these scales. Based on the number of transport equations solved, the models are divided in different categories as follows:

- **0-equation model:**
  - **The mixing-length model:** In this model the velocity scale is approximated as $u_o \sim l_m|\partial\langle u\rangle/\partial y|$ and the length scale is approximated as $l_o \sim l_m$ where, l_m is the Prandtl's mixing length and it signifies length up to which momentum is transported by mixing. We get, $\nu_t \sim l_m^2|\partial\langle u\rangle/\partial y|$. The problem is only partially solved as determination of l_m is yet to be done. l_m is flow specific and that is a major drawback of this model.
- **1-equation model:** The mixing-length model estimates u_o as a function of the mean velocity gradient. Kolmogorov in 1942 and Prandtl in 1945 suggested that a better velocity scale is based on the turbulent kinetic energy ($\langle k\rangle = \langle u_i' u_i'/2\rangle$), $u_o \sim \sqrt{\langle k\rangle}$. These models require solving of the transport equation of TKE. Readers are referred to Pope (2001) for more details. One major drawback of this model, like the mixing-length model, is that l_m still needs to be specified.
- **2-equation models:** Two most famous classes of models in this category are the $k-\epsilon$ and $k-w$ models. In $k-\epsilon$ models, along with the TKE transport equation, the transport equation of dissipation of TKE (ϵ) is solved. Using these two turbulent quantities, the length scale and velocity scale are constructed as, $u_o \sim \sqrt{\langle k\rangle}$ and $l_o \sim \langle k\rangle^{1.5}/\epsilon$. The main advantage of this model is that the exclusive specification of l_m is not needed as it is constructed using k and ϵ. The $k-\epsilon$ class of models are further divided into low-Re and high-Re $k-\epsilon$ models. The **high-Re** models are used for flows with very high Reynolds number and thus a very thin near-wall region (viscous sub-layer and buffer layer). In these models, the near-wall region is not solved and the first computation point lies in the log-law region. Suitable boundary conditions considering the wall-effect is devised using the

wall-functions. For low Reynolds number flows, the width of the near wall region is not negligible anymore. Also, if accurate near wall prediction of certain turbulent quantities (like k) is needed, near-wall region should be solved. For this, **low-Re** models are proposed. In this type of models, suitable damping functions are introduced in the model equations to reproduce the near-wall behaviour accurately, such that now the equations can be integrated all the way up to the wall. Various researchers have their own way of devising these damping functions and this is where a lot of models differ from each other.

$k-w$ models solves the transport equation of specific dissipation $w = \langle k \rangle / \epsilon$ as the second turbulent quantity alongside $\langle k \rangle$, instead of ϵ. These models are known to provide superior performance in the near-wall region that led (Menter, 1993) to propose another model which solves $k-w$ like equations near the wall, and $k-\epsilon$ like equations away from the wall.

- **V2F model:** This model was proposed by Durbin in 1991 (Durbin, 1991). In this model, alongwith the usual $k-\epsilon$ equations, two additional equations are solved, one for the wall-normal fluctuations $\langle v'^2 \rangle$ and another is an elliptic equation to model the pressure-velocity correlation term in the transport equation of $\langle v'^2 \rangle$. The salient feature of this model is that the use of damping function in the equation of ν_t to model the near wall effects is eliminated. This is because, the near wall damping functions are used to capture the inviscid effects of wall blocking that arise due to the impermeability kinematic boundary condition on v'. However, since now ν_t is modeled using $u_o \sim \sqrt{\langle v'^2 \rangle}$ and $l_o \sim \sqrt{\langle v'^2 \rangle}\langle k \rangle / \epsilon$, the wall-blocking effect is taken care in the computation of $\langle v'^2 \rangle$ with the help of an elliptic model equation to model the pressure-velocity term.

2-3-1-2 Reynolds stress models

In these models, the transport equations of Reynolds stress components are solved together with a transport equation to model the dissipation rate ϵ. The important terms in this model that needs closure are: the turbulent diffusion term, pressure-velocity correlation term and the anisotropic dissipation term. There are different closure models to model these terms.

For more details on turbulence modeling refer Pope (2001) or Wilcox et al. (1998).

2-3-2 Turbulent Heat Flux Modeling

So and Speziale (1999) presented a detailed review on heat flux models. A detailed description of the heat flux models, as presented therein, are not reproduced here. However, the most common ones are briefly discussed.

2-3-2-1 Gradient diffusion hypothesis

Like the turbulent viscosity hypothesis, there is a similar hypothesis for scalars, called the **gradient-diffusion hypothesis**. For turbulent channel flows, the turbulent scalar flux in the wall-normal direction is given by,

$$\langle \rho v'' \phi'' \rangle = -\sigma_t \partial \{\phi\} / \partial y, \tag{2-35}$$

where ϕ is any scalar and σ_t is the turbulent conductivity of that scalar. Using this hypothesis, turbulent heat flux can be written as,

$$\langle \rho v'' h'' \rangle = -\alpha_t \partial\{h\}/\partial y, \tag{2-36}$$

where α_t is λ_t/c_p. The main task now is to find a suitable approximation for α_t.

- **Constant Pr_t model:** This technique of modeling the heat flux is widely used in the industry due to its simplicity. However, this model is not always accurate and reliable. For example, it fails in cases where buoyancy effects are dominant (So and Speziale, 1999).

  The eddy conductivity is modeled as,

  $$\alpha_t = \frac{\mu_t}{Pr_t}. \tag{2-37}$$

  In the constant turbulent Prandtl number model, Pr_t is assumed to be constant in the flow field, and a value of 0.9 is widely used. This suggests a strong analogy between momentum and thermal mixing.

- **2-equation models:** In these models, α_t is modeled using turbulent quantities. α_t has dimensions of $\mathrm{m^2\,s^{-1}\,kg\,m^{-3}}$. However, to maintain similarity with the modeling of ν_t, we define eddy diffusivity with the dimensions of $\mathrm{m^2\,s^{-1}}$ as,

  $$\Gamma_t = \frac{\lambda_t}{\langle\rho\rangle c_p} = \frac{\alpha_t}{\langle\rho\rangle}. \tag{2-38}$$

  We can write,

  $$\Gamma_t \sim u_o^2 t_o, \tag{2-39}$$

  where u_o is a velocity scale of large eddies responsible for mixing and t_o is a time scale.

  The velocity and time scales are estimated using velocity turbulence quantities like TKE (k) and its dissipation (ϵ) and using thermal turbulence quantities like enthalpy variance ($k_h = h''h''/2$) and its dissipation (ϵ_h). This implies that α_t gets influenced by the turbulent quantities computed by turbulent stress models and thus, heat flux models are influenced by the accuracy of turbulent stress models.

After discussing about the governing equations in the dimensional form and also about the closure models, in the next chapter we will see how does the governing and model equations look like when they are semi-locally scaled.

Chapter 3

Semi-Local Scaling

The velocity scale and the viscous length scale are defined as $u_\tau = \sqrt{\tau_w/\rho_w}$ and $\delta_v = \nu_w/u_\tau$ respectively and are used in the classical scaling framework of constant property flows to characterize the inner layer. τ_w is the wall shear stress and ν represents kinematic viscosity. The dimensionless wall-normal co-ordinate is defined as $y^+ = y/\delta_v$, which can be interpreted as the local Reynolds number. The friction Reynolds number based on the half channel height is defined as $Re_\tau = h_c/\delta_v$, where h_c is the half channel height. Classical scaling is developed based on the properties at the wall. For constant properties, the properties in the flow domain are the same as the properties at the wall, but for variable property flows, this is not true. Thus, the characteristic scales defined using properties at the wall would not be a right choice to characterize the inner layer of variable property flows. Semi-local scaling, which was first introduced by Huang et al. (1995), has been applied mathematically to scale the Navier-Stokes equation by Patel et al. (2015). In semi-local scaling, the velocity scale and the viscous length scale are defined using the local properties as,

$$u^*_\tau = \sqrt{\tau_w/\langle\rho\rangle}, \qquad \delta^*_v = \langle\nu\rangle/u^*_\tau. \tag{3-1}$$

The semi-locally scaled wall-normal co-ordinate then becomes,

$$y^* = \frac{y}{\delta^*_v} = \frac{y}{h_c} Re^*_\tau, \tag{3-2}$$

where the semi-local Reynolds number is defined as,

$$Re^*_\tau = h_c/\delta^*_v. \tag{3-3}$$

Properties in the $\langle . \rangle$ operator indicate averaged local property at a point in the domain. The semi-local Prandtl number based on local properties is defined as,

$$Pr^* = \langle\mu\rangle c_p/\langle\lambda\rangle. \tag{3-4}$$

Like the friction velocity, u^*_τ, the semi-local friction temperature is defined as,

$$\theta^*_\tau = \frac{q_w}{\langle\rho\rangle c_p u^*_\tau}. \tag{3-5}$$

Knowing now the basics of semi-local scaling and understanding its essence, it would be interesting for the reader to know the motivation behind semi-local scaling and its importance. This is discussed in the next section.

3-1 Motivation Behind Using Semi-Local Scaling

Based on the analysis of Patel et al. (2015, 2016), we know that semi-local scaling characterizes variable property flows better than wall-based scaling. The best proof of this is the fact that solving RANS models in semi-locally scaled form provides much better results compared to just solving them in their conventional form (Pecnik and Patel, 2017; Otero Rodriguez et al., 2018). However, a clear explanation of why the same constant property models with the same model constants work for the different variable property cases, is not provided. An attempt to provide a clear explanation is made in this section.

Figure 3-1 shows the TKE production (scaled by $\rho_w u_\tau^3/h_c$) of three constant property cases of Moser et al. (1999) with $Re_\tau = 590$, $Re_\tau = 395$ and $Re_\tau = 180$. Generally in literature, this quantity is scaled with δ_v and not h_c. Figure 3-2 shows the TKE production of these cases but now scaled using $\rho_w u_\tau^3/\delta_v$ (in other words, dividing the production curves in figure 3-1 by their respective Re_τ). As seen, the cases collapse almost perfectly (except the low Reynolds number case with $Re_\tau = 180$, of Moser et al. (1999)). This collapse shows that the scaled production is universal for the constant property cases. Now let us do the same with the variable property cases. Figure 3-3 shows the TKE production for the different low-Mach number cases, as described in table 4-1 in the next chapter, scaled by $\langle\rho\rangle u_\tau^{*^3}/h_c$. As seen, the constant property case (CP) and constant semi-local Reynolds number cases (CRe_τ^*, CRe_τ^*2 and $\mathrm{CRe}_\tau^*\mathrm{CPr}^*$) are almost perfectly collapsing. Apart from this there is no sign of similarity with CP for other cases. Figure 3-4 shows the TKE production for these cases when scaled by $\rho u_\tau^{*^3}/\delta_v^*$ (effectively dividing the production term in figure 3-3 by Re_τ^*) and just like what happened with constant property cases in figure 3-2, we get nearly collapsing profiles in the region $y^* > 10$ (this universal profile is the same as what was obtained in figure 3-2. CP is equivalent to Moser395 in figure 3-2). This universal collapse is also observed for other TKE budget terms. Zhang et al. (2018) shows the nearly collapsing budget profiles, when semi-locally scaled, for different high-Mach number variable property cases analysed by them.

The collapsing TKE budget profiles, when semi-locally scaled, hints towards similarity in the dynamics of variable property cases and constant property cases. A major support of the similar dynamics in variable property and constant property cases also comes from Patel et al. (2015, 2016) where it is shown that the turbulent structures when scaled by semi-local viscous length scale (δ_v^*), become similar to constant property structures scaled by wall-based viscous length scale (δ_v), beyond $y^* \approx 10$. This is shown in figure 3-5 taken from Patel et al. (2016) which shows that the spanwise spacing of streaks (scaled by semi-local viscous length scale) becomes similar for the constant and variable property cases beyond $y^* \approx 10$. Figure 3-6 provides additional justification for similar dynamics. It shows the mixing length scaled by δ_v^* for the low-Mach number cases described in table 4-1, and as clearly seen, it becomes universal beyond $y^* \approx 10$. The universal collapse of mixing length is also shown in Patel et al. (2016).

Note the fact that we arrived from figure 3-1 to a collapsing profile in figure 3-2 by dividing by Re_τ and from figure 3-3 to a collapsing profile in figure 3-4 by dividing by Re_τ^*. This means

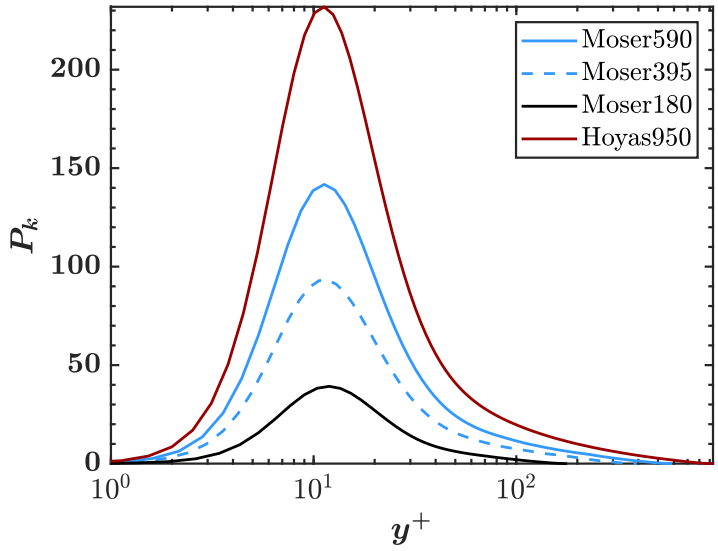

Figure 3-1: Production of TKE scaled by $\rho_w u_\tau^3/h_c$ for the constant property cases of Moser et al. (1999) (Re_τ =590, 395, 180) and Hoyas and Jiménez (2006) (Re_τ =950) available online on https://turbulence.oden.utexas.edu/.

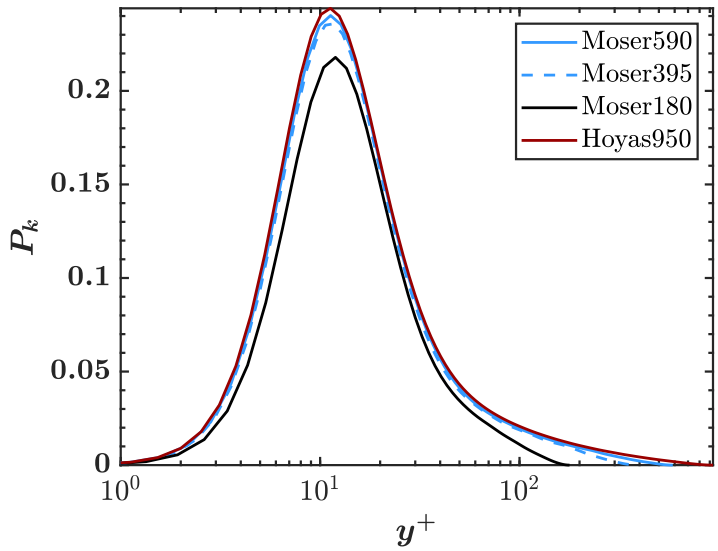

Figure 3-2: Production of TKE scaled by $\rho_w u_\tau^3/\delta_v$ for the cases described in figure 3-1.

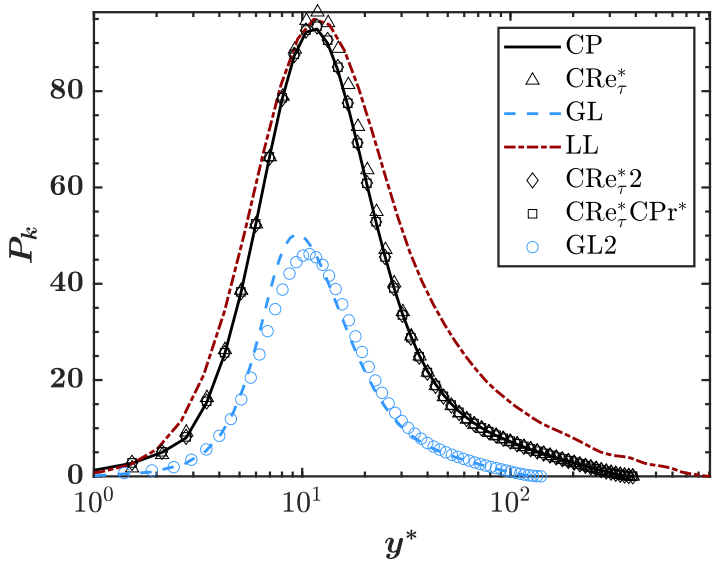

Figure 3-3: Production of TKE scaled by $\langle\rho\rangle u_\tau^{*^3}/h_c$ for the low-Mach number cases described in table 4-1 in the next chapter.

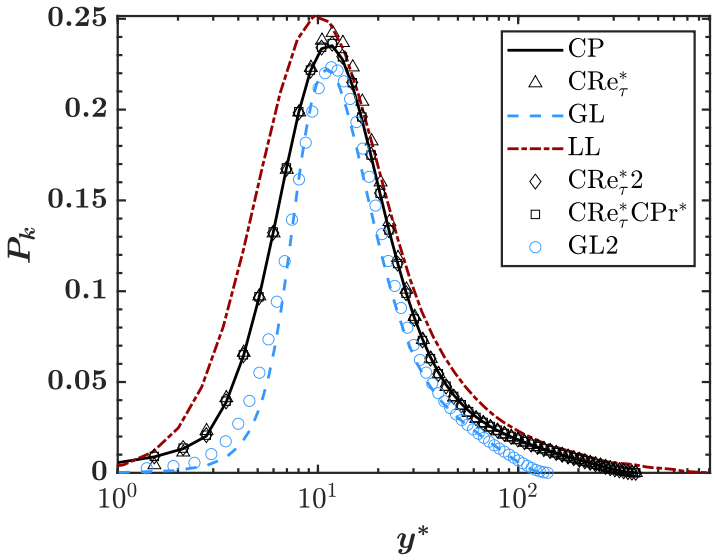

Figure 3-4: Production of TKE scaled by $\langle\rho\rangle u_\tau^{*^3}/\delta_v^*$ for the low-Mach number cases described in table 4-1 in the next chapter. CP is equivalent to Moser395 described in figure 3-1.

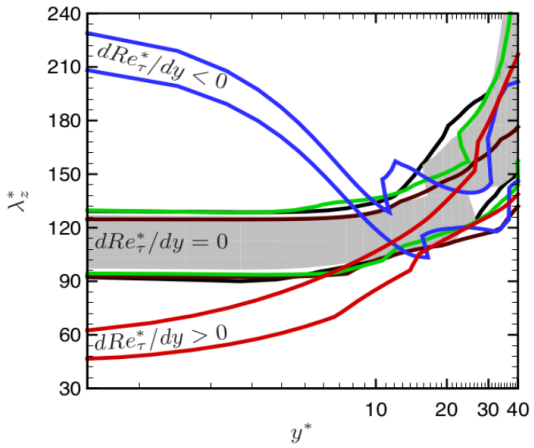

Figure 3-5: λ_z^* as a function of y^* obtained using bands of pre-multiplied spanwise spectra $k_z E_{\hat{u}'\hat{u}'}/\hat{u}'\hat{u}'$ with values larger than 96% of its maximum value; $\lambda_z^* = \lambda_z/\delta_v^*$ is semi-locally scaled wavelength; Wavelength corresponding to the maximum value of pre-multiplied spanwise spectra implies mean streak spacing in the spanwise direction; black, brown, green, blue and red lines correspond to case CP395 (constant property with $Re_\tau = 395$), CP150 (constant property with $Re_\tau = 150$), CP550 (constant property with $Re_\tau = 550$), GL (gas-like fluid) and LL (liquid-like fluid), respectively (Refer Patel et al. (2016) for more details on the cases); the grey region corresponds to case CRe_τ^* (constant $Re_\tau^* = 395$). Image is taken unedited from Patel et al. (2016).

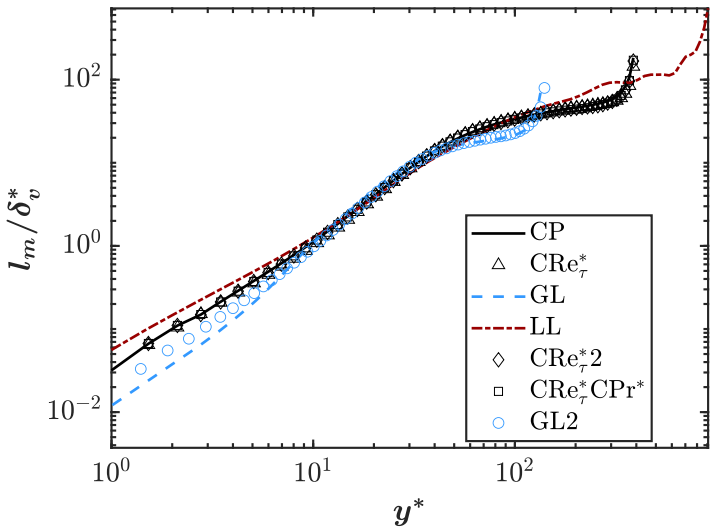

Figure 3-6: Mixing length l_m scaled by semi-local viscous length scale (δ_v^*). CP is equivalent to Moser395 described in figure 3-1.

that the TKE production $P_k/(\langle\rho\rangle u_\tau^{*^3}/h_c)$ at a certain y^* will be similar for a constant property flow and a variable property flow provided Re_τ of constant property flow is equal to the local Re_τ^* at that point. Same can also be said for other TKE budget terms. This implies that there exists a piecewise or pointwise similarity between semi-locally scaled variable property and constant property flows, provided that their Reynolds number are the same. It is important to note that this piecewise similarity and hence characterization by Re_τ^* is a result of scaling with length scale h_c. However, if we choose to scale with δ_v^* then we expect universality and no Reynolds number dependence on the TKE evolution (figure 3-2 and 3-4). Pecnik and Patel (2017) and Otero Rodriguez et al. (2018) choose to solve the model equations in the semi-locally scaled form with h_c as a length scale to non-dimensionalize the equations. This implies that the idea of piecewise similarity can be applied here and we can say that solving RANS model equations for a variable property flow implicitly means that we are solving them piecewise for different constant property flows with different Re_τ, such that $Re_\tau = Re_\tau^*$. Thus, the success of using the same models as constant property flows, but in semi-local form, is inevitable. It is stressed that near the wall ($y^* < 10$), there is no similarity between variable and constant property cases as also depicted by structure modulation seen in figure 3-5 (refer Patel et al. (2016) for more details on structure modulation). However, the error in the overall RANS solution caused by the non-similarity in this region is small due to viscous domination in this region. That means even if the value of μ_t computed in this region is not accurate, it does not matter because $\mu_t << \mu$.

The piecewise similarity is justified physically only if a point under consideration is influenced by neighbours where the semi-local Reynolds number is approximately similar to that at the point. Only then we can say that approximately the dynamics depends only on the local Re_τ^* and these dynamics are similar to those of constant property at $Re_\tau = Re_\tau^*$. This will be checked using a length scale argument as discussed next.

Consider a point in the domain and let us draw a rectangle about the point ranging from $+l_m$ to $-l_m$. l_m (mixing length) is a length scale signifying distance over which momentum is transported (Tennekes and Lumley, 1972). Let us define a length scale signifying the variation of Re_τ^* as,

$$\mathcal{L} = \frac{Re_\tau^*}{dRe_\tau^*/dy}. \tag{3-6}$$

Length scale $\mathcal{L}$ is compared with mixing length l_m and their ratio, for two variable property cases, is plotted in Figure 3-7.

Figure 3-7 shows that in the entire inner layer, $\mathcal{L} >> l_m$. This leads to the conclusion that inside the hypothetical rectangle we drew, the variation in Re_τ^* is minimal.

The similarity between the variable and constant property flows, that can be seen when semi-locally scaled, is the main motivation behind solving the RANS models, that were originally developed for constant property flows, in semi-locally scaled form. Doing this for variable property flows tremendously improved the estimation of shear stress as seen in Pecnik and Patel (2017); Otero Rodriguez et al. (2018). Will this also be effective for heat flux modeling? This is the question that is answered in chapter 5.

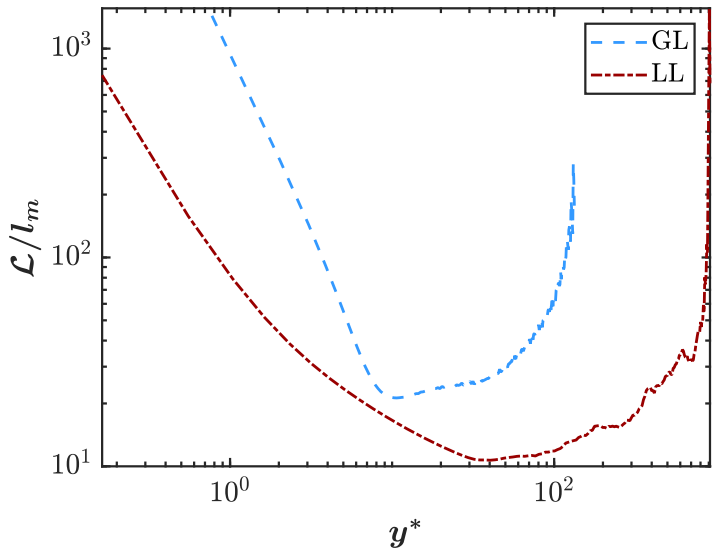

Figure 3-7: Ratio of the length scale defined in equation (3-6) and mixing-length scale (l_m).

3-2 Semi-Local Equations

In this section we shall present the governing equations, transport equations of TKE, enthalpy variance and turbulent heat flux in semi-local form. Table 3-1 shows which equations have already been derived (with reference) and also which equations will be derived as a part of this thesis.

Equation	Source
Continuity	Pecnik and Patel (2017)
Momentum	Pecnik and Patel (2017)
Energy	This work
TKE	Pecnik and Patel (2017)
Enthalpy Variance	This work
Turbulent Heat Flux	This work

Table 3-1: List of equations in semi-local form

Some relations between the semi-local quantities and quantities defined using the wall properties, that are important for derivations are,

$$u_\tau^* = u_\tau \sqrt{\frac{\rho_w}{\langle\rho\rangle}}, \quad \theta_\tau^* = \theta_\tau \sqrt{\frac{\rho_w}{\langle\rho\rangle}}, \quad Re_\tau^* = \frac{\sqrt{\langle\rho\rangle/\rho_w}}{\langle\mu\rangle/\mu_w} Re_\tau, \quad Pr^* = \frac{\langle\mu\rangle/\mu_w}{\langle\lambda\rangle/\lambda_w} Pr_w. \tag{3-7}$$

Until now, the equations were written in their dimensional form. But from here onward, their non-dimensional forms will be dealt with. In order to clearly differentiate, the following nomenclature is decided: for any variable, γ,

- γ- Dimensional variable,

- $\hat{\gamma}$ - Semi-locally scaled variable,
- $\tilde{\gamma}$ - Classically scaled variable.

In order to arrive at the non-dimensional form of any equation, the variables in the equation must be represented by their non-dimensional counterparts multiplied by a characteristic scale. For example, if x_i is a length variable then it is represented as $\hat{x}_i h_c$ where $\hat{x}_i$ is the non-dimensional representation and h_c is the characteristic scale (Refer table 3-2 for more such examples of different quantities). The equation then needs to be simplified to finally obtain its non-dimensional form.

Quantity		**Classical scales**	**Semi-local scales**
Length	x_i	$\tilde{x}_i h_c$	$\hat{x}_i h_c$
Time	t	$\tilde{t} h_c / u_\tau$	$\hat{t} h_c / u_\tau^*$
Velocity	u_i	$\tilde{u}_i u_\tau$	$\hat{u}_i u_\tau^*$
Pressure	p	$\tilde{p} \rho_w u_\tau^2$	$\hat{p} \langle\rho\rangle u_\tau^{*^2}$
Enthalpy	h	$\tilde{h} c_p \theta_\tau$	$\hat{h} c_p \theta_\tau^*$
Density	ρ	$\tilde{\rho} \rho_w$	$\hat{\rho} \langle\rho\rangle$
Dynamic viscosity	μ	$\tilde{\mu} \mu_w$	$\hat{\mu} \langle\mu\rangle$
Thermal conductivity	λ	$\tilde{\lambda} \lambda_w$	$\hat{\lambda} \langle\lambda\rangle$
Turbulent KE	k	$\tilde{k} u_\tau^2$	$\hat{k} u_\tau^{*^2}$
Eddy viscosity	μ_t	$\tilde{\mu}_t \rho_w u_\tau h_c$	$\hat{\mu}_t \langle\rho\rangle u_\tau^* h_c$
Dissipation of TKE (per unit mass)	ϵ	$\tilde{\epsilon} u_\tau^3 / h_c$	$\hat{\epsilon} u_\tau^{*^3} / h_c$
Enthalpy variance	k_h	$\tilde{k}_h (c_p \theta_\tau)^2$	$\hat{k}_h (c_p \theta_\tau^*)^2$
Eddy conductivity	α_t	$\tilde{\alpha}_t \rho_w u_\tau h_c$	$\hat{\alpha}_t \langle\rho\rangle u_\tau^* h_c$
Dissipation of k_h (per unit mass)	ϵ_{kh}	$\tilde{\epsilon}_{kh} u_\tau (c_p \theta_\tau)^2 / h_c$	$\hat{\epsilon}_{kh} u_\tau^* (c_p \theta_\tau^*)^2 / h_c$

Table 3-2: Representation of different quantities in their non-dimensional form multiplied by a characteristic scale.

Some assumptions in the derivations performed to arrive at the semi-local equations are as follows:

1. Streamwise variations of the wall shear stress (τ_w) are zero or very small. Also, variations in the wall properties in the streamwise direction are neglected. As the wall properties and τ_w, also, do not vary in the spanwise direction, we conclude that they are mere constants and can be pulled out of the spatial derivatives. This assumption is valid for fully developed channel flows.
2. Characteristic scales, u_τ^*, $\langle\rho\rangle$, etc., are assumed to be independent of time and are pulled

out of the time derivative $\partial(.)/\partial t$.

3-2-1 Governing Equations: Instantaneous Form

- **Continuity equation**

Derivation of the semi-local instantaneous continuity equation is performed in Pecnik and Patel (2017). The final result is,

$$t^*_\tau \frac{\partial \hat{\rho}}{\partial t} + \frac{\partial \hat{\rho}\hat{u}_i}{\partial \hat{x}_i} + \hat{\rho}\hat{u}_i \underbrace{\frac{1}{2\langle\rho\rangle}\frac{\partial\langle\rho\rangle}{\partial \hat{x}_i}}_{d_i} = 0. \tag{3-8}$$

The last term arises because density is not constant in the domain and thus, it is a function of spatial co-ordinates. This term is an "individual property dependent" term as it needs individual property (density) profile (or data) for its computation.

- **Momentum equation**

Derivation of the semi-local instantaneous momentum equation is performed in Pecnik and Patel (2017). The final result is,

$$t^*_\tau \hat{\rho}\frac{\partial \hat{u}_i}{\partial t} + \hat{\rho}\hat{u}_j\frac{\partial \hat{u}_i}{\partial \hat{x}_j} - \underbrace{\hat{\rho}\hat{u}_i\hat{u}_j d_j}_{\text{(I)}} = -\frac{\partial \hat{p}}{\partial \hat{x}_i} + \frac{\partial \hat{\tau}_{ij}}{\partial \hat{x}_j} - \underbrace{\frac{\partial \hat{D}_{ij}}{\partial \hat{x}_j}}_{\text{(II)}}. \tag{3-9}$$

Pecnik and Patel (2017) also had a term, $\hat{\rho}\hat{f}_i$, indicating the body force term. But to be consistent with the instantaneous momentum equation (2-2), we assume the body force term to be incorporated in the pressure, p, as was done in Pope (2001).

Other terms in the equation are defined as,

$$\hat{\tau}_{ij} = \hat{\mu}/Re^*_\tau \left[\left(\partial\hat{u}_i/\partial\hat{x}_j + \partial\hat{u}_j/\partial\hat{x}_i\right) - 2/3\left(\partial\hat{u}_k/\partial\hat{x}_k\right)\delta_{ij}\right], \tag{3-10}$$

$$\hat{D}_{ij} = \hat{\mu}/Re^*_\tau \left[\left(\hat{u}_i d_j + \hat{u}_j d_i\right) - 2/3\left(\hat{u}_k d_k\right)\delta_{ij}\right]. \tag{3-11}$$

Due to semi-local scaling, we have additional property dependent terms (term (I) and (II)). These terms are based on the derivative of density term, d_i. The viscosity coefficient in the momentum equation is replaced by $\hat{\mu}/Re^*_\tau$ due to semi-local scaling.

An interesting thing to note (which is not previously discussed in literature) is that, if we introduce the definition of van Driest velocity as,

$$\partial u_i^{vD} = \sqrt{\langle\rho\rangle/\rho_w}\partial\tilde{u}_i, \tag{3-12}$$

with the help of equations (3-7, 3-12), the viscous diffusion term and the term (II) in equation (3-9) can be combined together to form, $\partial\tau_{ij}^{vD}/\partial\hat{x}_j$, where,

$$\tau_{ij}^{vD} = \hat{\mu}/Re^*_\tau \left[\left(\partial u_i^{vD}/\partial\hat{x}_j + \partial u_j^{vD}/\partial\hat{x}_i\right) - 2/3\left(\partial u_k^{vD}/\partial\hat{x}_k\right)\delta_{ij}\right]. \tag{3-13}$$

Thus, we have the final equation as,

$$t^*_\tau \hat{\rho}\frac{\partial \hat{u}_i}{\partial t} + \hat{\rho}\hat{u}_j\frac{\partial \hat{u}_i}{\partial \hat{x}_j} - \hat{\rho}\hat{u}_i\hat{u}_j d_j = -\frac{\partial \hat{p}}{\partial \hat{x}_i} + \frac{\partial \tau^{vD}_{ij}}{\partial \hat{x}_j}. \tag{3-14}$$

- **Energy equation**

A detailed derivation of the semi-local instantaneous energy equation is not found in any literature. However, the semi-local averaged energy equation for a fully developed turbulent channel flow was analysed in Patel et al. (2017). The instantaneous equation is derived in Appendix A.

The final equation obtained is,

$$t^*_\tau \hat{\rho}\frac{\partial \hat{h}}{\partial t} + \hat{\rho}\hat{u}_j\frac{\partial \hat{h}}{\partial \hat{x}_j} - \underbrace{\hat{\rho}\hat{u}_j\hat{h}d_j}_{\text{(III)}} = Ec^*_{\theta_\tau}\left(t^*_\tau\frac{\partial \hat{p}}{\partial t} + \hat{u}_j\frac{\partial \hat{p}}{\partial \hat{x}_j}\right) + \frac{\partial \hat{q}_j}{\partial \hat{x}_j} - \underbrace{\frac{\partial \hat{D}_j}{\partial \hat{x}_j}}_{\text{(IV)}} + \hat{\Phi}, \tag{3-15}$$

where $\hat{q}_j$ is the conductive heat flux defined as,

$$\hat{q}_j = \hat{\alpha}/(Re^*_\tau Pr^*)\partial\hat{h}/\partial\hat{x}_j, \tag{3-16}$$

and the density dependent term (term (IV)), which is analogous to term (II) in the momentum equation (3-9), is defined as,

$$\hat{D}_j = \hat{\alpha}/(Re^*_\tau Pr^*)\hat{h}d_j. \tag{3-17}$$

$Ec^*_{\theta_\tau}$ is defined as ${u^*_\tau}^2/(c_p\theta^*_\tau)$ and comes in front of the pressure term because of the difference in scales with which pressure is scaled ($\langle\rho\rangle {u^*_\tau}^2$) and with which the enthalpy equation is scaled ($\langle\rho\rangle u^*_\tau c_p\theta^*_\tau/h_c$). More about the importance of this parameter is discussed in section 6-3.

$\hat{\Phi}$ is the semi-local form of volumteric heat source. It is defined as,

$$\hat{\Phi} = \frac{\Phi}{\langle\rho\rangle u^*_\tau c_p\theta^*_\tau/h_c}. \tag{3-18}$$

Like in the momentum equation, due to semi-local scaling, we have additional property dependent terms (term (III) and (IV)). The thermal conductivity, α, in the energy equation modifies to $\hat{\alpha}/(Re^*_\tau Pr^*)$ due to semi-local scaling.

Analogous to what we did for the momentum equation, if we introduce van Driest enthalpy as,

$$\partial h^{vD} = \sqrt{\langle\rho\rangle/\rho_w}\partial\tilde{h}, \tag{3-19}$$

we can combine the conductive heat flux term and term (IV) to form $\partial q^{vD}_j/\partial\hat{x}_j$ where,

$$q^{vD}_j = \hat{\alpha}/(Re^*_\tau Pr^*)\partial h^{vD}/\partial\hat{x}_j. \tag{3-20}$$

The final equation then becomes,

$$t^*_\tau \hat{\rho}\frac{\partial \hat{h}}{\partial t} + \hat{\rho}\hat{u}_j\frac{\partial \hat{h}}{\partial \hat{x}_j} - \hat{\rho}\hat{u}_j\hat{h}d_j = Ec^*_{\theta_\tau}\left(t^*_\tau\frac{\partial \hat{p}}{\partial t} + \hat{u}_j\frac{\partial \hat{p}}{\partial \hat{x}_j}\right) + \frac{\partial q^{vD}_j}{\partial \hat{x}_j} + \hat{\Phi}. \tag{3-21}$$

Comparing equations (3-14, 3-21), we can notice that in semi-local scales, molecular diffusion of momentum and energy depends on the gradient of van Driest velocity and van Driest enthalpy respectively.

3-2-2 Governing Equations: Averaged Form

Getting to the semi-locally scaled Reynolds Averaged Navier Stokes equations from the semi-local instantaneous form of the equations is not different from what we did in section 2-2. An important identity to note is,

$$\langle \hat{\rho}\hat{\gamma} \rangle = \{\hat{\gamma}\}. \tag{3-22}$$

- **Continuity equation**

The continuity equation in RANS form is derived as,

$$\left\langle t_\tau^* \frac{\partial \hat{\rho}}{\partial t} + \frac{\partial \hat{\rho}\hat{u}_i}{\partial \hat{x}_i} + \hat{\rho}\hat{u}_i d_i \right\rangle = t_\tau^* \underbrace{\frac{\partial \langle \hat{\rho} \rangle}{\partial t}}_{=0} + \frac{\partial \langle \hat{\rho}\hat{u}_i \rangle}{\partial \hat{x}_i} + \langle \hat{\rho}\hat{u}_i \rangle d_i = 0. \tag{3-23}$$

Using identity (3-22) we get,

$$\frac{\partial \{\hat{u}_i\}}{\partial \hat{x}_i} + \{\hat{u}_i\} d_i = 0. \tag{3-24}$$

- **Momentum equation**

Rewriting the left-hand side of equation (3-14) as,

$$t_\tau^* \hat{\rho} \frac{\partial \hat{u}_i}{\partial t} + \hat{\rho}\hat{u}_j \frac{\partial \hat{u}_i}{\partial \hat{x}_j} - \hat{\rho}\hat{u}_i\hat{u}_j d_j = t_\tau^* \frac{\partial \hat{\rho}\hat{u}_i}{\partial t} + \frac{\partial \hat{\rho}\hat{u}_i\hat{u}_j}{\partial \hat{x}_j}. \tag{3-25}$$

Taking Reynolds average on both sides of the momentum equation, we have,

$$\left\langle t_\tau^* \frac{\partial \hat{\rho}\hat{u}_i}{\partial t} + \frac{\partial \hat{\rho}\hat{u}_j\hat{u}_i}{\partial \hat{x}_j} \right\rangle = \left\langle -\frac{\partial \hat{p}}{\partial \hat{x}_i} + \frac{\partial \tau_{ij}^{vD}}{\partial \hat{x}_j} \right\rangle. \tag{3-26}$$

We will show the detailed steps of only the advection term.

Advection term:

$$\frac{\partial \langle \hat{\rho}\hat{u}_i\hat{u}_j \rangle}{\partial \hat{x}_j} = \frac{\partial \langle \hat{\rho}(\{\hat{u}_i\} + \hat{u}_i'')(\{\hat{u}_j\} + \hat{u}_j'') \rangle}{\partial \hat{x}_j}, \tag{3-27}$$

$$= \frac{\partial (\langle \hat{\rho}\{\hat{u}_i\}\{\hat{u}_j\} \rangle + \langle \hat{\rho}\hat{u}_i''\{\hat{u}_j\} \rangle + \langle \hat{\rho}\{\hat{u}_i\}\hat{u}_j'' \rangle + \langle \hat{\rho}\hat{u}_i''\hat{u}_j'' \rangle)}{\partial \hat{x}_j}. \tag{3-28}$$

Using the identity in equation (2-22) and equation (3-22), we get,

$$\frac{\partial \langle \hat{\rho}\hat{u}_i\hat{u}_j \rangle}{\partial \hat{x}_j} = \frac{\partial \{\hat{u}_i\}\{\hat{u}_j\}}{\partial \hat{x}_j} + \frac{\partial \{\hat{u}_i''\hat{u}_j''\}}{\partial \hat{x}_j}. \tag{3-29}$$

The final momentum equation becomes,

$$t_\tau^* \frac{\partial \{\hat{u}_i\}}{\partial t} + \frac{\partial \{\hat{u}_i\}\{\hat{u}_j\}}{\partial \hat{x}_j} = -\frac{\partial \langle \hat{p} \rangle}{\partial \hat{x}_i} + \frac{\partial \langle \tau_{ij}^{vD} \rangle}{\partial \hat{x}_j} - \frac{\partial \{\hat{u}_i''\hat{u}_j''\}}{\partial \hat{x}_j}. \tag{3-30}$$

- **Energy equation**

Detailed derivation of the energy equation is not presented here as the steps are very similar to what was done for the momentum equation.

The final equation obtained is,

$$t^*_\tau \frac{\partial\{\hat{h}\}}{\partial t} + \frac{\partial\{\hat{u}_j\}\{\hat{h}\}}{\partial \hat{x}_j} = Ec^*_{\theta_\tau}\left(t^*_\tau \frac{\partial\langle\hat{p}\rangle}{\partial t} + \left\langle \hat{u}_j \frac{\partial \hat{p}}{\partial \hat{x}_j}\right\rangle\right) + \frac{\partial\langle q^{vD}_j\rangle}{\partial \hat{x}_j} - \frac{\partial\{\hat{u}''_j\hat{h}''\}}{\partial \hat{x}_j} + \langle\hat{\Phi}\rangle. \tag{3-31}$$

3-2-3 Semi-Local Turbulent Kinetic Energy (TKE) Transport Equation

This equation is derived in Pecnik and Patel (2017). The final result is,

$$t^*_\tau \frac{\partial\{\hat{k}\}}{\partial t} + \frac{\partial\{\hat{k}\}\{\hat{u}_j\}}{\partial \hat{x}_j} = \hat{P}_k - \hat{\epsilon}_k + \hat{T}_k + \hat{C}_k + \hat{\mathcal{D}}_k. \tag{3-32}$$

The details about the terms in equation (3-32) are presented in table 3-3.

Term	Definition
$\hat{P}_k = -\left\{\hat{u}''_i\hat{u}''_j\right\}\frac{\partial\left\{u^{vD}_i\right\}}{\partial \hat{x}_j}.$	Production of TKE.
$\hat{\epsilon}_k = \left\langle \hat{\tau}'_{ij}\frac{\partial \hat{u}'_i}{\partial \hat{x}_j}\right\rangle.$	Dissipation of TKE.
$\hat{T}_k = \frac{\partial}{\partial \hat{x}_j}\left(\left\langle \hat{u}'_i\hat{\tau}'_{ij}\right\rangle - \left\{\hat{u}''_j\hat{k}\right\} - \left\langle \hat{p}'\hat{u}'_j\right\rangle\right).$	Total diffusion.
$\hat{C}_k = \left\langle \hat{p}'\frac{\partial \hat{u}'_j}{\partial \hat{x}_j}\right\rangle - \langle\hat{u}''_j\rangle\frac{\partial\langle\hat{p}\rangle}{\partial \hat{x}_j} + \langle\hat{u}''_i\rangle\frac{\partial\langle\hat{\tau}_{ij}\rangle}{\partial \hat{x}_j}.$	Compressibility term.
$\hat{\mathcal{D}}_k = \left(\{\hat{u}_j\}\{\hat{k}\} + \left\{\hat{u}''_j\hat{k}\right\}\right)d_j - \left\langle \hat{u}''_i\frac{\partial \hat{D}_{ij}}{\partial \hat{x}_j}\right\rangle.$	Mathematical artifacts of semi-local scaling.

Table 3-3: Terms in the TKE equation.

$\hat{\tau}_{ij}$ is defined in equation (3-10) and $\hat{D}_{ij}$ is defined in equation (3-11). The transport equation is simplified for a fully developed channel and its model form is solved for estimating eddy viscosity and hence the turbulent shear stress (Pecnik and Patel, 2017; Otero Rodriguez et al., 2018).

3-2-4 Semi-Local Enthalpy Variance Transport Equation

Pecnik and Patel (2017) derived the transport equation for turbulent kinetic energy in semi-local scales. They started with an instantaneous momentum equation in semi-local scales. In the similar manner, here we derive the counterpart of TKE for thermal turbulence i.e. the enthalpy variance equation in semi-local scales starting with the instantaneous enthalpy equation in semi-local scales.

The recipe of derivation is very similar as we would have for a constant property enthalpy variance (or thermal variance) equation. If $\mathcal{H}(\hat{h}) = 0$ denotes the instantaneous enthalpy equation in semi-local form, then the transport equation of enthalpy variance is obtained as,

$$\overline{\hat{h}''\mathcal{H}(\hat{h})} = 0, \tag{3-33}$$

where $\overline{(.)}$ is another way of denoting Reynolds averaging.

Detailed derivation of the equation is shown in Appendix A. The final equation is,

$$t^*_\tau \frac{\partial\{\hat{k}_h\}}{\partial t} + \frac{\partial\{\hat{k}_h\}\{\hat{u}_j\}}{\partial\hat{x}_j} = \hat{P}_{kh} - \hat{\epsilon}_{kh} + \hat{T}_{kh} + \hat{D}_{kh} + \hat{B}_{kh} + \hat{Pr}_{kh} + \hat{\Phi}_{kh}, \tag{3-34}$$

where $\hat{k}_h = \hat{h''}\hat{h''}/2$ is half of enthalpy variance and is analogous to TKE. Each term in equation (3-34) is described in table 3-4.

Some terms used in table 3-4 are,

$$\hat{q}_j = \frac{\hat{\alpha}}{Re^*_\tau Pr^*}\frac{\partial\hat{h}}{\partial\hat{x}_j}, \tag{3-35}$$

$$\hat{D}_j = \frac{\hat{\alpha}}{Re^*_\tau Pr^*}\hat{h}d_j, \tag{3-36}$$

$$d_j = \frac{1}{2\langle\rho\rangle}\frac{\partial\langle\rho\rangle}{\partial\hat{x}_j}. \tag{3-37}$$

For a fully developed channel, the Equation (3-34) simplifies to,

$$\hat{P}_{kh} - \hat{\epsilon}_{kh} + \hat{T}_{kh} + \hat{D}_{kh} + \hat{B}_{kh} + \hat{Pr}_{kh} + \hat{\Phi}_{kh} = 0, \tag{3-38}$$

with y being the direction in which mean quantities can vary and x, z are homogeneous directions.

The main goal of deriving this equation is to solve for eddy conductivity and hence turbulent heat flux in chapters 5 and 6. In chapter 6 this equation is also used to study the effects of viscous heating on enthalpy variance.

Term	Definition
$\hat{P}_{kh} = -\{\hat{h''}\hat{u''_j}\}\frac{\partial\{h^{vd}\}}{\partial\hat{x}_j}.$	Production of enthalpy variance.
$\hat{\epsilon}_{kh} = \left\langle \hat{q}'_j \frac{\partial\hat{h}''}{\partial\hat{x}_j} \right\rangle.$	Dissipation of enthalpy variance.
$\hat{T}_{kh} = \hat{T}^m_{kh} + \hat{T}^t_{kh}.$	Total diffusion.
$\hat{T}^m_{kh} = \frac{\partial}{\partial\hat{x}_j}\left\langle \hat{h}''\hat{q}'_j \right\rangle.$	Molecular diffusion.
$\hat{T}^t_{kh} = -\frac{\partial}{\partial\hat{x}_j}\{\hat{u''_j}\hat{k}_h\}.$	Turbulent diffusion.
$\hat{B}_{kh} = \langle\hat{h}''\rangle\frac{\partial\langle\hat{q}_j\rangle}{\partial\hat{x}_j} + \langle\hat{h}''\rangle\langle\hat{\Phi}\rangle.$	Favre artifact term. This term arises due to non-zero $\langle\hat{h}''\rangle$ which is a consequence of Favre averaging.
$\hat{D}_{kh} = \{\hat{u}_j\}\{\hat{k}_h\}d_j + \{\hat{u''_j}\hat{k}_h\}d_j - \left\langle \hat{h''}\frac{\partial\hat{D}_j}{\partial\hat{x}_j} \right\rangle.$	Mathematical artifacts of semi-local scaling.
$\hat{Pr}_{kh} = Ec^*_\tau\left(t^*_\tau\left\langle\hat{h}''\frac{\partial\hat{p}}{\partial t}\right\rangle + \left\langle\hat{h}''\hat{u}_j\frac{\partial\hat{p}}{\partial\hat{x}_j}\right\rangle\right).$	Contribution due to pressure terms in the enthalpy equation.
$\hat{\Phi}_{kh} = \langle\hat{h}''\hat{\Phi}'\rangle.$	Contribution by fluctuations in the volumetric heat source.

Table 3-4: Terms in the enthalpy variance equation.

3-2-5 Semi-Local Turbulent Heat Flux Transport Equation

We aim to derive the budget for $\langle \hat{u}_i'' \hat{h}'' \rangle$ which signifies turbulent heat flux in the x_i direction where $i = 1, 2, 3$ stands for streamwise, wall-normal and spanwise directions respectively. Let $\mathcal{N}(\hat{u}_i) = 0$ denote the semi-local instantaneous momentum equation for $\hat{u}_i$ and $\mathcal{H}(\hat{h}) = 0$ denote the semi-local enthalpy equation. The heat flux budget is derived as,

$$\overline{\hat{h}'' \mathcal{N}(\hat{u}_i) + \hat{u_i}'' \mathcal{H}(\hat{h})} = 0, \tag{3-39}$$

where $\overline{(.)}$ is another way of denoting Reynolds averaging.

Detailed steps of derivation are shown in Appendix A. The final equation obtained is,

$$t_\tau^* \frac{\partial \{\hat{u}_i'' \hat{h}''\}}{\partial t} + \frac{\partial \{\hat{u}_i'' \hat{h}''\}\{u_j\}}{\partial \hat{x}_j} = \hat{P}_{u_i h} - \hat{\epsilon}_{u_i h} + \hat{T}_{u_i h} + \hat{H}_{u_i h} + \hat{D}_{u_i h} + \hat{B}_{u_i h} + \hat{Pr}_{u_i h} + \hat{\Phi}_{u_i h}, \tag{3-40}$$

where the terms are described in table 3-5.

Some terms used in table 3-5 are introduced before and rewritten below for convenience,

$$\hat{q}_j = \hat{\alpha}/(Re_\tau^* Pr^*) \partial \hat{h}/\partial \hat{x}_j, \tag{3-41}$$

$$\hat{\tau}_{ij} = \hat{\mu}/Re_\tau^* \left[(\partial \hat{u}_i/\partial \hat{x}_j + \partial \hat{u}_j/\partial \hat{x}_i) - 2/3 \left(\partial \hat{u}_k/\partial \hat{x}_k \right) \delta_{ij} \right], \tag{3-42}$$

$$\hat{D}_j = \frac{\hat{\alpha}}{Re_\tau^* Pr^*} \hat{h} d_j, \tag{3-43}$$

$$\hat{D}_{ij} = \hat{\mu}/Re_\tau^* \left[(\hat{u}_i d_j + \hat{u}_j d_i) - 2/3 \left(\hat{u}_k d_k \right) \delta_{ij} \right], \tag{3-44}$$

$$d_j = \frac{1}{2\langle \rho \rangle} \frac{\partial \langle \rho \rangle}{\partial \hat{x}_j}. \tag{3-45}$$

For a fully developed channel flow, the equation simplifies to,

$$\hat{P}_{u_i h} - \hat{\epsilon}_{u_i h} + \hat{T}_{u_i h} + \hat{H}_{u_i h} + \hat{D}_{u_i h} + \hat{B}_{u_i h} + \hat{Pr}_{u_i h} + \hat{\Phi}_{u_i h} = 0, \tag{3-46}$$

with y being the direction in which mean quantities can vary and x, z are homogeneous directions.

This equation is derived mainly to study the effects of viscous heating on turbulent heat flux in chapter 6. This equation can also be used for second order closure models for turbulent heat flux modeling in variable property flows, but it is not done in this thesis.

In this chapter, we have presented the mathematics related to semi-local scaling. In the next chapter one would gain the knowledge of different variable property cases analysed in this study.

Term	Definition
$\hat{P}_{u_i h} = -\{\hat{u}_i''\hat{u}_j''\}\frac{\partial\{h^{vD}\}}{\partial\hat{x}_j} - \{\hat{u}_j''\hat{h}''\}\frac{\partial\{u_i^{vD}\}}{\partial\hat{x}_j}.$	Production of turbulent heat flux.
$\hat{\epsilon}_{u_i h} = \left\langle \hat{q}_j' \frac{\partial\hat{u}_i''}{\partial\hat{x}_j} \right\rangle + \left\langle \hat{\tau}_{ij}' \frac{\partial\hat{h}''}{\partial\hat{x}_j} \right\rangle.$	Dissipation of turbulent heat flux.
$\hat{T}_{u_i h} = \frac{\partial}{\partial\hat{x}_j}\left(\langle\hat{u}_j''\hat{q}_j'\rangle + \langle\hat{h}''\hat{\tau}_{ij}'\rangle - \{\hat{u}_i''\hat{h}''\hat{u}_j''\}\right).$	Total diffusion.
$\hat{H}_{u_i h} = \left\langle \hat{h}'' \frac{\partial\hat{p}}{\partial\hat{x}_i} \right\rangle.$	Enthalpy - pressure gradient correlation term .
$\hat{B}_{u_i h} = \langle\hat{u}_i''\rangle\frac{\partial\langle\hat{q}_j\rangle}{\partial\hat{x}_j} + \langle\hat{h}''\rangle\frac{\partial\langle\hat{\tau}_{ij}\rangle}{\partial\hat{x}_j} + \langle\hat{u}_i''\rangle\langle\hat{\Phi}\rangle.$	Favre artifact term. This term arises due to non-zero $\langle\hat{h}''\rangle$ and $\langle\hat{u}_i''\rangle$ which is a consequence of Favre averaging.
$\hat{D}_{u_i h} = \{\hat{u}_j\}\{\hat{u}_i''\hat{h}''\}d_j + \{\hat{u}_i''\hat{h}''\hat{u_j''}\}d_j - \left\langle \hat{u}_i'' \frac{\partial\hat{D}_j}{\partial\hat{x}_j} \right\rangle - \left\langle \hat{h}'' \frac{\partial\hat{D}_{ij}}{\partial\hat{x}_j} \right\rangle.$	Mathematical artifacts of semi-local scaling.
$\hat{Pr}_{u_i h} = Ec_\tau^*\left(t_\tau^*\left\langle\hat{u}_i''\frac{\partial\hat{p}}{\partial t}\right\rangle + \left\langle\hat{u}_i''\hat{u}_j\frac{\partial\hat{p}}{\partial\hat{x}_j}\right\rangle\right).$	Contribution due to pressure terms in the enthalpy equation.
$\hat{\Phi}_{u_i h} = \langle\hat{u}_i''\hat{\Phi}'\rangle.$	Contribution by fluctuations in the volumetric heat source.

Table 3-5: Terms in the turbulent heat flux budget.

Chapter 4

Description of Cases

In this chapter we will describe different cases that will be analysed in this thesis. All the cases are based on calorifically perfect fluids such that,

$$\frac{c_p}{c_{p_w}} = 1. \tag{4-1}$$

A summary of all the cases analysed is shown in table 4-1. In table 4-1 Ma_b is Mach number based on bulk velocity and speed of sound defined at the wall. Re_{τ_w} is friction Reynolds number defined using wall properties and $Re^*_{\tau_c}$ is defined using properties at the channel centre. Similarly Pr_w and Pr^*_c are Prandtl numbers defined at the wall and channel centre respectively. The wall and channel centre values give an idea about the variation of the parameters in the domain.

4-1 Low-Mach Number Cases

Table 4-2 describes the property laws and figure 4-1 shows property distribution for the low-Mach number cases. Figure 4-2 shows the distribution of semi-local Reynolds and Prandtl number for these cases.

- CP stands for "constant property" and signifies incompressible constant property cases.
- GL possesses gas-like fluid property laws and thus we can see the viscosity increasing and density decreasing with temperature (figure 4-1).
- LL signifies liquid-like property laws.
- CRe^*_τ is a special case in which the property laws are such that the semi-local Reynolds number is constant in the domain. This case helps to isolate the individual property variation effects (like intercomponent energy transfer discussed in chapter 7).

- $\mathrm{CRe}_\tau^*\mathrm{CPr}^*$ is another special case in which the property laws are such that not only the semi-local Reynolds number but also the semi-local Prandtl number Pr^* is constant in the domain.

The difference between GL and GL2 (or CRe_τ^* and CRe_τ^*2) is that the amount of volumetric heating is different and hence, the property variations are different, however, the property laws are the same.

4-2 High-Mach Number Cases

These are high-Mach number **ideal gas** cases that were discussed in Trettel and Larsson (2016). Viscosity and thermal conductivity are computed using the relation,

$$\frac{\mu}{\mu_w} = \frac{\lambda}{\lambda_w} = \left(\frac{T}{T_w}\right)^{0.75}. \tag{4-2}$$

Density is computed using the continuity equation but because of the wall-normal variation of pressure being very small, an approximate law for density follows from the ideal gas equation of state,

$$\frac{\rho}{\rho_w} \approx \left(\frac{T}{T_w}\right)^{-1}. \tag{4-3}$$

Figure 4-3 shows the property distribution in the domain and figure 4-4 shows the distribution of semi-local Reynolds number (Re_τ^*) and modified Eckert number ($Ec_{\theta_\tau}^*$). Distribution of semi-local Prandtl number (Pr^*) is not shown as it is constant in the domain for all the cases and takes a value of 0.7. A case with name "MxRy" implies that the bulk Mach number is "x" and the semi-local Reynolds number at the channel center is "y".

4-3 High-Mach Number Cases with Constant Re_τ^*

These are high-Mach number cases but with viscosity and thermal conductivity laws such that both Re_τ^* and Pr^* are constant in the domain. **Ideal gas** equation of state is followed for these cases. The property laws are,

$$\frac{\mu}{\mu_w} = \frac{\lambda}{\lambda_w} = \left(\frac{\rho}{\rho_w}\right)^{0.5} \approx \left(\frac{T}{T_w}\right)^{-0.5}. \tag{4-4}$$

Using the laws mentioned in equation (4-4), the profile of Re_τ^* is not strictly constant. This is because for a strictly constant Re_τ^* we must have,

$$\frac{\langle\mu\rangle}{\langle\mu_w\rangle} = \sqrt{\frac{\langle\rho\rangle}{\langle\rho_w\rangle}}, \tag{4-5}$$

but due to non-zero fluctuations in properties we cannot strictly maintain equation (4-5) while using equation (4-4) as the property laws.

Figure 4-5 shows the property distribution in the domain and figure 4-6 shows the distribution of Re^*_τ and $Ec^*_{\theta_\tau}$.

In the following two chapters, using DNS data we will analyse thermal turbulence in low-Mach number and high-Mach number cases. Using the knowledge about the physics and governing parameters, we shall try to solve RANS equations for these cases using 2-equation turbulent stress and 2-equation heat flux models.

Casename	Ma_b	Re_{τ_w}	$Re^*_{\tau_c}$	Pr_w	Pr^*_c	Heating
CP[1]	NA	395	395	1	1	UH
CRe^*_τ[1]	NA	395	395	1	0.34	UH
GL[1]	NA	950	137	1	3.10	UH
LL[1]	NA	150	945	1	0.16	UH
CRe^*_τ2[1]	NA	395	395	1	0.71	UH
$\mathrm{CRe}^*_\tau\mathrm{CPr}^*$[1]	NA	395	395	1	1	UH
GL2[1]	NA	395	143	1	1.81	UH
M0.7R400[2]	0.7	437	396	0.7	0.7	VH
M0.7R600[2]	0.7	652	591	0.7	0.7	VH
M1.7R600[2]	1.7	972	596	0.7	0.7	VH
M3.0R200[2][3]	3.0	650	208	0.7	0.7	VH
M3.0R600[2]	3.0	1876	601	0.7	0.7	VH
M4.0R200[2][3]	4.0	1017	203	0.7	0.7	VH
$\mathrm{M0.7CRe}^*_\tau$[3]	0.7	602	602	0.7	0.7	VH
$\mathrm{M3.0CRe}^*_\tau$[3]	3.0	606	606	0.7	0.7	VH

Table 4-1: Description of the cases analysed in this thesis. [1] - low-Mach number cases studied by Patel (2017). [2] - high-Mach number cases of Trettel and Larsson (2016). [3] - cases that are simulated in this thesis. UH stands for uniform heating and VH stands for viscous heating.

Casename	ρ/ρ_w	μ/μ_w	λ/λ_w
CP[1]	1	1	1
CRe^*_τ[1]	$(T/T_w)^{-1}$	$(T/T_w)^{-0.5}$	1
GL[1]	$(T/T_w)^{-1}$	$(T/T_w)^{0.7}$	1
LL[1]	1	$(T/T_w)^{-1}$	1
CRe^*_τ2[1]	$(T/T_w)^{-1}$	$(T/T_w)^{-0.5}$	1
$\mathrm{CRe}^*_\tau\mathrm{CPr}^*$[1]	$(T/T_w)^{-1}$	$(T/T_w)^{-0.5}$	$(T/T_w)^{-0.5}$
GL2[1]	$(T/T_w)^{-1}$	$(T/T_w)^{0.7}$	1

Table 4-2: Constitutive relations for density, viscosity and thermal conductivity as a function of temperature.

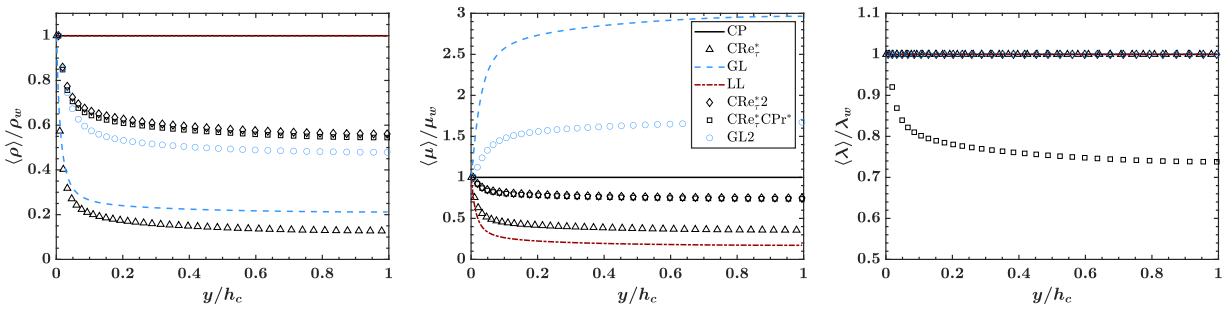

Figure 4-1: Distribution of density (left), viscosity (centre) and thermal conductivity (right) for the low-Mach number cases described in table 4-1.

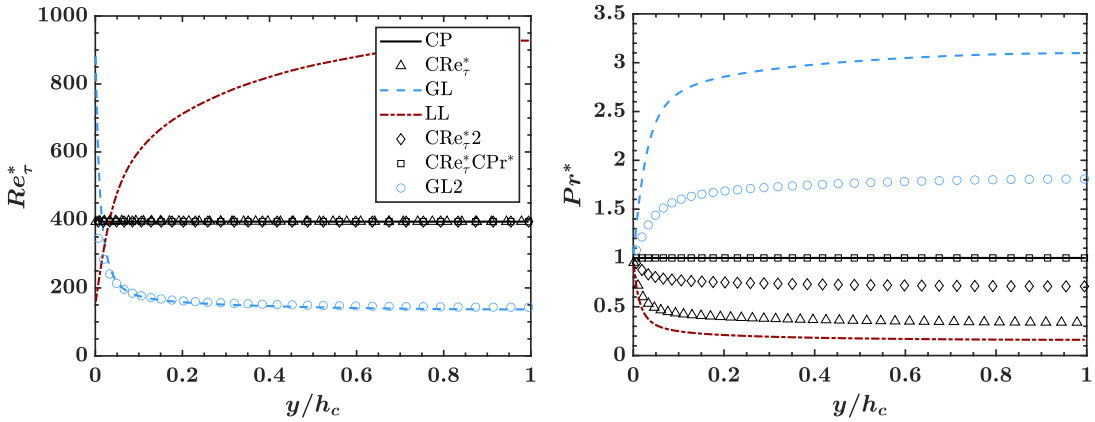

Figure 4-2: Semi-local Reynolds (left) and Prandtl (right) number distribution for the low-Mach number cases described in table 4-1.

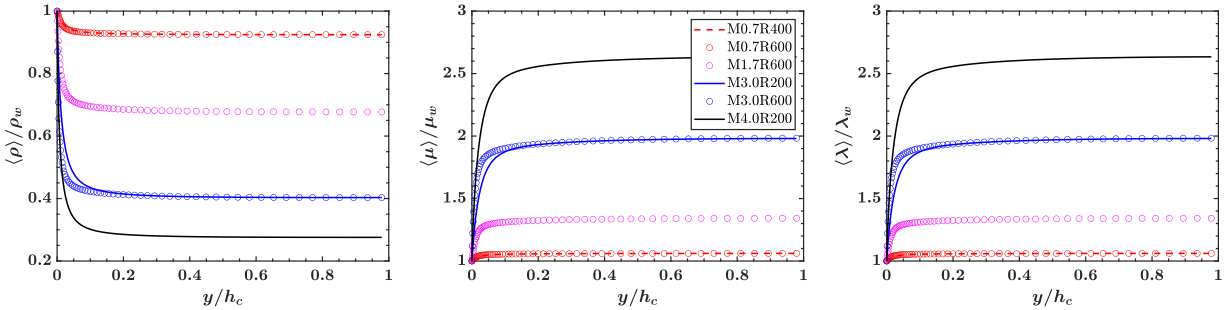

Figure 4-3: Distribution of density (left), viscosity (centre) and thermal conductivity (right) for the high-Mach number cases of Trettel and Larsson (2016) described in table 4-1.

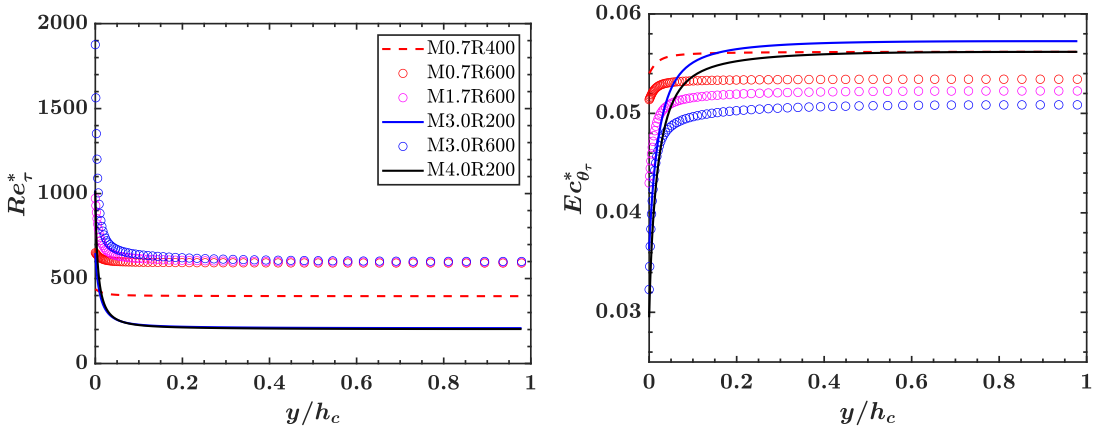

Figure 4-4: Semi-local Reynolds (left) and modified Eckert (right) number distribution for the high-Mach number cases of Trettel and Larsson (2016) described in table 4-1.

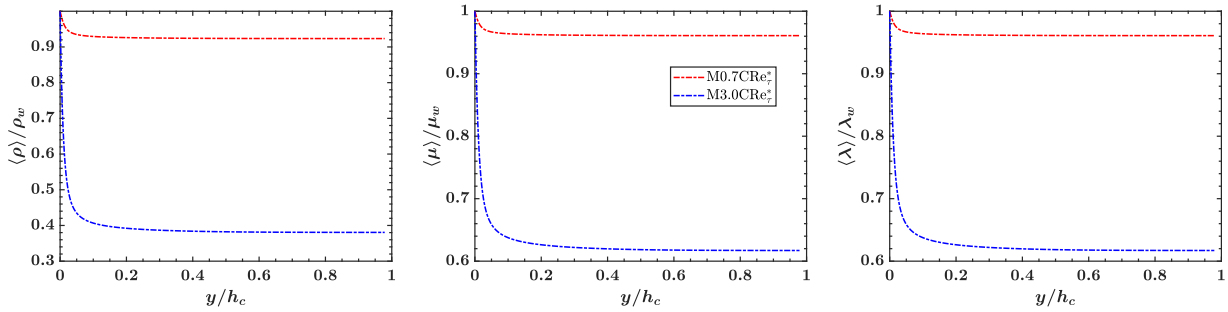

Figure 4-5: Distribution of density (left), viscosity (centre) and thermal conductivity (right) for the high-Mach number constant Re^*_τ cases described in table 4-1.

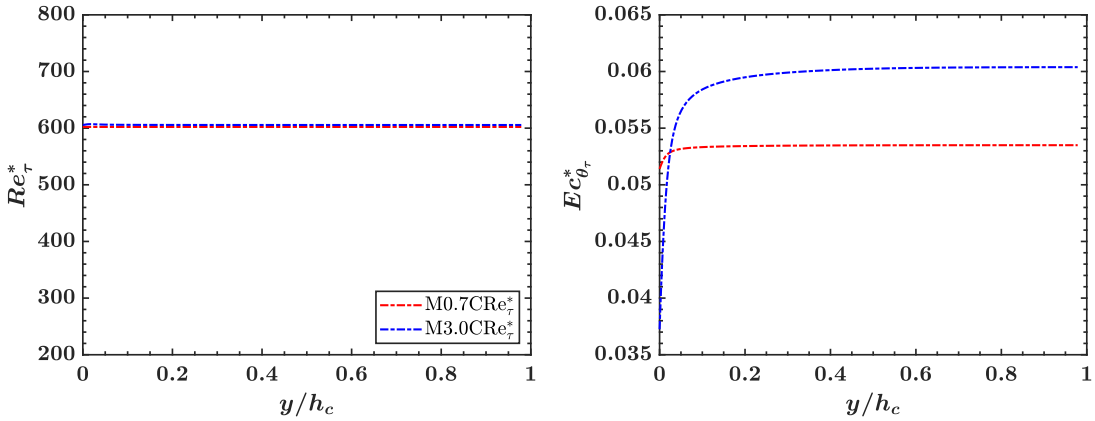

Figure 4-6: Semi-local Reynolds (left) and modified Eckert (right) number distribution for the high-Mach number constant Re^*_τ cases described in table 4-1.

Chapter 5

Low-Mach Number Cases with Uniform Heating

In this chapter we will first simplify the enthalpy variance (k_h) equation (equation (3-38) derived in section 3-2-4) for the low-Mach number cases and check if the additional artifact terms (B_{kh} and D_{kh}) are small or dominant for the low-Mach number cases of Patel et al. (2017) with uniform heating source. We shall also analyse the governing parameters for thermal turbulence in these cases. Using this knowledge, in the end, we check if implementing heat flux models in semi-local form provides improvement in results or not, compared to solving them in their conventionally scaled form.

The k_h equation for a fully developed channel flow derived in section 3-2-4 is,

$$\hat{P}_{kh} - \hat{\epsilon}_{kh} + \hat{T}_{kh} + \hat{D}_{kh} + \hat{B}_{kh} + \hat{Pr}_{kh} + \hat{\Phi}_{kh} = 0. \tag{5-1}$$

In the low-Mach number approximation, the scale of kinetic energy is negligible compared to the scale of enthalpy ($u_\tau^{*^2} << c_p\theta_\tau^*$). In other words, we can say that $Ec_{\theta_\tau}^* \to 0$. Hence,

$$\hat{Pr}_{kh} = Ec_\tau^* \left(t_\tau^* \left\langle \hat{h}'' \frac{\partial \hat{p}}{\partial t} \right\rangle + \left\langle \hat{h}'' \hat{u}_j \frac{\partial \hat{p}}{\partial \hat{x}_j} \right\rangle \right) \approx 0. \tag{5-2}$$

Also, the low-Mach number cases analysed in this chapter are of Patel et al. (2017). These cases have user specified uniform heat source to produce the temperature gradient. Thus, for cases with uniform and user specified constant heat source,

$$\Phi' = 0, \tag{5-3}$$

which gives,

$$\hat{\Phi}_{kh} = \langle \hat{h}'' \hat{\Phi}' \rangle = 0. \tag{5-4}$$

For low-Mach number cases with uniform heating, the k_h transport equation further simplifies to,

$$\hat{P}_{kh} - \hat{\epsilon}_{kh} + \hat{T}_{kh} + \hat{D}_{kh} + \hat{B}_{kh} = 0. \tag{5-5}$$

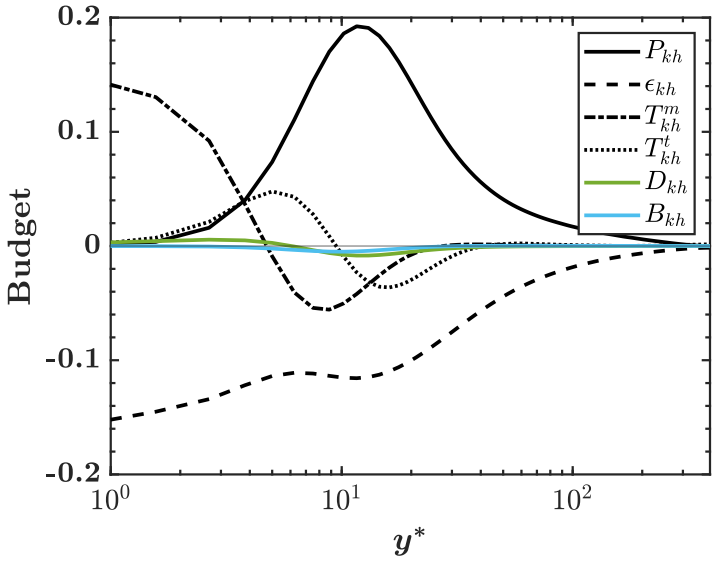

Figure 5-1: Semi-local k_h budget scaled by $\langle\rho\rangle u^*_\tau(c_p\theta^*_\tau)^2/\delta^*_v$ (effectively dividing equation (5-5) by Re^*_τ) for the case CRe$^*_\tau$2.

5-1 The Artifact Terms in k_h Equation

First three terms on the left hand side of equation (5-5) are familiar terms as we have them also in the enthalpy variance equation for a constant property flow. However, due to variable properties, we have two additional terms, $\hat{B}_{kh}$ and $\hat{D}_{kh}$. Note that the additional terms occur mainly due to density variation in the domain. For cases with constant density these terms are zero. In this section, we will present the magnitudes of these additional terms in comparison with other budget terms.

To do this, in-house DNS data of Patel et al. (2017) was post-processed. We will show the results for cases CRe$^*_\tau$2, CRe$^*_\tau$CPr* and GL2 (cases are described in table 4-1). These cases comprise of different distributions of properties, Re^*_τ and Pr^* and hence conclusions drawn from them are general and can be also accepted for other low-Mach number cases.

The enthalpy variance budget for the cases CRe$^*_\tau$2, CRe$^*_\tau$CPr* and GL2 are presented in figures 5-1, 5-2 and 5-3 respectively.

As seen from the budgets presented in figures 5-1 to 5-3, the additional terms are indeed small compared to other budget terms. Thus, the equation (5-5) can be further simplified as,

$$\hat{P}_{kh} - \hat{\epsilon}_{kh} + \hat{T}_{kh} \approx 0. \tag{5-6}$$

We notice that the only dominant terms in the enthalpy variance budget of low-Mach number cases analysed in this thesis are the production, dissipation and diffusion terms. If we can also show that the terms in the budget are governed only by Re^*_τ and Pr^*, then there would exist a very strong analogy between the semi-locally scaled equation and an equation for constant property governed by Re_τ and Pr_w. The same in analysed in the next section.

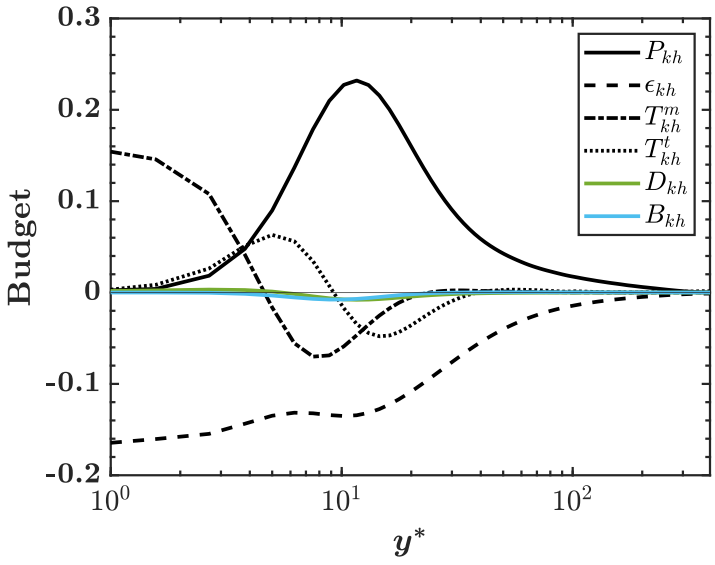

Figure 5-2: Semi-local k_h budget scaled by $\langle\rho\rangle u_\tau^*(c_p\theta_\tau^*)^2/\delta_v^*$ (effectively dividing equation (5-5) by Re_τ^*) for the case CRe$_\tau^*$CPr*.

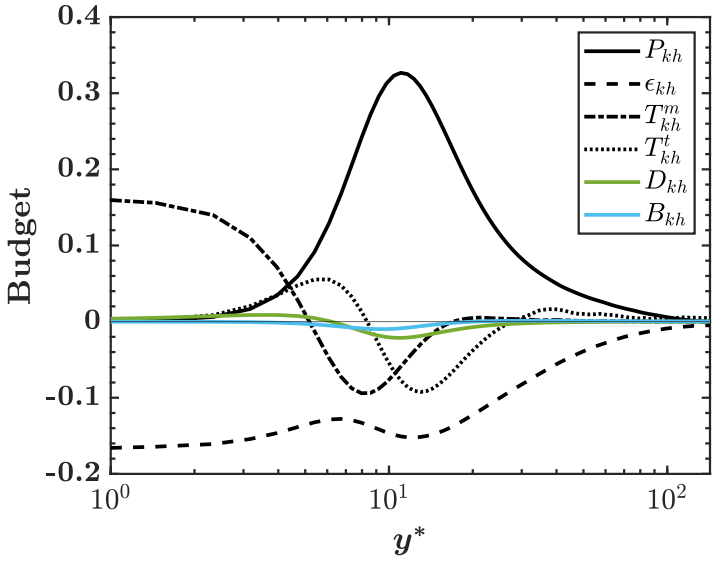

Figure 5-3: Semi-local k_h budget scaled by $\langle\rho\rangle u_\tau^*(c_p\theta_\tau^*)^2/\delta_v^*$ (effectively dividing equation (5-5) by Re_τ^*) for the case GL2.

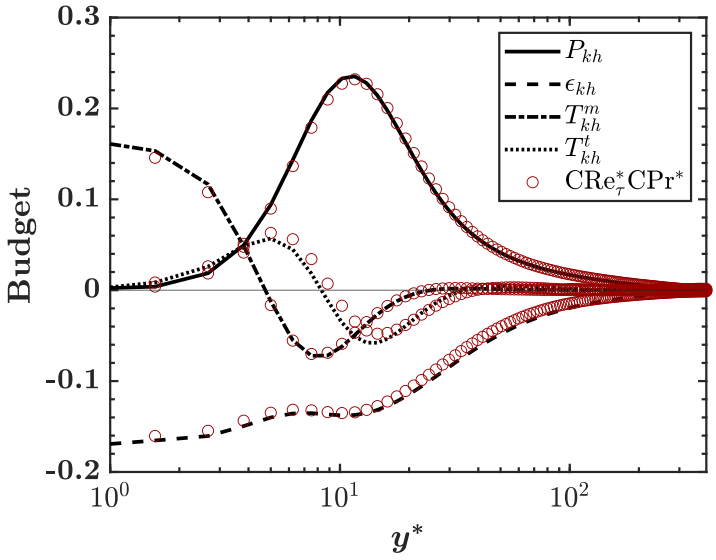

Figure 5-4: Semi-local k_h budget scaled by $\langle\rho\rangle u^*_\tau(c_p\theta^*_\tau)^2/\delta^*_v$ for the cases CP and $\mathrm{CRe}^*_\tau\mathrm{CPr}^*$.

5-2 Governing Parameters

In this section, the k_h budget for a constant property case and a variable property case (with the same Re^*_τ and Pr^* as constant property) are compared. Figure 5-4 shows the k_h budget for CP and $\mathrm{CRe}^*_\tau\mathrm{CPr}^*$ in semi-locally scaled form. The collapse of the budget in figure 5-4 for CP and $\mathrm{CRe}^*_\tau\mathrm{CPr}^*$, is a sufficient proof to conclude that the governing parameters for thermal turbulence in the low-Mach number cases analysed by Patel et al. (2017), up to a leading order, are Re^*_τ and Pr^*. This implies that fully developed channel flows with very different types of fluids with very different property laws can exhibit similar thermal turbulence (in semi-local form) as far as their semi-local Reynolds number and semi-local Prandtl number are quasi-similar. It is stressed that for similar turbulence we need individually similar profiles of Re^*_τ and Pr^* and not just similar semi-local Peclet number ($Re^*_\tau Pr^*$) profile because some terms in a thermal turbulence quantity's budget are mainly governed by Re^*_τ and some have influence of Pr^* as well. Figure 5-5 shows the budget for CP and $\mathrm{CRe}^*_\tau\mathrm{CPr}^*$, but in classically scaled form. The non-collapse, despite the same Reynolds number at the wall (Re_τ), signifies the importance of semi-local scaling for thermal turbulence.

Figure 5-6 shows the k_h budget of CP and $\mathrm{CRe}^*_\tau 2$ in semi-local form. Keeping similar Pr^* is important especially near the wall, as it is clear from the near-wall non-collapse of the budgets of CP and $\mathrm{CRe}^*_\tau 2$ with different Pr^* profiles and the same Re^*_τ profiles. Away from the wall in the log-law region and beyond ($y^* > 30$), Prandtl number becomes less important in thermal turbulence as can be seen from the collapsing budget in that region despite different Pr^*. This is because, away from the wall, for moderately high Reynolds number flows, the convective effect becomes more dominant than molecular (or diffusive) effects and convective effects are mainly governed by Re^*_τ. Note that, for very low Prandtl number fluids the molecular effects are dominant for thermal turbulence even beyond $y^* = 30$ and in that case, we would not expect a collapse in the log-law region if Pr^* is different. Kawamura et al. (1999) (in section 3.4) also mentions about the effect of Prandtl number being small for high Reynolds number flows due to dominant convective effect.

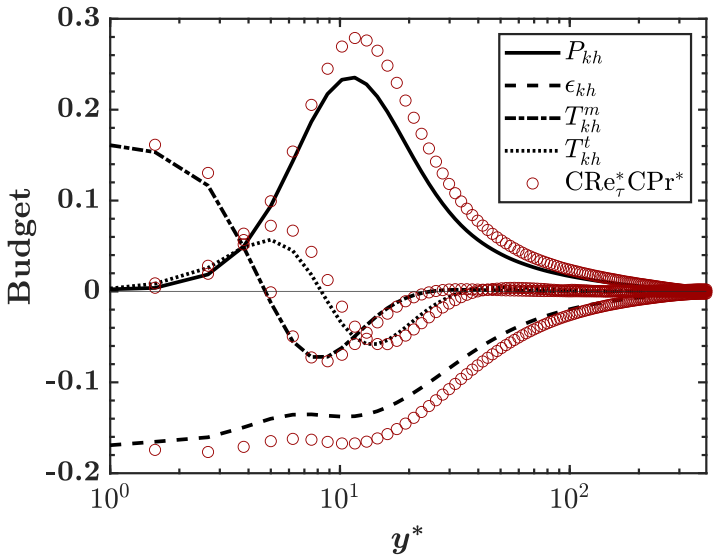

Figure 5-5: Classical k_h budget scaled by $\rho_w u_\tau (c_p \theta_\tau)^2/\delta_v$ (classically scaled) for the cases CP and $\mathrm{CRe}^*_\tau\mathrm{CPr}^*$.

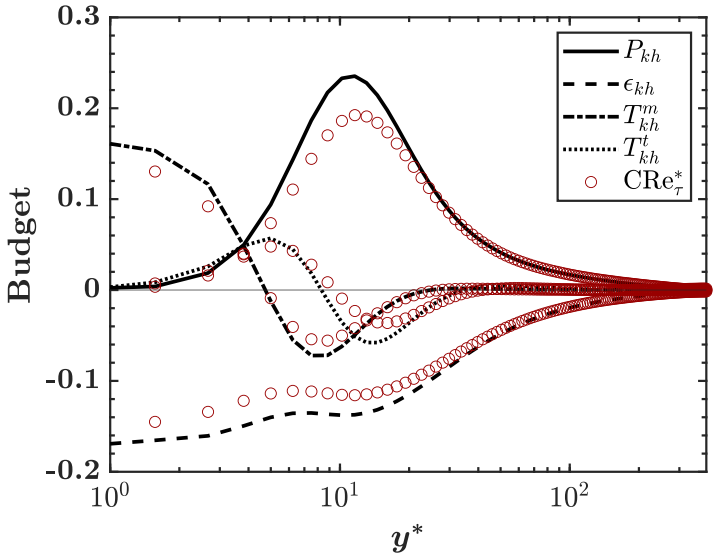

Figure 5-6: Semi-local k_h budget scaled by $\langle\rho\rangle u^*_\tau (c_p \theta^*_\tau)^2/\delta^*_v$ for the cases CP and CRe^*_τ.

The fact that thermal turbulence is governed by Re_τ^* and Pr^* profiles and also using the piecewise similarity arguments made in section 3-1, we can expect that the thermal turbulence (in semi-locally scaled form) at any point in the flow field is equivalent to a constant property thermal turbulence at Re_τ and Pr of the same value as Re_τ^* and Pr^* defined at the point. This motivates us to use the same heat flux model as was developed for a constant property flow and solve it in semi-local scales for various variable property cases. This is presented in the next section.

5-3 Solving Heat Flux Model in Semi-Local Form

5-3-1 Model Equations and Implementation

The RANS model used in this study is the one developed by Nagano and Shimada (1996) (2-equation turbulent stress and 2- equation heat flux models) for solving both, turbulent shear stress and heat flux. The model developed by Nagano and Shimada has been rigorously built to take care of the near wall effects. Near the wall, turbulent Reynolds number drops drastically and also the scale separation between energy containing eddies and dissipating eddies is reduced. This calls for modification of the High-Re form of the model equations. Some terms that are small in the high turbulent Reynolds number region also become dominant near the wall and needs modeling to capture the near wall behaviour accurately. These factors are taken care in this model. Also, multiple time and length scales (energy containing and dissipative) are used to model the eddy viscosity and eddy diffusivity. Another feature of the heat flux model presented is that the model is built considering the effect Prandtl number has on the near wall behaviour. The model is validated for a wide range of Reynolds and Prandtl numbers. For more details refer the original paper (Nagano and Shimada, 1996).

The simplified k_h equation (5-6) is rewritten here as,

$$\hat{P}_{kh} - \hat{\epsilon}_{kh} + \hat{T}_{kh} \approx 0. \tag{5-7}$$

Writing the detailed form of each term using table 3-4 we get,

$$-\{\hat{h''}\hat{v''}\}\frac{\partial\{h^{vd}\}}{\partial\hat{y}} - \left\langle \hat{q}'_j \frac{\partial \hat{h}''}{\partial \hat{x}_j} \right\rangle + \frac{\partial}{\partial\hat{y}}\left(\left\langle \hat{h}''\hat{q}'_y \right\rangle - \{\hat{v''}\hat{k}_h\}\right) = 0. \tag{5-8}$$

The term representing molecular diffusion $\left\langle \hat{h}''\hat{q}'_y \right\rangle$ can be simplified as,

$$\left\langle \hat{h}''\hat{q}'_y \right\rangle = \left\langle \hat{h}'' \left(\hat{\alpha}/(Re_\tau^* Pr^*)\partial\hat{h}/\partial\hat{y}\right)' \right\rangle. \tag{5-9}$$

Assuming effects of fluctuations of α are negligible and thus,

$$\hat{\alpha} = 1 + \frac{\alpha'}{\langle\alpha\rangle} \approx 1. \tag{5-10}$$

Also, we can split $\partial\hat{h}/\partial\hat{y}$ into Favre mean and fluctuations as,

$$\frac{\partial\hat{h}}{\partial\hat{y}} = \frac{\partial\{\hat{h}\}}{\partial\hat{y}} + \frac{\partial\hat{h}''}{\partial\hat{y}}, \tag{5-11}$$

then we finally simplify equation (5-9) to,

$$\left\langle \hat{h}''\hat{q}'_y \right\rangle \approx \left\langle \hat{h}'' \frac{1}{Re^*_\tau Pr^*} \left(\frac{\partial\{\hat{h}\}}{\partial\hat{y}} + \frac{\partial\hat{h}''}{\partial\hat{y}} \right)' \right\rangle = \left\langle \frac{\hat{h}''}{Re^*_\tau Pr^*} \frac{\partial\hat{h}''}{\partial\hat{y}} \right\rangle = \underbrace{\frac{1}{Re^*_\tau Pr^*} \frac{\partial\langle\hat{k_h}\rangle}{\partial\hat{y}}}_{\text{A}}. \tag{5-12}$$

The term "A" in equation (5-12) is a very recognizable form of the molecular diffusion of k_h. Inline with common modeling methods, the turbulent diffusion term is modeled using gradient diffusion hypothesis and the production term is modeled using eddy diffusivity. The modelled form of k_h equation becomes,

$$\hat{\alpha}_t \left(\frac{\partial\{h^{vD}\}}{\partial\hat{y}} \right)^2 + \frac{\partial}{\partial\hat{y}} \left[\left(\frac{1}{Re^*_\tau Pr^*} + \frac{\hat{\alpha}_t}{\sigma_{kh}} \right) \frac{\partial\{\hat{k}_h\}}{\partial\hat{y}} \right] - \hat{\epsilon}_{kh} = 0, \tag{5-13}$$

where σ_{kh} is a model function/constant. If we compare the equation (5-13) with its dimensional counterpart, we arrive at a simple recipe that can be used to arrive at semi-local form of model equation of any quantity starting from its dimensional model equation. The recipe is summarized as,

- Replace all the variables with their semi-local notations, except for $\langle\alpha\rangle$ and $\langle\rho\rangle$ and $\partial\{h\}$ (or $\partial\{T\}$).
- $\langle\alpha\rangle$ is replaced by $1/(Re^*_\tau Pr^*)$.
- $\langle\rho\rangle$ is replaced by 1.
- Gradient of the mean enthalpy (or temperature) $\partial\{h\}$ is replaced by $\partial\{h^{vD}\}$.

A similar recipe is also proposed in Pecnik and Patel (2017) pertaining to turbulent stress modeling. Some additional points to note are,

- If a model equation uses Re_τ, Pr, y^+, etc. then they should be replaced with their semi-local counterpart like Re^*_τ, Pr^*, y^*, etc.
- Apart from above mentioned points the recipe mentioned in Pecnik and Patel (2017) should also be considered.

Now that we have a robust recipe in place, we can very easily convert the model equations of Nagano and Shimada (1996) into semi-locally scaled form. For more details on the model equations and model constants, refer the Appendix of Nagano and Shimada (1996).

In-house MATLAB code of Pecnik et al. (2018) is modified to implement the model. We solve the semi-locally scaled form of the equations but the variables are represented in their conventionally (wall-based) scaled form. The advantages of doing so is mentioned in Otero Rodriguez et al. (2018) in section 2. To reconvert the variables we need information on scale relations presented in section 3-2 and also in table 3-2.

We will show the steps for the production term of equation (5-13) as follows (averaging symbols are omitted for the sake of brevity):

$$\hat{\alpha}_t \left(\frac{\partial h^{vd}}{\partial\hat{y}} \right)^2 = \tilde{\alpha}_t \frac{\rho_w u_\tau h_c}{\rho u^*_\tau h_c} \left(\sqrt{\frac{\rho}{\rho_w}} \frac{\partial\tilde{h}}{\partial\tilde{y}} \right)^2 = \sqrt{\frac{\rho}{\rho_w}} \tilde{\alpha}_t \left(\frac{\partial\tilde{h}}{\partial\tilde{y}} \right)^2. \tag{5-14}$$

Repeating this for other terms gives,

$$\sqrt{\frac{\rho}{\rho_w}}\tilde{\alpha}_t\left(\frac{\partial\tilde{h}}{\partial\tilde{y}}\right)^2+\frac{\partial}{\partial\tilde{y}}\left[\frac{1}{\sqrt{\rho/\rho_w}}\left(\frac{\alpha/\alpha_w}{Re_\tau Pr}+\frac{\tilde{\alpha}_t}{\sigma_{kh}}\right)\frac{\partial\rho/\rho_w\tilde{k}_h}{\partial\tilde{y}}\right]-\left(\frac{\rho}{\rho_w}\right)^{1.5}\tilde{\epsilon}_{kh}=0. \tag{5-15}$$

Dividing the equation by $\sqrt{\rho/\rho_w}$ and using notations as explained in section 3-2, we can write,

$$\tilde{\alpha}_t\left(\frac{\partial\tilde{h}}{\partial\tilde{y}}\right)^2+\frac{1}{\sqrt{\tilde{\rho}}}\frac{\partial}{\partial\tilde{y}}\left[\frac{1}{\sqrt{\tilde{\rho}}}\left(\frac{\alpha/\alpha_w}{Re_\tau Pr}+\frac{\tilde{\alpha}_t}{\sigma_{kh}}\right)\frac{\partial\tilde{\rho}\tilde{k}_h}{\partial\tilde{y}}\right]-\tilde{\rho}\tilde{\epsilon}_{kh}=0. \tag{5-16}$$

The strong similarity between equation (5-16) above and the equation of TKE presented in Otero Rodriguez et al. (2018) is evident. This confirms that the effects of variable inertia on the evolution of enthalpy variance (k_h) is similar to that on the evolution of TKE (k). If we compare equation (5-16) to an equation which we would have obtained just by classical scaling, we note the difference in the diffusion term which is exactly what was observed for TKE in Otero Rodriguez et al. (2018).

Now that we know how to derive a semi-locally scaled model equation and also how to rewrite it in terms of conventional variables, the rest is coding the equations and plotting the results. Nagano and Shimada (1996) solves for k and ϵ in their turbulent stress model and for k_h (they actually do it for thermal variance but in semi-local scales both thermal and enthalpy variances are equivalent as c_p in semi-local scales is 1 for the calorifically perfect cases analysed in this thesis) and ϵ_{kh} in their heat flux model. The implementation is validated in Appendix C.

From the results of Otero Rodriguez et al. (2018), we know that turbulent stress models performs exceptionally well when solved in semi-local scales and thus, we will follow that. However, since our goal is to see the effect of semi-local scaling on heat flux models, we shall solve the heat flux model in both conventionally scaled form and in semi-locally scaled form and the results will be compared.

5-3-2 Results for Low-Mach Number cases

Results are presented in figures 5-9 to 5-12 for cases CP, CRe$^*_\tau$, GL and LL (table 4-1). These cases were also analysed in Otero Rodriguez et al. (2018). The results plotted are for the transformed velocity $\{u^*\}$ defined in Patel et al. (2016) as,

$$\{u^*\}=\int_0^{\{u^{vD}\}}\left(1+\frac{y}{Re^*_\tau}\frac{dRe^*_\tau}{dy}\right)d\{u^{vD}\}, \tag{5-17}$$

normalised mean temperature defined in Otero Rodriguez et al. (2018) as,

$$\frac{\{T\}-T_w}{\{T^{max}_{DNS}\}-T_w},$$

TKE (k), its dissipation (ϵ), enthalpy variance (k_h) and its dissipation (ϵ_{kh}). T^{max}_{DNS} is the centreline temperature computed from DNS. All the turbulent quantities are presented in conventionally scaled form, for instance, k in the image is k/u^2_τ. Another important thing to

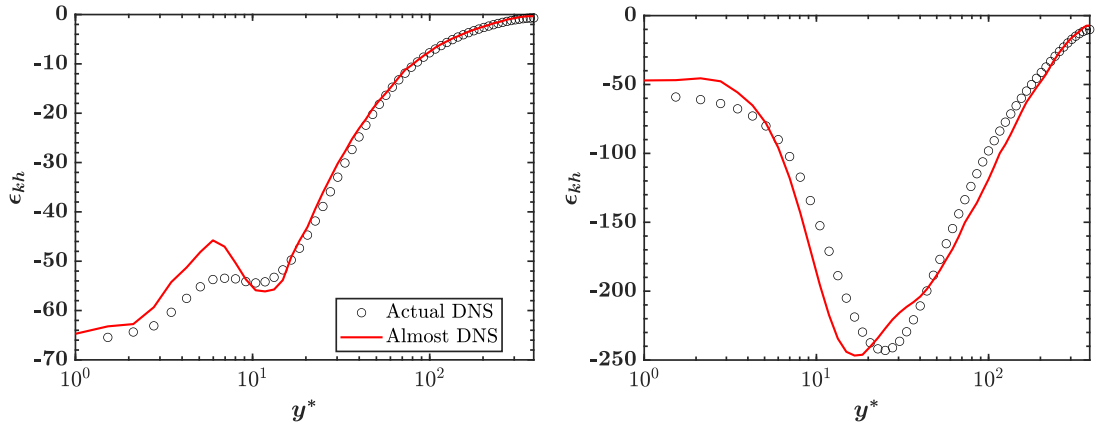

Figure 5-7: Comparison of ϵ_{kh} computed using the model k_h equation (with other terms taken from DNS) with the actual DNS values. Results are shown for the case CP (left) and CRe$^*_\tau$ (right).

note is that the dissipation of enthalpy variance (ϵ_{kh}) presented in the figures 5-11 and 5-12 (for cases GL and LL) are not strictly DNS values. Due to unavailability of DNS data files, it was not possible to post-process and compute it. Thus, it is computed from a typical "model k_h" equation but with other terms in the equation taken from DNS. Figure 5-7 compares the dissipation (ϵ_{kh}) computed from DNS and that computed from the model equation (with all other terms taken from DNS) for cases CP and CRe$^*_\tau$. As seen, the accuracy is not very high but reasonable enough for modeling conclusions.

The solution of RANS using the semi-locally scaled Nagano and Shimada model follows DNS data accurately for all the cases except the GL case. At first sight one would attribute this to the low Reynolds number of gas-like case away from the wall (≈ 150) and call it a low-Re effect. However, apart from the low Reynolds number effect, the error is also attributable to the high Prandtl number of the gas-like case away from the wall as seen in figure 4-2. As explained in section 3-1, the major reason behind the success of modeling in semi-local scales is the similarity between variable property cases and constant property cases beyond $y^* \approx 10$. However, near the wall, for cases with Re^*_τ gradients, there is structure modulation as can also be seen in figure 3-5, and this similarity fails. For higher Prandtl number cases, the strong thermal turbulence region shifts to lower y^* (in other words, the region where values of α_t actually begin to matter). This is evident from figure 5-8 which shows the production of thermal variance normalized by the maximum value (another measure of this would be to see the peaks of turbulent heat flux). Clearly the peak of production for the GL case shifts to $y^* \approx 8.5$ compared to the peaks occurring for other cases beyond $y^* \approx 11.8$. Because of this shift towards the wall for GL case and considering the fact that using a constant property like model in this region will not produce accurate results due to structure modulation, one can explain the error in GL case. The only other case with Re^*_τ gradient and hence at the risk of error due to structure modulation is LL. However, as seen in figure 5-8, the production peak for LL (due to low Prandtl number) is far in the safe region and hence the effect of structure modulation on thermal turbulence is negligible.

For all the variable property cases, the solution obtained using semi-locally scaled model is much better than the solution obtained by solving classically scaled equations. Not just mean

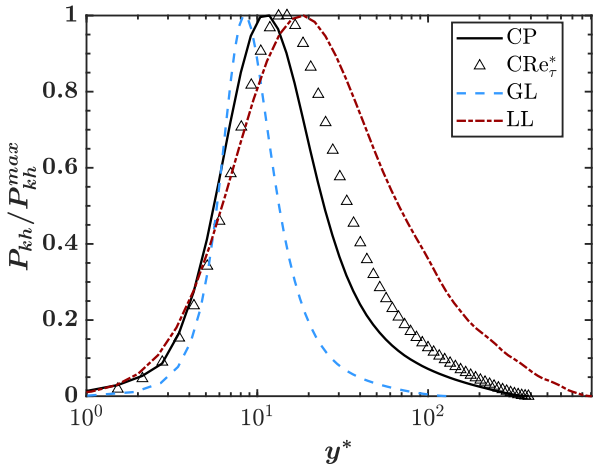

Figure 5-8: Production of thermal variance P_{kh} normalized by its maximum value.

temperature but also turbulent quantities are correctly predicted. It is worth noting that the major advantage of solving in semi-local scales over conventional scales is obtained for cases with varying density in the domain. This is the reason why for LL (constant ρ), the results are nearly similar with both the implementations but for CRe$^*_\tau$ (varying ρ) the improvement is noteworthy. This supports the conclusion that semi-local scaling indeed takes care of the variable inertia effects.

For low-Mach number cases, we now know that solving heat flux model equations in semi-local scales for thermal turbulence captures physics (variable inertia effects) more accurately than just solving them in conventional scales. At this point, it is interesting to see the results of semi-locally scaled heat flux models for high-Mach number cases. But before that a detailed understanding about the physics behind viscous heating is required as it is what separates the thermal turbulence in low and high-Mach number cases. This analysis is presented in the next chapter.

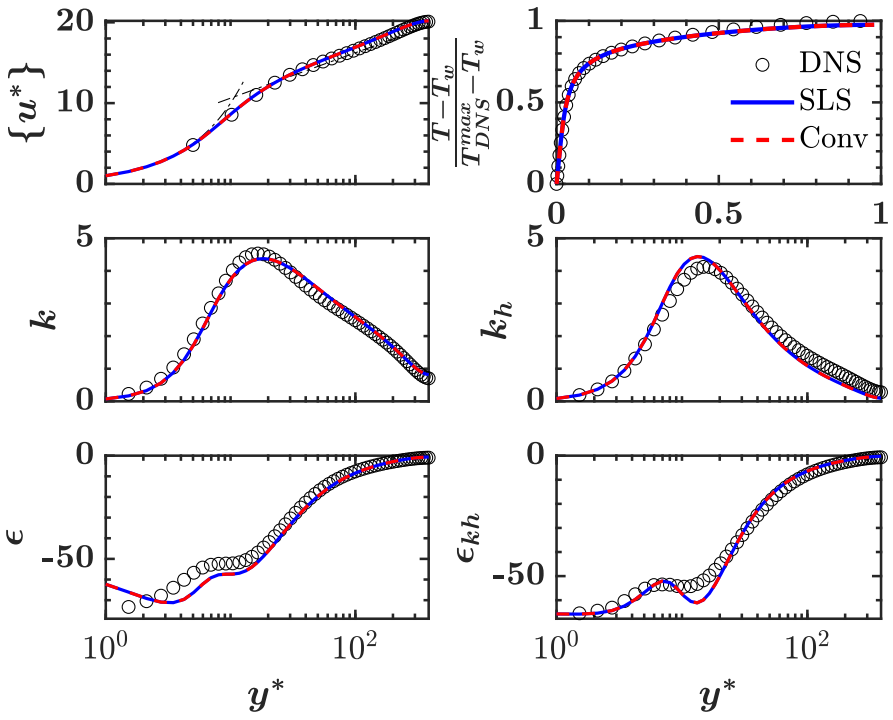

Figure 5-9: RANS results for the case CP. "SLS" stands for solving the model in semi-local scales and "Conv" stands for solving it in conventional form. All turbulent quantities in the figure are classically scaled. X-axis for the top right image is y/h_c and not y^*.

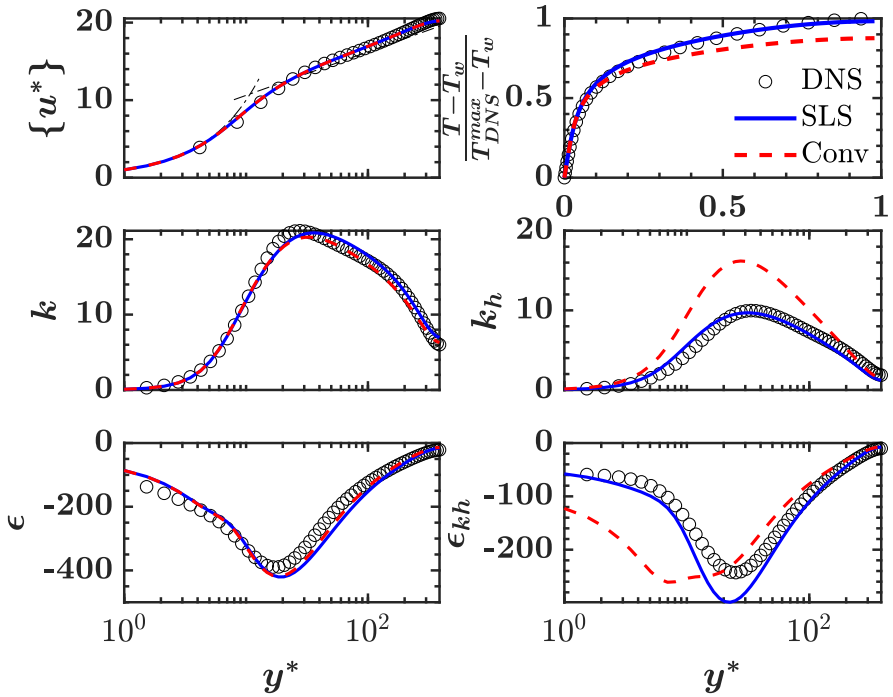

Figure 5-10: RANS results for the case CRe$^*_\tau$. "SLS" stands for solving the model in semi-local scales and "Conv" stands for solving it in conventional form. All turbulent quantities in the figure are classically scaled. X-axis for the top right image is y/h_c and not y^*.

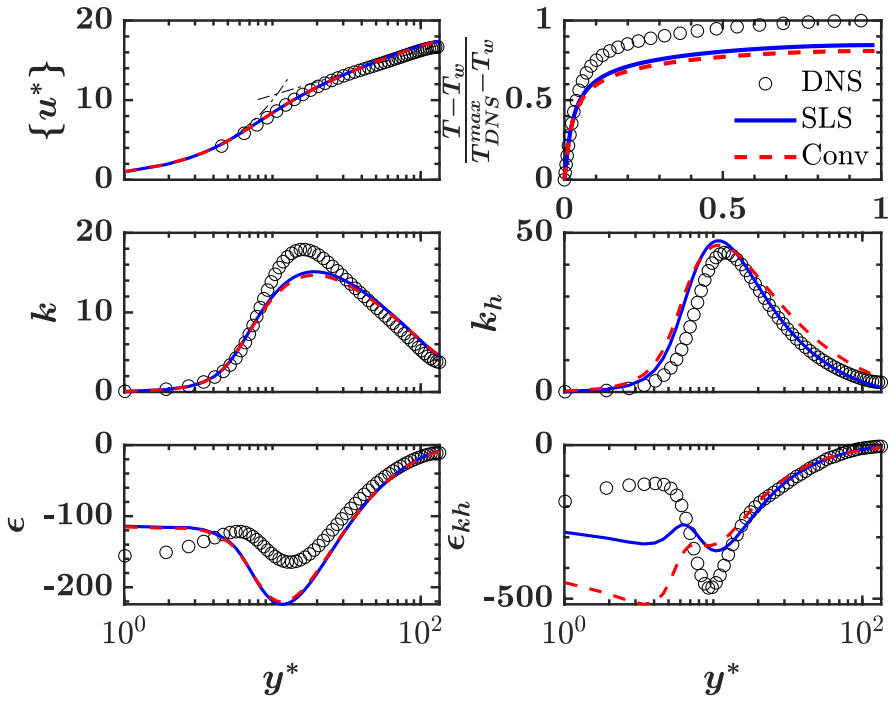

Figure 5-11: RANS results for the case GL. "SLS" stands for solving the model in semi-local scales and "Conv" stands for solving it in conventional form. All turbulent quantities in the figure are classically scaled. X-axis for the top right image is y/h_c and not y^*.

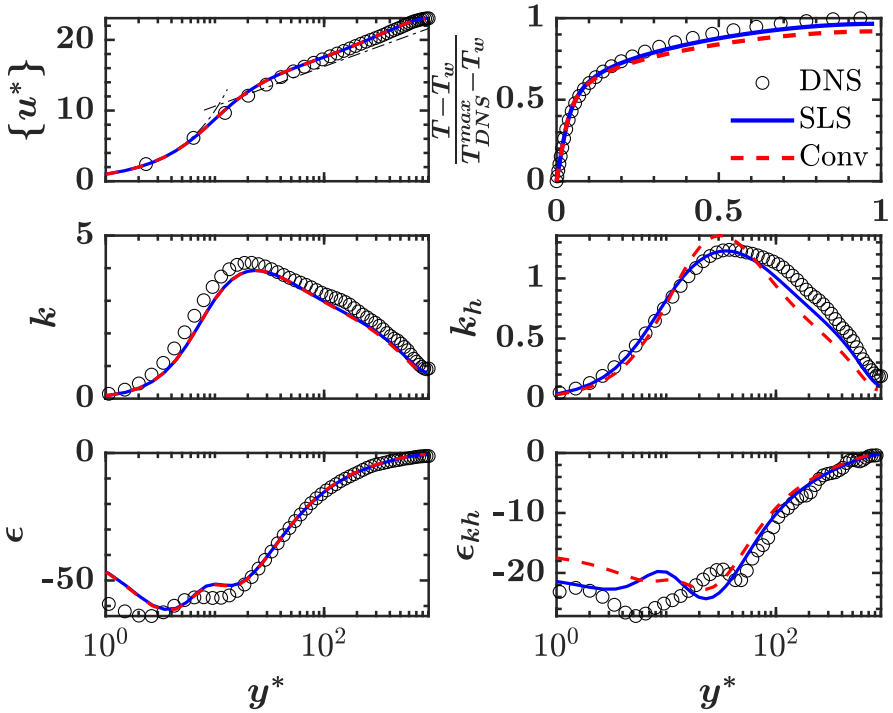

Figure 5-12: RANS results for the case LL. "SLS" stands for solving the model in semi-local scales and "Conv" stands for solving it in conventional form. All turbulent quantities in the figure are classically scaled. X-axis for the top right image is y/h_c and not y^*.

Chapter 6

High-Mach Number Cases with Viscous Heating

In this chapter we will analyse thermal turbulence in high-Mach number cases with viscous heating. We will first compare these cases with the low-Mach number cases (with uniform heat source) as discussed in the previous chapter. We will show that the conclusions made in Patel et al. (2017) pertaining to scalar transport in variable property flows will not necessarily hold for high-Mach number cases with viscous heating. An analysis showing the effect of viscous heating source on the mean enthalpy equation, enthalpy variance equation and turbulence heat flux equation is presented. Later in the chapter, the governing parameters for thermal turbulence in high-Mach number cases with viscous heating are discussed. The chapter is concluded with heat flux modeling in semi-local scales for these cases.

For the high-Mach number cases, the volumetric heating source Φ (in the energy equation (2-10)), unlike low-Mach number cases, is not constant anymore and is coupled to velocity turbulence as,

$$\Phi = \tau_{ij} \frac{\partial u_i}{\partial x_j}. \tag{6-1}$$

Equation (6-1) is called aerodynamic heating or viscous heating. In the low-Mach number approximation the viscous heating is assumed to be negligible and thus to produce significant temperature gradients, fictitious user specified heat sources are added.

In semi-local scales Φ is,

$$\hat{\Phi} = Ec_{\theta^*_\tau} \hat{\tau}^{vD}_{ij} \frac{\partial u^{vD}_i}{\partial \hat{x}_j}. \tag{6-2}$$

6-1 Comparison with Uniform Heating Cases

In previous section we analysed low-Mach number cases of Patel et al. (2017) in which the temperature gradient (and variable property effect) was produced using user-specified uniform

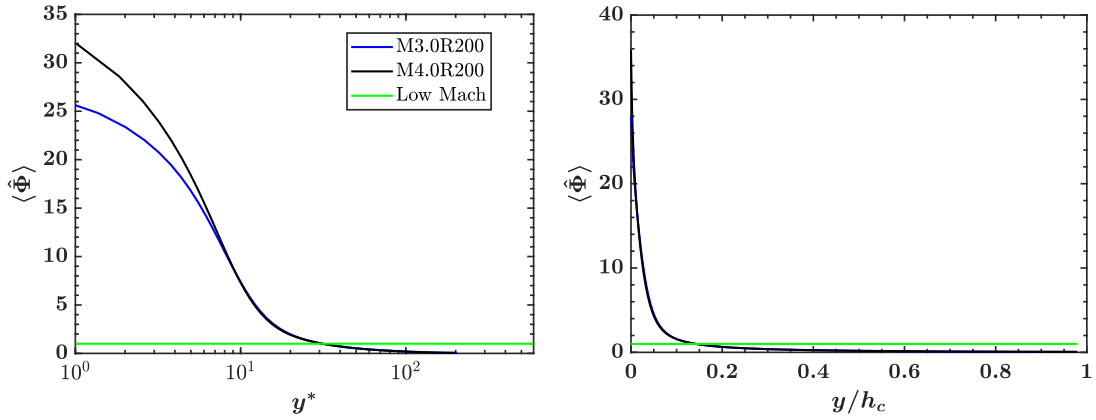

Figure 6-1: The distribution of viscous heating source (high-Mach number) and uniform heat source (low-Mach number) in semi-local scales.

volumetric heating sources. The major difference between those cases and the high-Mach number cases with viscous heating, is that now the volumetric sources are not uniform but are governed by dissipation of kinetic energy. This leads to a very non-uniform distribution of the heat source, with maximum concentration near the wall because that is where we have the highest gradients in velocity. Because of this disparity in the distribution of the heat source, maximum temperature change occurs near the wall and, unlike low-Mach number cases, the change in temperature away from the wall is negligible due to the negligible heat source. This fundamental difference leads to major differences between the cases with uniform heating and with viscous heating (will henceforth be referred to as UH and VH respectively in this section).

Table 6-1 presents the mean enthalpy equation in semi-local scales for UH and VH.

UH	VH
$\frac{\partial}{\partial\hat{y}}\left[\left(\frac{1}{Re_\tau^* Pr^*}+\hat{\alpha}_t\right)\frac{\partial\{h^{vD}\}}{\partial\hat{y}}\right]=-1.$	$\frac{\partial}{\partial\hat{y}}\left[\left(\frac{1}{Re_\tau^* Pr^*}+\hat{\alpha}_t\right)\frac{\partial\{h^{vD}\}}{\partial\hat{y}}\right]=-\langle\hat{\Phi}\rangle.$

Table 6-1: The mean enthalpy equation for UH (low-Mach number) and VH (high-Mach number) cases

Figure 6-1 shows $\langle\hat{\Phi}\rangle$ for the cases M3.0R200 and M4.0R200 as described in table 4-1 and for a low-Mach number case. We can clearly see the non-uniformity in distribution of $\langle\hat{\Phi}\rangle$ and also the fact that near the wall it is very high. An interesting thing to note from table 6-1 is that the uniform user specified volumetric heating source, in semi-local scales, for UH cases is equal to 1.

When the RHS of equations presented in table 6-1 are integrated, we get local heat flux (q_y/q_w) as,

$$q_y/q_w = 1 - \frac{y}{h_c}, \tag{6-3}$$

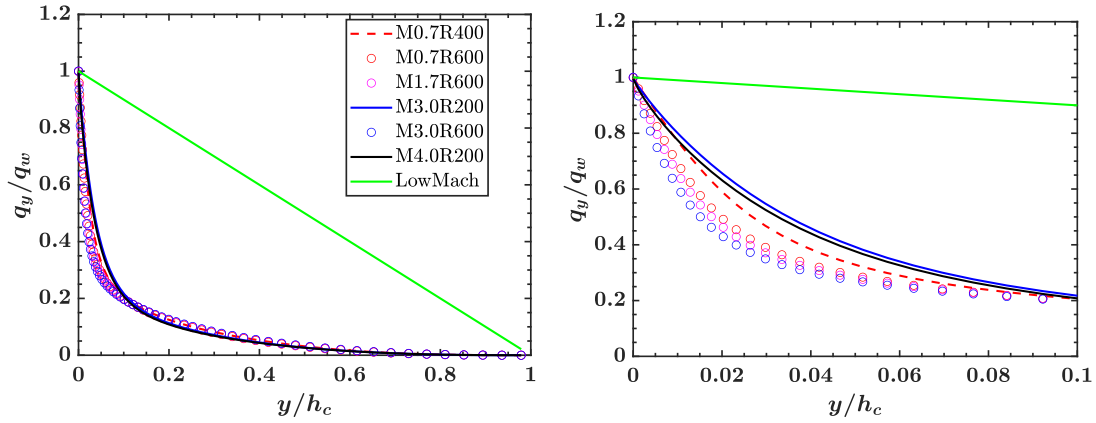

Figure 6-2: Local heat flux (q_y) normalized by heat flux at the wall (q_w). In the image on the right, the distribution only in the inner layer is shown.

and,

$$q_y/q_w = \int_1^{\hat{y}} -\langle\hat{\Phi}\rangle d\hat{y}, \tag{6-4}$$

respectively for UH and VH. This implies that the local heat flux q_y/q_w varies linearly in UH cases but for the VH cases, the profile of q_y/q_w is not necessarily linear. To check this, we plot q_y/q_w for a low-Mach number case and for Trettel and Larsson cases (table 4-1) in figure 6-2. As seen, due to the highly non-uniform distribution of viscous heating, q_y/q_w changes non-linearly in the near wall region for high-Mach number cases. In the inner layer, the approximation $q_y \approx q_w$ is true for low-Mach number cases but not for the high-Mach number cases as seen in figure 6-2 (right).

This leads us to the major conclusion of this section. Due to this fundamental difference between UH and VH cases, the conclusions obtained in Patel et al. (2017), considering UH cases, will not necessarily hold for VH cases and are very specific. For instance, the derivation of the extended van Driest temperature transformation,

$$\{\theta^*\} = \int_0^{\{\theta^{vD}\}} \left(1 + \frac{y}{Re_\tau^*}\frac{dRe_\tau^*}{dy}\right) d\{\theta^{vD}\}, \tag{6-5}$$

is based on the assumption that in the inner layer $q_y \approx q_w$, which is not true for VH cases and thus, we would expect it to fail. The transformed mean temperature ($\{\theta^*\}$) is plotted in figure 6-3 for the cases of Trettel and Larsson (2016) specified in table 4-1. For low-Mach number cases with the same Prandtl number (Pr), the transformed mean temperature profile should collapse. However, for high-Mach number, even though the Prandtl number (Pr) for all the cases is the same, the profiles do not collapse. Also in figure 6-3 (right), we can see that there is no log-law region for the high-Mach number cases (incompressible case CP is added for reference). This is an effect due to viscous heating as was also observed in Morinishi et al. (2004) for temperature profiles scaled by wall friction temperature θ_τ.

The effects of viscous heating on thermal turbulence is discussed in the next section.

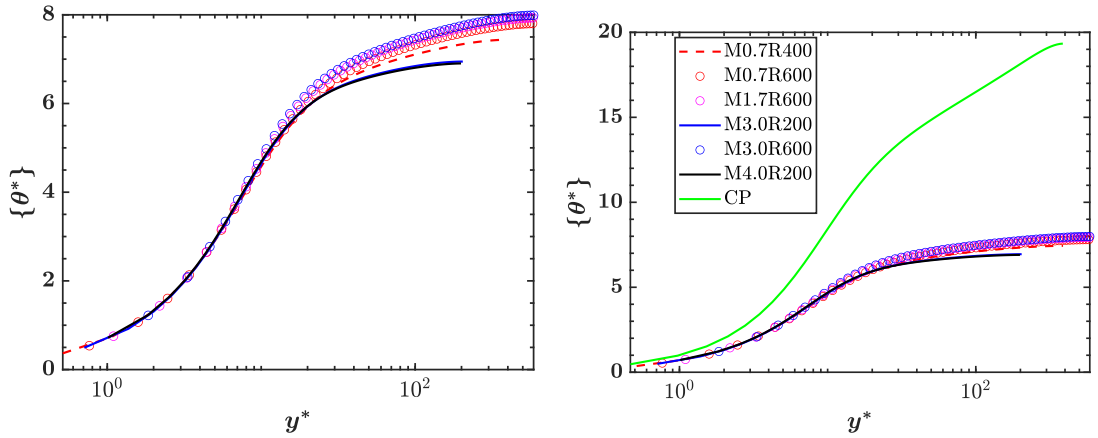

Figure 6-3: The transformed mean temperature $\{\theta^*\}$ for the high-Mach number cases of Trettel and Larsson (2016). In the image on the right, the curves are compared with $\{\theta^*\}$ for a low-Mach number case (CP).

6-2 Effects of Viscous Heating on Thermal Turbulence

There are two ways in which viscous heating can affect thermal turbulence:

- By changing the volumetric heat source in the mean enthalpy equation and hence affecting the mean enthalpy (or temperature) distribution.
- By correlating with turbulent fluctuations and resulting in additional source/sink in the transport equations of thermal quantities, such as enthalpy variance and turbulent heat flux.

6-2-1 Effects on the Mean Enthalpy Equation

This has already been discussed in the previous section (section 6-1) in which the VH cases were compared with the UH cases.

6-2-2 Effects on the Enthalpy Variance (k_h) Budget

The enthalpy variance equation (3-38) for fully developed channel flows is rewritten here as,

$$\hat{P}_{kh} - \hat{\epsilon}_{kh} + \hat{T}_{kh} + \hat{D}_{kh} + \hat{B}_{kh} + \hat{Pr}_{kh} + \hat{\Phi}_{kh} = 0. \tag{6-6}$$

For the low-Mach number cases, $\hat{\Phi}_{kh}$ was neglected due to the uniform and constant nature of Φ. However, in high-Mach number cases, this term cannot be neglected. In this section we will analyse the importance of $\hat{\Phi}_{kh}$ in the evolution of k_h and also discuss the physical mechanism behind $\hat{\Phi}_{kh}$.

Let us first study the form of Φ. Rewriting equation (6-1),

$$\Phi = \tau_{ij}\frac{\partial u_i}{\partial x_j}. \tag{6-7}$$

The RHS can be expanded as,

$$\Phi = \langle \tau_{ij} \rangle \frac{\partial \{u_i\}}{\partial x_j} + \langle \tau_{ij} \rangle \frac{\partial u_i''}{\partial x_j} + \tau_{ij}' \frac{\partial \{u_i\}}{\partial x_j} + \tau_{ij}' \frac{\partial u_i''}{\partial x_j}. \tag{6-8}$$

For a fully developed channel we have,

$$\Phi = \langle \tau_{xy} \rangle \frac{\partial \{u\}}{\partial y} + \langle \tau_{ij} \rangle \frac{\partial u_i''}{\partial x_j} + \tau_{xy}' \frac{\partial \{u\}}{\partial y} + \tau_{ij}' \frac{\partial u_i''}{\partial x_j}. \tag{6-9}$$

We can write the fluctuations in Φ as,

$$\Phi' = \underbrace{\langle \tau_{ij} \rangle \frac{\partial u_i''}{\partial x_j}}_{\text{I}} + \underbrace{\tau_{xy}' \frac{\partial \{u\}}{\partial y}}_{\text{II}} + \underbrace{\tau_{ij}' \frac{\partial u_i''}{\partial x_j} - \left\langle \tau_{ij}' \frac{\partial u_i''}{\partial x_j} \right\rangle}_{\text{III}}. \tag{6-10}$$

Term III signifies fluctuations in TKE dissipation and can be written as ϵ'. Equation (6-10) has an assumption of $\langle u_i'' \rangle \approx 0$. We want to analyse how Φ' is correlated to the fluctuations in streamwise velocity and thus we will study their correlation coefficient. Consider the correlation,

$$\langle u'' \Phi' \rangle = \underbrace{\langle \tau_{ij} \rangle \left\langle u'' \frac{\partial u_i''}{\partial x_j} \right\rangle}_{\text{I}} + \underbrace{\left\langle u'' \tau_{xy}' \right\rangle \frac{\partial \{u\}}{\partial y}}_{\text{II}} + \underbrace{\langle u'' \epsilon' \rangle}_{\text{III}}, \tag{6-11}$$

whose correlation coefficient is defined as,

$$R_{u\Phi} = \frac{\langle u'' \Phi' \rangle}{u_{rms} \Phi_{rms}}. \tag{6-12}$$

Figure 6-4 shows the contributions to the correlation coefficient from each term in equation (6-11) for the case M3.0R200. As seen, the terms I and II on the RHS of equation (6-11) contribute the most near the wall. Another point to note is that the contributions from the term I and II are almost identical. With some assumptions we can show that both these terms (I and II) approximately represent,

$$\langle \mu \rangle \frac{\partial \{u\}}{\partial y} \left\langle u'' \frac{\partial u''}{\partial y} \right\rangle,$$

and hence, their contributions are also similar. Contribution by term III (in equation (6-11)) is small near the wall, but away from the wall, the total contribution comes from this term. The total correlation coefficient (computed without any assumptions and simplifications) is high and positive near the wall. This signifies that the fluctuations in Φ (Φ') are positively correlated to u'' which is not possible if the fluctuations were generated due to mere passive mixing. Because if it was the case then the correlation coefficient should be negative near the wall as the distribution of $\langle \Phi \rangle$ decreases away from the wall and that of $\{u\}$ increases.

Near the wall, the very high velocity gradients provide an important contribution to dissipation and hence to Φ. The role of turbulent dissipation is very small near the wall. This is clear from figure 6-5 which shows the contributions to $\langle \Phi \rangle$ from dissipation due to mean velocity gradients (dissipation of mean KE, $\langle \tau_{12} \rangle \partial \langle u \rangle / \partial y$) and dissipation of TKE (ϵ) for the

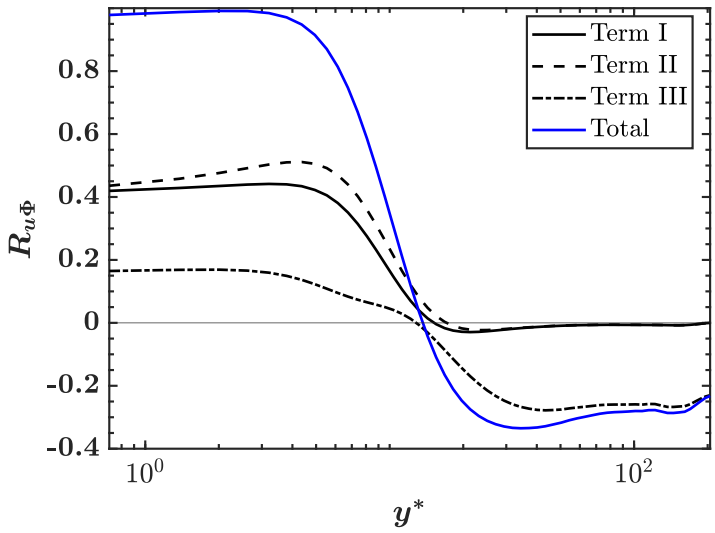

Figure 6-4: Contributions from the individual terms in equation (6-11) to the total correlation coefficient (equation (6-12)) for the case M3.0R200.

case M3.0R200. However, away from the wall, the gradients in streamwise velocity are small and thus, the main contribution to Φ comes from the TKE dissipation (ϵ). Near the wall, the fluctuations in Φ (Φ') are generated because of fluctuations in the streamwise velocity u'' modifying the instantaneous velocity gradients. A positive u'' is coupled with a positive gradient $\partial u''/\partial y$ in the near wall region. A positive gradient $\partial u''/\partial y$ causes the instantaneous velocity gradient to increase and thus increasing Φ, resulting in a positive fluctuation Φ'. This explains the positive correlation near the wall. However, away from the wall, the fluctuations are generated due to passive mixing of ϵ and hence the correlation coefficient is negative. The TKE dissipation ϵ acts on very small scales and hence is a local quantity. u'' is mainly related to large scales and has no direct impact on TKE dissipation. Note that this is true only away from the wall where turbulent Reynolds number and hence scale separation is high. Near the wall, there is no clear distinction between large and small scales and hence u'' can directly affect ϵ. This is evident from the positive correlation coefficient coming from term III near the wall in figure 6-4. Phenomenologically, away from the wall, a fluid parcel leaving source "A" and reaching destination point "B" would also carry with it the dissipation at "A" to "B". This would create fluctuations in ϵ at "B" due to passive mixing.

To summarize, near the wall, Φ' is generated by u'' affecting the instantaneous velocity gradients. Mathematically,

$$\Phi' \approx \langle \tau_{ij} \rangle \frac{\partial u_i''}{\partial x_j} + \tau_{xy}' \frac{\partial \{u\}}{\partial y}, \tag{6-13}$$

and,

$$\langle u'' \Phi' \rangle \approx \langle \tau_{ij} \rangle \left\langle u'' \frac{\partial u_i''}{\partial x_j} \right\rangle + \left\langle u'' \tau_{xy}' \right\rangle \frac{\partial \{u\}}{\partial y}. \tag{6-14}$$

Away from the wall, Φ' is generated by passive mixing of TKE dissipation ϵ. Mathematically,

$$\Phi' \approx \epsilon', \tag{6-15}$$

and,

$$\langle u'' \Phi' \rangle \approx \langle u'' \epsilon' \rangle. \tag{6-16}$$

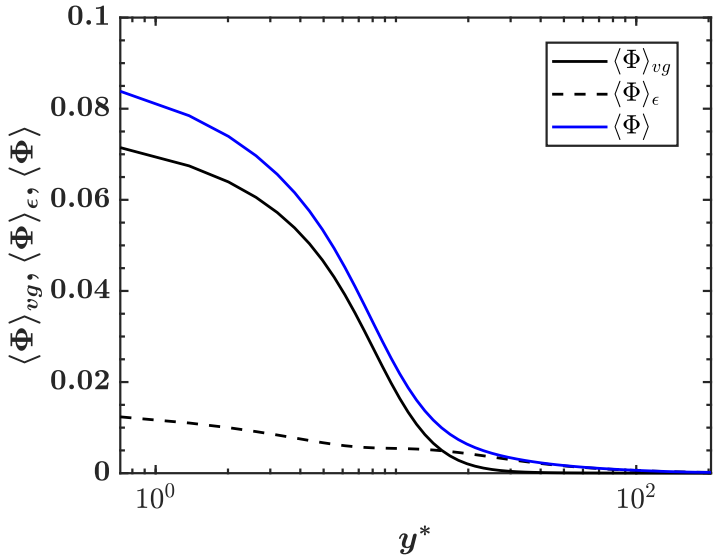

Figure 6-5: Contributions to the mean viscous heating $\langle\Phi\rangle$ from dissipation due to mean velocity gradients $\langle\Phi\rangle_{vg}$ and from TKE dissipation $\langle\Phi\rangle_\epsilon$ for the case M3.0R200. Note that the values are not semi-locally scaled but are unscaled.

The above analysis proves that the fluctuations in Φ are not simply caused by passive mixing of the mean heat sources $\langle\Phi\rangle$, especially near the wall. Viscous heating effects, therefore, cannot be modelled by just providing a user defined varying volumetric heat source distribution such that it represents $\langle\Phi\rangle$. The heat sources also need to be coupled to velocity gradients and turbulence.

After studying the mechanism of how Φ' is generated, we want to know how does it correlate with the enthalpy fluctuations. Since Φ is directly present in the enthalpy equation (2-16), one would expect fluctuations Φ' leading to enthalpy fluctuations, or in other words we can say that Φ' contributes to an additional source in the enthalpy variance (k_h) equation which is nothing but the Φ_{kh} term.

Figure 6-6 and 6-7 show the enthalpy variance budget in semi-local scales for the cases M3.0R200 and M3.0CRe$^*_\tau$. As seen, the production due to the viscous heating ($\hat{\Phi}_{kh}$) is as large as the conventional production term ($\hat{P}_{kh}$), however, its peak is much closer to the wall. This is expected due to very high $\hat{\Phi}_{rms}$ near the wall (figure 6-8). The artifact terms ($\hat{B}_{kh}$ and $\hat{D}_{kh}$) are small like we had in the low-Mach number cases. However, due to very low production ($\hat{P}_{kh}$), these terms might become relatively important. The term due to pressure, $\hat{Pr}_{kh}$ is small in the entire domain.

Figure 6-9 shows the two mechanisms of production, i.e. by passive mixing ($\hat{P}_{kh}$) and by fluctuations in Φ ($\hat{\Phi}_{kh}$) for the case M3.0R200. The same figure also plots the correlation coefficient defined as,

$$R_{h\Phi} = \frac{\langle \hat{h}'' \hat{\Phi}' \rangle}{\hat{h}_{rms} \hat{\Phi}_{rms}}. \tag{6-17}$$

Near the wall, $\hat{\Phi}_{kh}$ is a dominant source term. This implies that fluctuations in enthalpy near the wall are generated due to fluctuations in viscous heat source Φ. Since Φ is a source term in the enthalpy transport equation, we would expect the correlation between the fluctuations

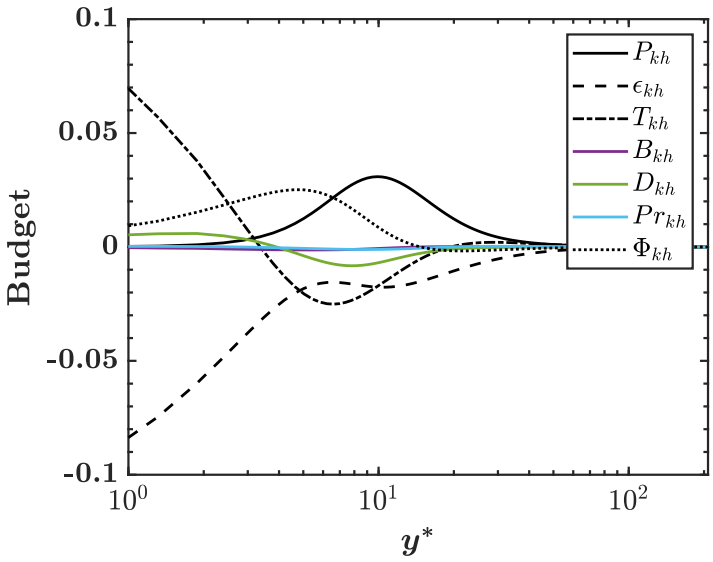

Figure 6-6: Semi-local k_h budget for the case M3.0R200 scaled by $\langle\rho\rangle u_\tau^*(c_p\theta_\tau^*)^2/\delta_v^*$ (effectively dividing equation (6-6) by Re_τ^*).

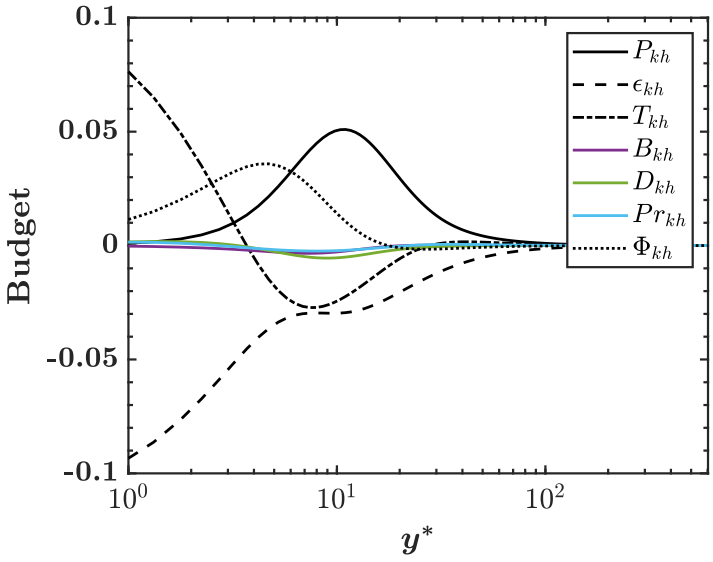

Figure 6-7: Semi-local k_h budget for the case M3.0CRe$_\tau^*$ scaled by $\langle\rho\rangle u_\tau^*(c_p\theta_\tau^*)^2/\delta_v^*$ (effectively dividing equation (6-6) by Re_τ^*).

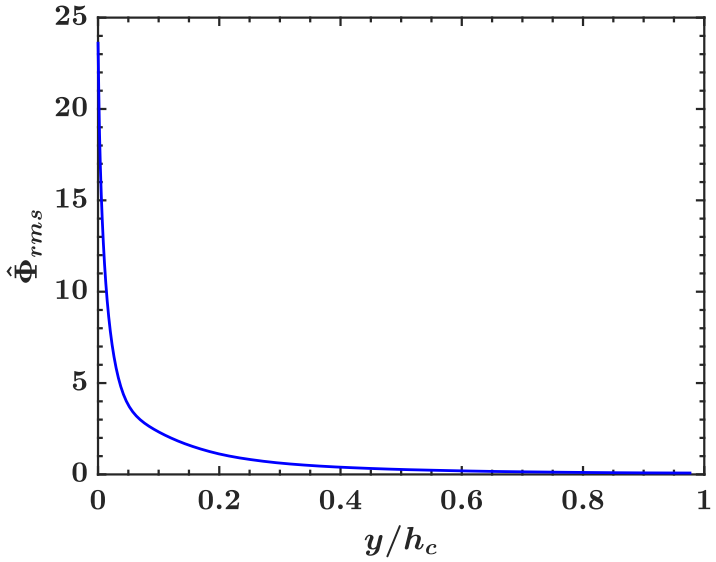

Figure 6-8: $\hat{\Phi}_{rms}$, signifying the magnitude of fluctuations in viscous heating ($\hat{\Phi}'$). The values are semi-locally scaled.

to be positive and figure 6-9 shows exactly that. However, away from the wall, passive mixing dominates and $\hat{P}_{kh}$ becomes the dominant production term. Thus, the coefficient changes sign. The mechanism of generation of enthalpy fluctuations near the wall can be summarized as follows: Fluctuations in the streamwise velocity u'' affect the instantaneous streamwise velocity gradients and hence the viscous heating source Φ. This leads to fluctuations in the source term (Φ) in the enthalpy equation, causing fluctuations in enthalpy.

In figure 6-9, we have seen that the $\hat{\Phi}_{kh}$ term is a dominant production term near the wall. Its effect on k_h is clearly seen in figure 6-10 which compares the k_h profile and the k profile (normalized by their maximums) for the M3.0R200 case. For a $Pr = 0.7$ fluid, the peaks should occur nearly at the same y^* location, but due to the additional production term near the wall, the peak of k_h is shifted towards the wall.

Now that we have studied the effect of viscous heating on enthalpy variance and its budget, we are interested to study its effect on the quantity of engineering importance, i.e. the turbulent heat flux.

6-2-3 Effects on the Turbulent Heat Flux Budget

In this section we will present the budget of wall-normal turbulent heat flux in semi-local scales. The equation for turbulent heat flux in semi-local scales is derived and presented in section 3-2-5. Figure 6-11 shows the budget for wall-normal turbulent heat flux (-$\langle\hat{v}''\hat{h}''\rangle$) in semi-local scales for the case M3.0CRe$^*_\tau$. (Note the minus sign. The equations we derived are for $\langle\hat{u}_i''\hat{h}''\rangle$ and thus to obtain budget for $-\langle\hat{u}_i''\hat{h}''\rangle$, each term in equation (3-46) should be multiplied by -1.)

Like for the constant property budget, the enthalpy – pressure gradient correlation term ($\hat{H}_{u_ih}$) acts as a major sink term to balance most of the production ($\hat{P}_{u_ih}$). The dissipation $\hat{\epsilon}_{u_ih}$ has notable values only in the near wall region. Also, we can see that the artifact terms

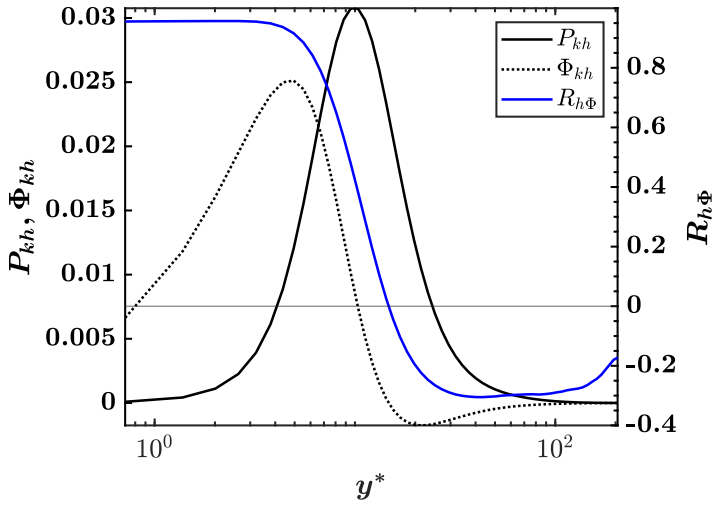

Figure 6-9: Source terms in the k_h equation ($\hat{P}_{kh}$ and $\hat{\Phi}_{kh}$) on the left y-axis. Correlation coefficient defined in equation (6-17) on the right y-axis.

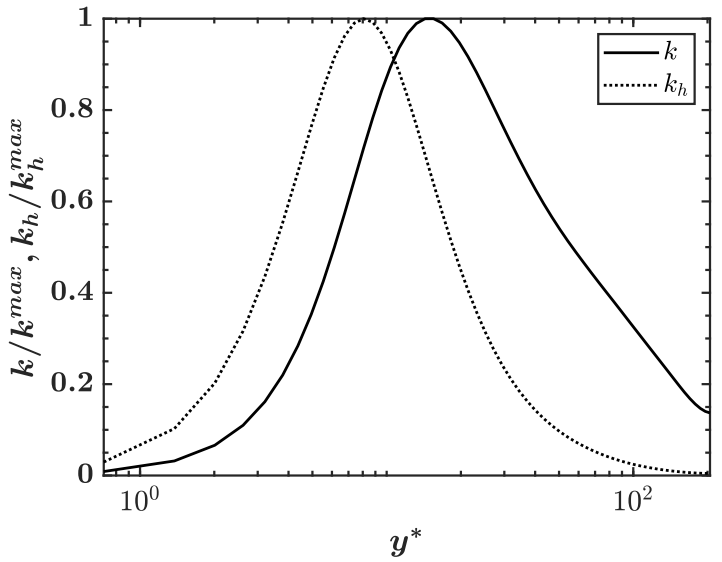

Figure 6-10: TKE and enthalpy variance normalized by their respective maximums for the case M3.0R200.

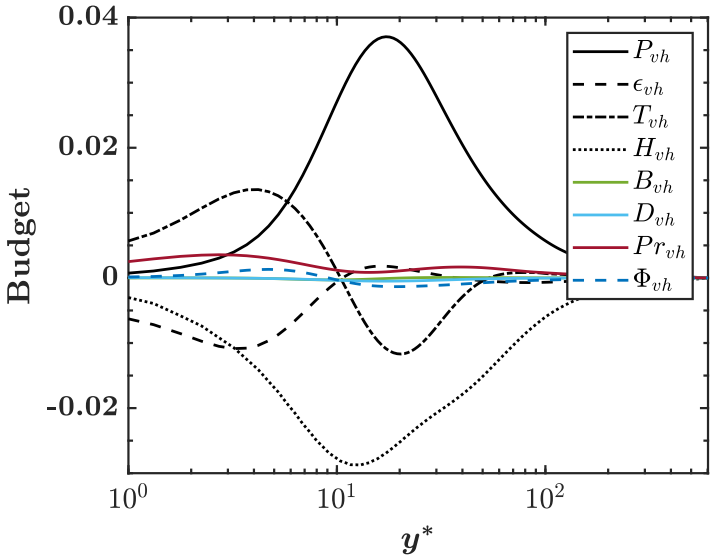

Figure 6-11: Semi-local wall-normal turbulent heat flux budget scaled by $\langle\rho\rangle u_\tau^{*^2}(c_p\theta_\tau^*)/\delta_v^*$ (effectively dividing equation (3-46) by Re_τ^*), for the case M3.0CRe$_\tau^*$.

$\hat{B}_{u_ih}$ and $\hat{D}_{u_ih}$ are small throughout the domain. The additional term due to viscous heating Φ_{u_ih} is negligible in the entire domain and thus, we can conclude that the direct contribution of viscous heating to the turbulent heat flux is negligible. However, it can affect the heat flux indirectly by affecting other terms in the budget. The term due to pressure ($\hat{Pr}_{u_ih}$) has notable values near the wall, however, in the entire domain the term is small compared to other budget terms.

Here, we come to an end of our analysis about the effects of viscous heating on thermal turbulence. We saw the effect of the viscous heating term as a whole. Looking at its formulation in equation (6-2), the term seems to be governed by Re_τ^* and $Ec_{\theta_\tau}^*$. In the next section we shall discuss more about these parameters and their importance in thermal turbulence.

6-3 Governing Parameters

The viscous heating term is a sink in the mean KE and TKE equations and a source in the enthalpy equation. In dimensional form they should be equal, however, in semi-local scales, the sink in KE equation is $\tau_{ij}^{vD}\partial u_i^{vD}/\partial\hat{x}_j$ but the source in the enthalpy equation is $Ec_{\theta_\tau}^*\tau_{ij}^{vD}\partial u_i^{vD}/\partial\hat{x}_j$. This is because both the equations are scaled differently. As an artifact of using different scales to scale kinetic energy ($u_\tau^{*^2}$) and enthalpy ($c_p\theta_\tau^*$), we get a new parameter, called the "modified Eckert number" ($Ec_{\theta_\tau}^* = u_\tau^{*^2}/(c_p\theta_\tau^*)$) in this thesis. Its form is very similar to the conventional Eckert number and hence the name.

We already know the importance of Re_τ^* and Pr^* in semi-locally scaled thermal turbulence as seen in section 5-2 for low-Mach number cases. However, for high-Mach number cases, due to viscous heating an additional parameter (modified Eckert number) is introduced. In the next section we will analyse the importance of this new parameter.

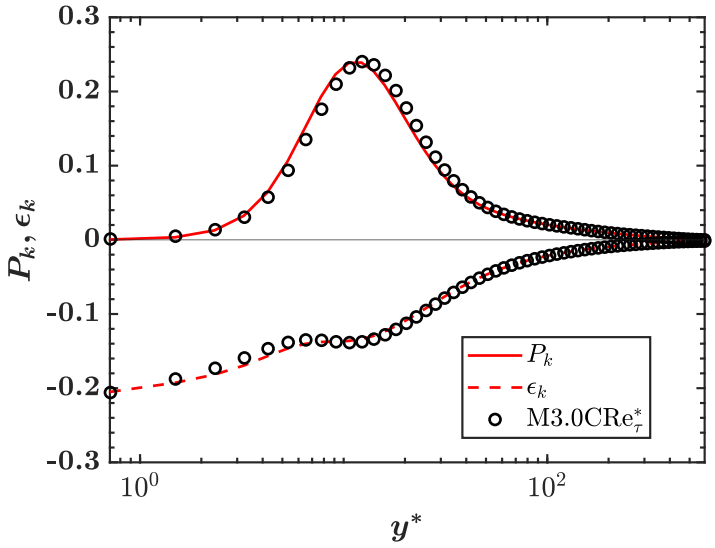

Figure 6-12: Semi-locally scaled production and dissipation of TKE for the cases M3.0CRe$^*_\tau$ and M0.7CRe$^*_\tau$.

6-3-1 Importance of $Ec^*_{\theta_\tau}$ in thermal turbulence

In this section, we want to know if we can just ensure similar Re^*_τ and Pr^* without considering about $Ec^*_{\theta_\tau}$ and still get similar thermal turbulence statistics for two cases. Answering this question requires setting up two cases with same Pr^* and Re^*_τ profiles but different $Ec^*_{\theta_\tau}$ profile. This will help us to isolate the effects of $Ec^*_{\theta_\tau}$ and comment on its importance in a better way.

For this purpose, the idea of setting up constant Re^*_τ high-Mach number cases (M0.7CRe$^*_\tau$ and M3.0CRe$^*_\tau$) was proposed. The cases are described in table 4-1. These cases have the same Re^*_τ and Pr^* profiles but due to very different Mach numbers, their $Ec_{\theta^*_\tau}$ profiles are different as seen in figure 4-6.

DNS simulations were performed for these cases using the code developed in-house by the Fluid Dynamics of Energy Systems team headed by Dr. R. Pecnik. The DNS code is described briefly in Appendix B. The same code is also used to simulate the M3.0R200 and M4.0R200 cases of Trettel and Larsson (2016) so as to compute the statistics that are not published by the authors. The validation of the code is presented in Appendix C.

In figure 6-12 we show the production and dissipation of TKE for the M3.0CRe$^*_\tau$ and M0.7CRe$^*_\tau$ cases. We see that indeed the profiles are very similar and hence reinforces our belief in Re^*_τ as a governing parameter for velocity turbulence. However, the peak for the Mach 3 case is slightly shifted away from the wall. This is due to the inter-component energy transfer affected by the density profile and not fully characterized by Re^*_τ. This is discussed in the next chapter.

In figure 6-13 we see the production $\hat{P}_{kh}$, dissipation $\hat{\epsilon}_{kh}$ and viscous heating term $\hat{\Phi}_{kh}$ for the two cases. As seen, the collapse is not as good as what we had in figure 6-12. The peaks of both $\hat{P}_{kh}$ and $\hat{\Phi}_{kh}$ are not fully characterized by Re^*_τ and Pr^*. This signifies the importance of $Ec^*_{\theta_\tau}$ in thermal turbulence.

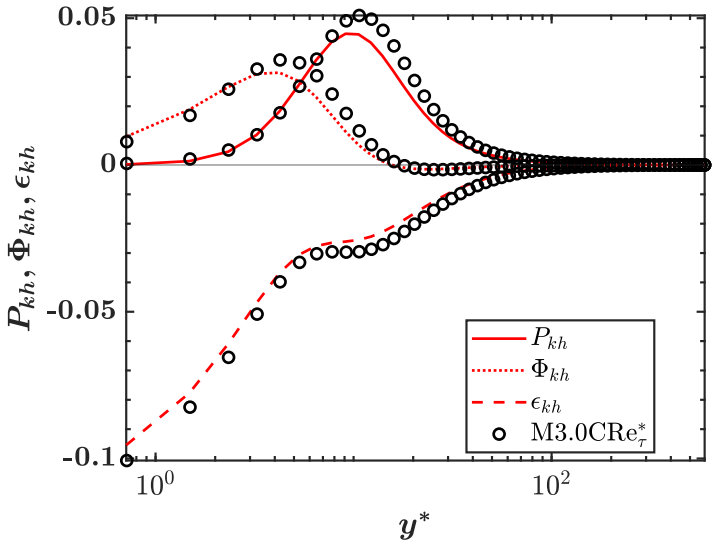

Figure 6-13: Semi-locally scaled production and dissipation of enthalpy variance for the cases M3.0CRe$^*_\tau$ and M0.7CRe$^*_\tau$.

In the next section, we will use the findings of this chapter to solve for turbulent heat flux in high-Mach number flows.

6-4 Heat Flux Modeling of High-Mach Number Cases

At this point, we know that the viscous heating term ($\hat{\Phi}_{kh}$) indeed plays a dominant role in the evolution of enthalpy variance, especially near the wall (section 6-2-2). We want to see how dominant is this role from a modeling perspective. In other words, we want to check if we can use the same model equations for high-Mach number cases as we did for low-Mach number cases. In section 5-3, we saw that solving heat flux models in semi-locally scaled form captures variable inertia effects better than solving them in conventionally scaled form. We will use that conclusion and solve the model equations for high-Mach number cases also in semi-locally scaled form. This will help to isolate only the effects or differences that arise due to viscous heating, as the variable property effects are taken care by semi-locally scaling the model equations.

For high-Mach number cases, the mean enthalpy equation will be modified as,

$$\frac{\partial}{\partial \hat{y}}\left[\left(\frac{1}{Re^*_\tau Pr^*}+\hat{\alpha}_t\right)\frac{\partial\{h^{vD}\}}{\partial \hat{y}}\right] = -\langle\hat{\Phi}\rangle. \tag{6-18}$$

To solve the mean enthalpy equation, we need an approximation for $\langle\hat{\Phi}\rangle$. Otero Rodriguez et al. (2018) have approximated this term as (when reformulated in semi-local scales),

$$\langle\hat{\Phi}\rangle = Ec^*_{\theta_\tau}\left(\frac{1}{Re^*_\tau}\left(\frac{\partial\{u^{vD}\}}{\partial\hat{y}}\right)^2+\hat{\mu}_t\left(\frac{\partial\{u^{vD}\}}{\partial\hat{y}}\right)^2\right). \tag{6-19}$$

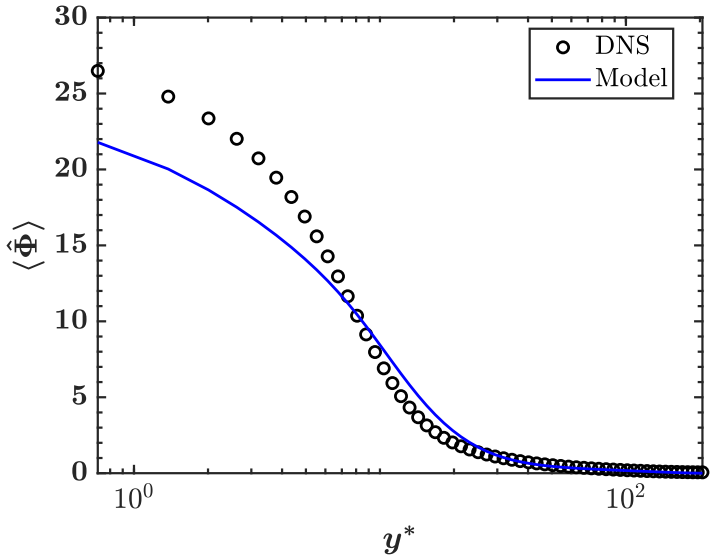

Figure 6-14: $\langle\hat{\Phi}\rangle$ computed using the model (equation (6-19)) and compared with DNS for the case M3.0R200. Values are semi-locally scaled.

The first term on the RHS is the contribution by dissipation of mean KE and the second term is the contribution by TKE. This formulation, even though seems to be reasonable from a modeling perspective, is not fully correct. This is because the second term on the right hand side of equation (6-19) is production of TKE (P_k), but the contribution to enthalpy is by dissipation of TKE (ϵ). In the log-law region and beyond, due to equilibrium nature of the flow, production and dissipation are nearly in balance. However, near the wall, this is not the case and thus the formulation is not completely correct. Near the wall the first term on the RHS of equation (6-19) dominates and the effect of this inaccuracy is overshadowed. Figure 6-14 shows accurate $\langle\hat{\Phi}\rangle$ (computed from DNS) and the one obtained using equation (6-19) for the case M3.0R200. The difference is not too large and is acceptable for modeling purpose. However, a better approximation would be to use ϵ computed from the turbulent stress model, instead of the production term.

The RANS results are presented in figure 6-15 for the case M3.0R200 when the model is solved in semi-local scales. The model equations are same as the ones used for low-Mach number cases without any modification to account for viscous heating effects. As seen, the predictions of mean temperature is not very inaccurate, however, the thermal turbulence quantities are far from accurate. This near-accurate mean temperature is mere coincidence and does not speak for robustness of the model as seen in figure 6-16, which shows the normalised mean temperature for cases M0.7R600 and M3.0R600. The computed mean temperature for these cases is not accurate showing deficiency in the model equations. The predictions of mean velocity and velocity turbulence quantities are acceptable. This implies that the turbulent stress model seems to capture the physics well, but due to viscous heating, the heat flux model is unable to completely capture the physics.

It is worth noting at this point that Otero Rodriguez et al. (2018) solved the mean temperature for high-Mach number cases using a simple constant turbulent Prandtl number model and the results were accurate. So why don't we simply use constant Pr_t model? The benefit of improving 2-equation heat flux models is because these models would even work in cases

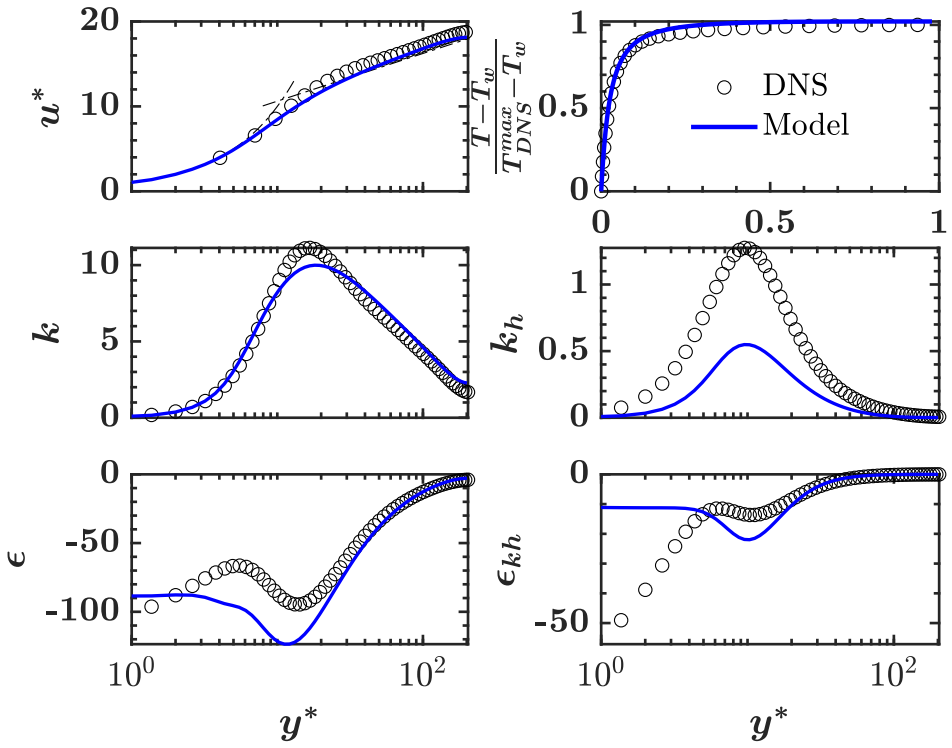

Figure 6-15: RANS results for the case M3.0R200 using the same Nagano and Shimada model as was used for low-Mach number cases. Turbulence quantities presented in the image are classically scaled. X-axis for the top right image is y/h_c and not y^*.

where the constant turbulent Prandtl number model fails. For instance, where the strong analogy between heat and momentum transport is not applicable. Nagano and Shimada (1996) solved developing thermal boundary layers in a fully developed velocity field and found that a constant Pr_t model does not work in the early stage of development due to dissimilarity between velocity and thermal fields, but their 2-equation heat flux model does. So and Speziale (1999) and Patel (2013) also mention about the failure of constant Pr_t models when the buoyancy effects are high.

In the following section we will discuss how the k_h and ϵ_{kh} model equations are affected due to viscous heating in high-Mach number cases. Note that this effect will be dominant only near the wall because that is where viscous heating effects are strong.

6-4-1 Model enthalpy variance (k_h) equation

Figure 6-6 and 6-7 represent the k_h budget in semi-local scales for two high-Mach number channel flows. We notice that apart from the usual terms that are modeled in the low-Mach number case, viscous heating source term seems to be a dominant production term near the wall and an attempt to model it is made in this section.

Near the wall, the correlation $\langle u''\Phi' \rangle$ can be approximated by equation (6-14). It is rewritten below as,

$$\langle u''\Phi' \rangle \approx \langle \tau_{ij} \rangle \left\langle u'' \frac{\partial u_i''}{\partial x_j} \right\rangle + \left\langle u'' \tau_{xy}' \right\rangle \frac{\partial \{u\}}{\partial y}. \tag{6-20}$$

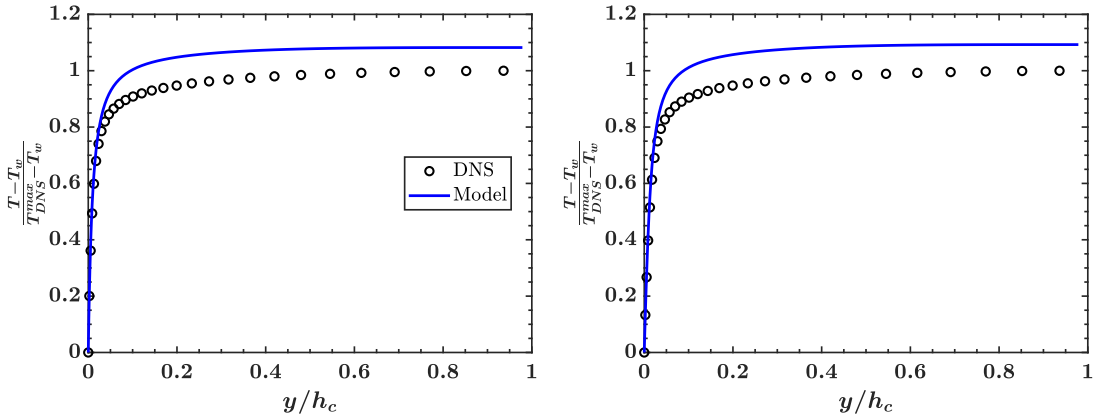

Figure 6-16: Normalised mean temperature for the cases M0.7R600 (left) and M3.0R600 (right).

In section 6-2-2, we also showed that the terms on the RHS, to a certain approximation, represent,

$$\langle \mu \rangle \frac{\partial \{u\}}{\partial y} \left\langle u'' \frac{\partial u''}{\partial y} \right\rangle,$$

which in semi-local scales can be written as,

$$\frac{1}{Re^*_\tau} \frac{\partial \{u^{vD}\}}{\partial \hat{y}} \left\langle \hat{u}'' \frac{\partial \hat{u}''}{\partial \hat{y}} \right\rangle.$$

Using this information, in semi-local scales we can write,

$$\langle \hat{u}'' \hat{\Phi}' \rangle \approx \frac{2}{Re^*_\tau} \frac{\partial \{u^{vD}\}}{\partial \hat{y}} \left\langle \hat{u}'' \frac{\partial \hat{u}''}{\partial \hat{y}} \right\rangle = \frac{2}{Re^*_\tau} \frac{\partial \{u^{vD}\}}{\partial \hat{y}} \underbrace{\frac{\partial \langle \hat{u}'' \hat{u}''/2 \rangle}{\partial \hat{y}}}_{\text{A}}. \tag{6-21}$$

We model term "A" as,

$$\frac{\partial \{\hat{k}\}}{\partial \hat{y}}.$$

The final model becomes,

$$\langle \hat{u}'' \hat{\Phi}' \rangle \approx C_u \frac{2}{Re^*_\tau} \frac{\partial \{u^{vD}\}}{\partial \hat{y}} \frac{\partial \{\hat{k}\}}{\partial \hat{y}}, \tag{6-22}$$

where C_u is a model constant and needs to be fine tuned for accurate predictions. We have chosen a value of 1.33 for C_u. Figure 6-17 compares our model with the DNS for some cases and the predictions appear reasonable.

In Figure 6-18 we present the correlation coefficient defined as,

$$R_{uh} = \frac{\langle \hat{u}'' \hat{h}'' \rangle}{\hat{u}_{rms} \hat{h}_{rms}}, \tag{6-23}$$

and as seen the coefficient is very high especially near the wall. Using this information about u'' and h'' being strongly correlated near the wall, and using equation (6-22), we propose the model for $\langle \hat{h}'' \hat{\Phi}' \rangle$ as,

$$\langle \hat{h}'' \hat{\Phi}' \rangle \approx C_h \frac{2}{Re^*_\tau} \frac{\partial \{u^{vD}\}}{\partial \hat{y}} \frac{\partial \sqrt{\{\hat{k}\}\{\hat{k}_h\}}}{\partial \hat{y}}, \tag{6-24}$$

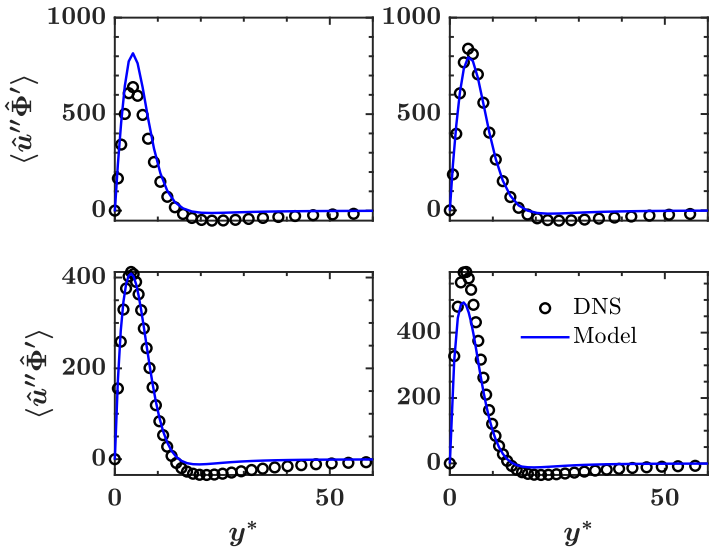

Figure 6-17: Comparison of the model for $\langle \hat{u}''\hat{\Phi}' \rangle$ proposed in equation (6-22) with DNS. Results are shown for M0.7CRe$^*_\tau$ (top left), M3.0CRe$^*_\tau$ (top right), M3.0R200 (bottom left) and M4.0R200 (bottom right). Values are semi-locally scaled.

where C_h is a model constant. After some fine tuning we have selected a value of 1.6 for the constant. Figure 6-19 compares our model with the DNS for some cases and the predictions appear accurate.

The best way to check if the model is good or not is to implement it and solve k_h. Figure 6-20 shows k_h without the model for $\hat{\Phi}_{kh}$, or in other words solution to equation,

$$\hat{P}_{kh} - \hat{\epsilon}_{kh} + \hat{T}_{kh} = 0. \tag{6-25}$$

The same figure also shows the results for k_h when we use equation (6-24) to model $\hat{\Phi}_{kh}$. In other words, the solution to equation,

$$\hat{P}_{kh} - \hat{\epsilon}_{kh} + \hat{T}_{kh} + \hat{\Phi}^{model}_{kh} = 0. \tag{6-26}$$

The production, dissipation and turbulent diffusion terms are taken directly from DNS and the viscous diffusion term is used to compute k_h by integration. The result without the model for $\hat{\Phi}_{kh}$ is unsatisfactory and is one of the major reasons for poor results obtained in figure 6-15 for the M3.0R200 case. However, with the model, the results are clearly improved. Note that in this analysis we have neglected the artifact terms ($\hat{B}_{kh}$ and $\hat{D}_{kh}$) and the term due to pressure ($\hat{Pr}_{kh}$) due to their insignificant magnitudes (figure 6-6 and 6-7).

Using the model proposed for $\hat{\Phi}_{kh}$, the RANS equations were again solved for the case M3.0R200 (results are not shown here) using the Nagano and Shimada model in semi-local form. There was no major improvement in the result. This is because the ϵ_{kh} equation proposed for the low-Mach number cases is not suitable for the high-Mach number cases. The error due to ϵ_{kh} was not reflected in figure 6-20 because we used DNS values for ϵ_{kh} as the main goal was to study the effectiveness of the proposed model for $\hat{\Phi}_{kh}$. In the next section the possible reason behind the failure of ϵ_{kh} model equation is discussed.

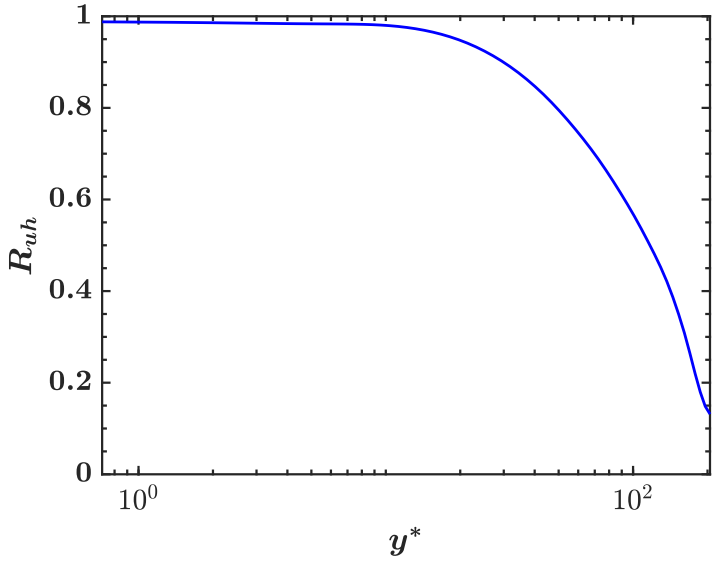

Figure 6-18: Coefficient of correlation between the fluctuations in streamwise velocity and enthalpy (defined in equation (6-23)).

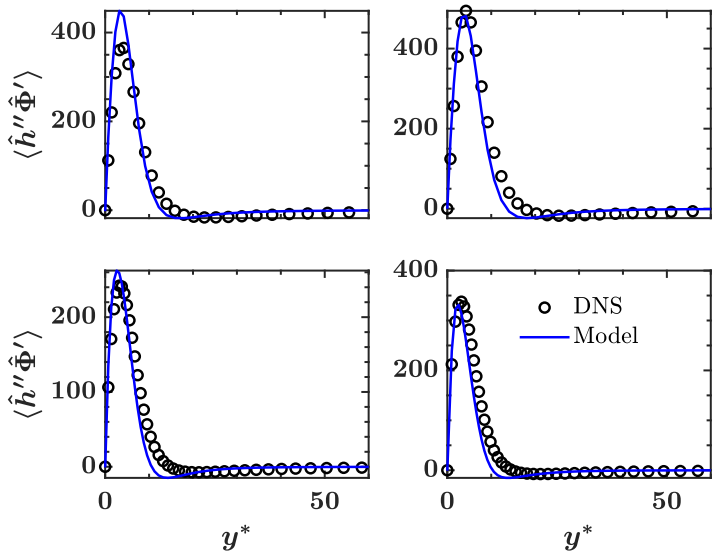

Figure 6-19: Comparison of the model for $\langle \hat{h}'' \hat{\Phi}' \rangle$ proposed in equation (6-24) with DNS. Results are shown for M0.7CRe$^*_\tau$ (top left), M3.0CRe$^*_\tau$ (top right), M3.0R200 (bottom left) and M4.0R200 (bottom right). Values are semi-locally scaled.

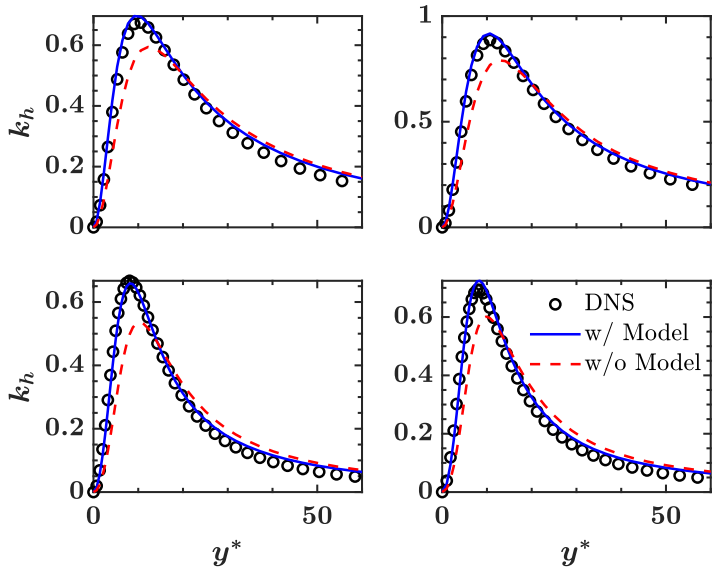

Figure 6-20: Comparison of k_h computed using the model for $\hat{\Phi}_{kh}$ and that computed without any model for $\hat{\Phi}_{kh}$, with DNS. Results are shown for M0.7CRe$^*_\tau$ (top left), M3.0CRe$^*_\tau$ (top right), M3.0R200 (bottom left) and M4.0R200 (bottom right). All values presented are semi-locally scaled.

6-4-2 Model ϵ_{kh} equation

The model equation of thermal variance dissipation (ϵ_{kh}) is proposed based on intelligent dimensional arguments (Launder, 1976). We can also refer this equation as an empirical equation for ϵ_{kh}. In Nagano and Shimada (1996), the equation of ϵ_{kh} (referred as ϵ_t in the paper) is rigorously modeled to take care of the near wall effects and Prandtl number (Pr) dependency. However, the channel cases tested in Nagano and Shimada (1996) are the ones with uniform internal heat source or with iso-flux boundary condition. They do not discuss if the ϵ_{kh} equation proposed will work for compressible cases with viscous heating. The question comes to mind - how are the viscous heating cases different and why would the model ϵ_{kh} equation not work for them? This question is answered in this section.

Launder (1976) was one of the pioneering work in heat flux modeling. Launder (1976) mentioned that coming up with a model equation for ϵ_{kh} is more difficult than that for ϵ (TKE dissipation) due to the increased number of parameters. For instance, time scales can be constructed as k/ϵ or as k_h/ϵ_{kh}. Nagano and Shimada (1996) models the source and sink terms in the dissipation equation as,

$$\frac{\epsilon_{kh}}{\mathcal{T}},$$

where $\mathcal{T}$ is a suitable time scale. The time scale for the production of ϵ_{kh} (or ϵ_t) is taken as k/P_k and k_h/P_{kh}. Similarly, the time scale for the dissipation of ϵ_{kh} is taken as k/ϵ and k_h/ϵ_{kh}. Thus, there are 4 terms representing the source and sink terms in the ϵ_{kh} model equation, one with each time scale. These terms are,

$$\frac{\epsilon_{kh}P_{kh}}{k_h}, \quad \frac{\epsilon_{kh}P_k}{k}, \quad \frac{\epsilon_{kh}\epsilon_{kh}}{k_h}, \quad \frac{\epsilon_{kh}\epsilon}{k}. \tag{6-27}$$

However, in the high-Mach number cases, we will have additional source/sink terms in the ϵ_{kh} equation due to viscous heating. Possibly, it is due to these terms, that the low-Mach number ϵ_{kh} model equation seems to be insufficient to capture the physics. Modeling these terms by just using a time scale as k_h/Φ_{kh} was tried but there was no significant improvement. Thus, a more rigorous approach needs to be adopted. Fixing the ϵ_{kh} equation for the high-Mach number cases is beyond the scope of this work and can be pursued as a continuation of this work in future studies. An appropriate action plan would be to first derive the exact ϵ_{kh} equation to see which new terms are dominant. A possible way to model these terms then needs to be figured out. Also, the possibility of the model constants in the ϵ_{kh} equation getting modified needs to be considered.

This brings us to the end of this section. In summary we can say that viscous heating does have notable effects on the model equations of k_h and ϵ_{kh}, especially near the wall. Thus, if we are to compute α_t using a two equation heat flux model, then we need to incorporate these effects in the model equations.

The next chapter is not strongly related to the content discussed until now but tells us an important condition in which semi-local scaling can be compromised. We will see why two high-Mach number cases (M0.7CRe$^*_\tau$ and M3.0CRe$^*_\tau$) are different despite having the same Re^*_τ.

Chapter 7

Effects of High Density Gradients on Inter-Component Energy Transfer

In the previous chapter, in figure 6-12, we saw that the TKE production profile of the case M3.0CRe$^*_\tau$ was slightly shifted away from the wall compared to that of the case M0.7CRe$^*_\tau$, despite having the same Re^*_τ profile. No matter how small the difference seems to be, it is important to investigate it in more detail as it will help us to understand the scenarios under which semi-local scaling can fail. In this chapter, a brief discussion on the possible reasons for this difference is presented.

Figure 7-1 shows the $\{u^*\}$ profile (equation (5-17), also known as the Trettel and Larsson transformation) for the high-Mach number cases that have the same semi-local Reynolds number at the channel centre. As seen, all the cases, except M3.0CRe$^*_\tau$, show a perfect collapse with the constant property "law of the wall", which is clear from these curves collapsing with the profile of the case Moser590 (incompressible case from Moser et al. (1999) with $Re_\tau = 590$). There is a shift observed in the log-law intercept for the case M3.0CRe$^*_\tau$, similar to what is commonly observed for boundary layers (Zhang et al., 2018).

We saw that the TKE production peak is shifted away from the wall for the case M3.0CRe$^*_\tau$. This is explained from figure 7-2. It shows the distribution of the semi-locally scaled wall-normal Reynolds stress for the case M3.0CRe$^*_\tau$ compared with Moser590. The rise of wall-normal Reynolds stress in the case of M3.0CRe$^*_\tau$ is delayed and a clear offset is seen. This delay in the rise of the active motions near the wall is the major reason why the TKE production peak is shifted away from the wall. This is because, the TKE production depends on the turbulent shear stress and the production of turbulent shear stress depends on wall-normal Reynolds stress. This delayed rise is also the possible reason behind the log-law shift observed in figure 7-1. This is because the collapse obtained in $\{u^*\}$ is due to the collapse of viscous shear stress (Patel et al., 2016). The viscous shear stress depends on the turbulent shear stress in the inner layer as,

$$\tau_{visc} \approx 1 - \tau_{turbulent}. \tag{7-1}$$

There is a direct effect of the delayed rise on $\tau_{turbulent}$ which in turn affects the viscous shear stress and hence the $\{u^*\}$ profile. Figure 7-3 shows the viscous and turbulent shear stresses

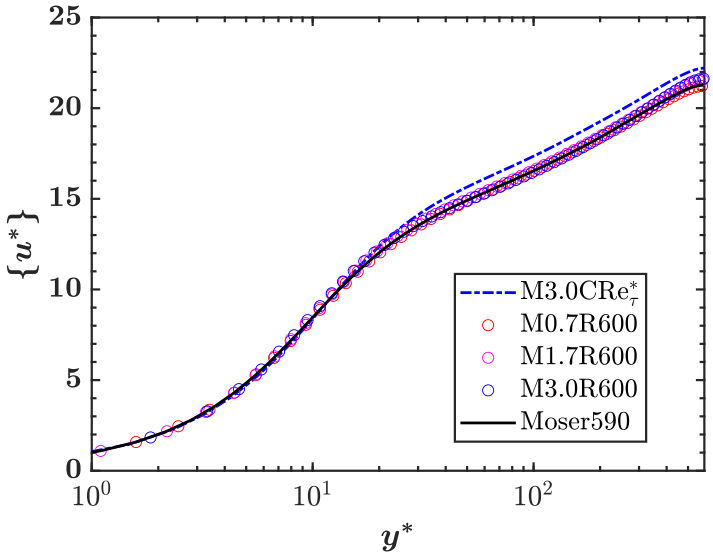

Figure 7-1: Universal velocity transformation (equation (5-17)) for the cases M3.0CRe$^*_\tau$, M0.7R600, M1.7R600, M3.0R600 and Moser590 (incompressible case from Moser et al. (1999) with $Re_\tau = 590$).

for the cases M3.0CRe$^*_\tau$ and Moser590. As seen, there is a clear effect of wall-normal Reynolds stress visible on the profile of turbulent shear stress and hence indirectly on the viscous shear stress.

The delayed rise of the wall-normal Reynolds stress (figure 7-2) can occur because of insufficient inter-component energy transfer from the streamwise component to the wall-normal component. This is clear from figure 7-4 which shows the semi-locally scaled pressure-strain correlation for the streamwise ($\hat{\Pi}_{11}$), wall-normal ($\hat{\Pi}_{22}$) and spanwise ($\hat{\Pi}_{33}$) components for the case M3.0CRe$^*_\tau$ compared with Moser590. Clearly, the reduced magnitude of $\hat{\Pi}_{11}$ is the reason why the other two components receive less energy and hence also explains the delayed rise of the wall-normal Reynolds stress.

The final question that remains unanswered is why is there a reduced energy transfer, or in other words, why $\hat{\Pi}_{11}$ reduces? Patel et al. (2016) discusses about reduced inter-component energy transfer for the cases with $dRe^*_\tau/dy < 0$ but this reasoning is not applicable here due to $dRe^*_\tau/dy = 0$ for both the cases. There can be two possible reasons for this effect:

- A "pure compressibility" effect, or
- A variable inertia effect (due to density gradients).

Initially, the reduced pressure-strain correlation seems to be a pure compressibility effect. Pantano and Sarkar (2002) analytically explained, using a Green's function analysis, that the streamwise pressure-strain correlation in compressible mixing layers is reduced compared to its incompressible counterpart due to finite speed of the pressure wave opposed to infinite speed in incompressible flows. However, Foysi et al. (2004) neglected the wave speed effect while writing the equation for pressure in channel flows with bulk Mach number as high as 3. In other words, they use the Poisson equation for pressure (and not a wave equation), but

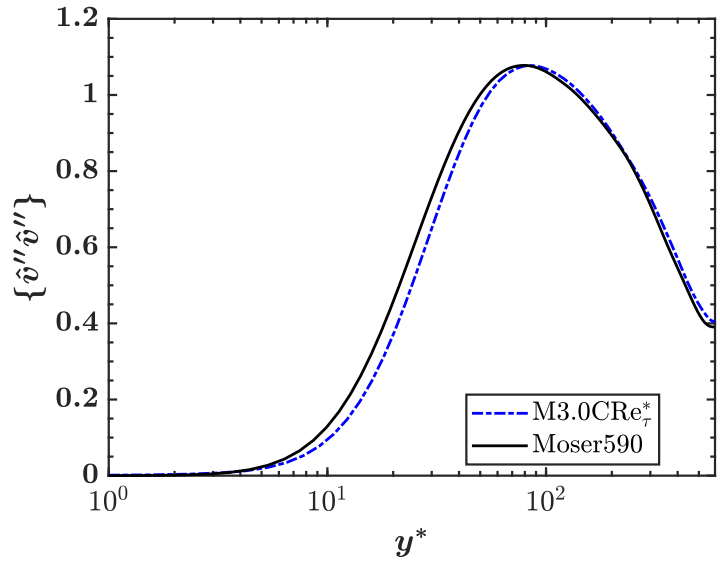

Figure 7-2: Semi-locally scaled wall-normal Reynolds stress ($\{\hat{v}''\hat{v}''\}$) for the cases M3.0CRe$^*_\tau$ and Moser590 (incompressible case from Moser et al. (1999) with $Re_\tau = 590$).

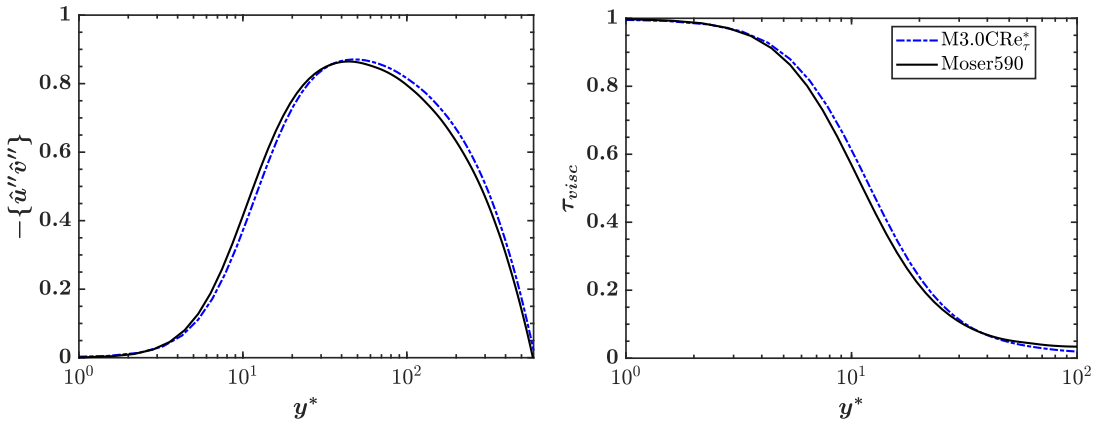

Figure 7-3: Semi-locally scaled turbulent (left) and viscous (right) shear stresses for the cases M3.0CRe$^*_\tau$ and Moser590 (incompressible case from Moser et al. (1999) with $Re_\tau = 590$).

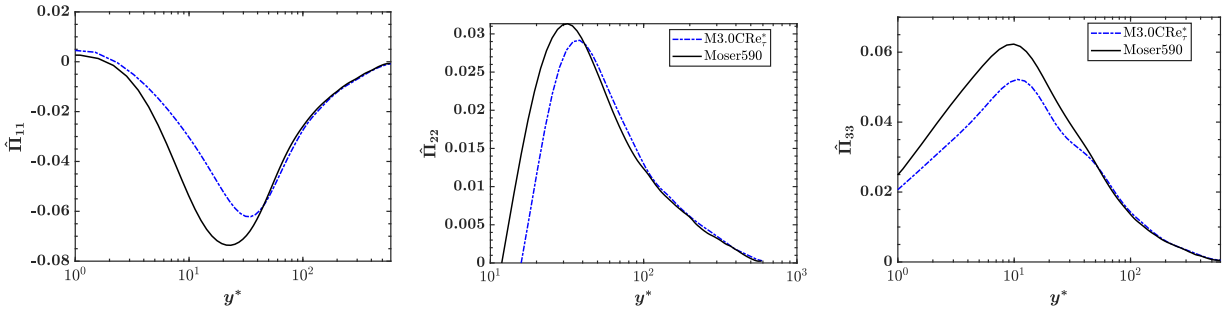

Figure 7-4: Semi-locally scaled pressure-strain correlation. Streamwise component $\hat{\Pi}_{11} = \langle \hat{p}' \partial \hat{u}'' / \partial \hat{x} \rangle$ (left), wall-normal component $\hat{\Pi}_{22} = \langle \hat{p}' \partial \hat{v}'' / \partial \hat{y} \rangle$ (centre) and spanwise component $\hat{\Pi}_{33} = \langle \hat{p}' \partial \hat{w}'' / \partial \hat{z} \rangle$ (right), for the cases M3.0CRe$^*_\tau$ and Moser590 (incompressible case from Moser et al. (1999) with $Re_\tau = 590$). The values are divided by Re^*_τ. Axis for $\hat{\Pi}_{22}$ is adjusted to only show the positive values.

they use source term contributions due to gradients in density. So we can call it a low-Mach number variable property formulation of the pressure Poisson equation. Foysi et al. (2004) explain the reduced pressure-strain correlation in high-Mach number channel flows as an effect arising due to decreasing density away from the wall.

As per the analysis of Patel et al. (2015, 2016); Pecnik and Patel (2017), Re^*_τ and the semi-local scaling characterize the variable inertia effects. If the characterization is perfect (without involving any assumptions), then the density effect that Foysi et al. (2004) explain, should not be there for two cases with the same Re^*_τ profiles, irrespective of their density profiles, when the equations are semi-locally scaled. In other words, the semi-locally scaled pressure-strain correlation should collapse for two cases with the same Re^*_τ profiles. However, this is not true as seen in figure 7-5, which shows the semi-locally scaled pressure-strain correlation for the low-Mach number cases CP, CRe$^*_\tau$ and CRe$^*_\tau$2. The same figure also shows the density profile for these cases. As seen, the correlation is not fully characterized by Re^*_τ and the difference between CP and the constant Re^*_τ cases intensifies as density gradients become more severe. This is a sufficient proof to say that the reduced pressure-strain correlation is an effect arising due to decreasing density away from the wall, as Foysi et al. (2004) explain. In semi-local sense, this implies that we cannot just scale the pressure-strain correlation by the "local" density, because of the non-locality of this correlation. This non-locality arises because of pressure being governed by a Poisson equation (a Poisson equation implies that any change anywhere in the domain will get instantly translated to all other points in the domain). Kim (1989) discusses this non-local effect on pressure and pressure-strain correlation in detail using a Green's function analysis.

To summarize, the reduced pressure-strain correlation is not a pure compressibility effect, is not an effect due to Re^*_τ gradients, but is an individual property effect which is not fully characterized by semi-local scaling. This tells us about the conditions in which semi-local scaling can fail (like very steep density gradients near the wall). Another interesting question still remains to be answered: Why for the cases of Trettel and Larsson (2016) (table 4-1), despite having steep near-wall density gradients, the transformation seems to work fine (figure 7-1)? The answer again lies in the profile of wall-normal Reynolds stress which is shown in figure 7-6 for the cases M3.0R600 and Moser590. As seen, the delayed rise is also observed in

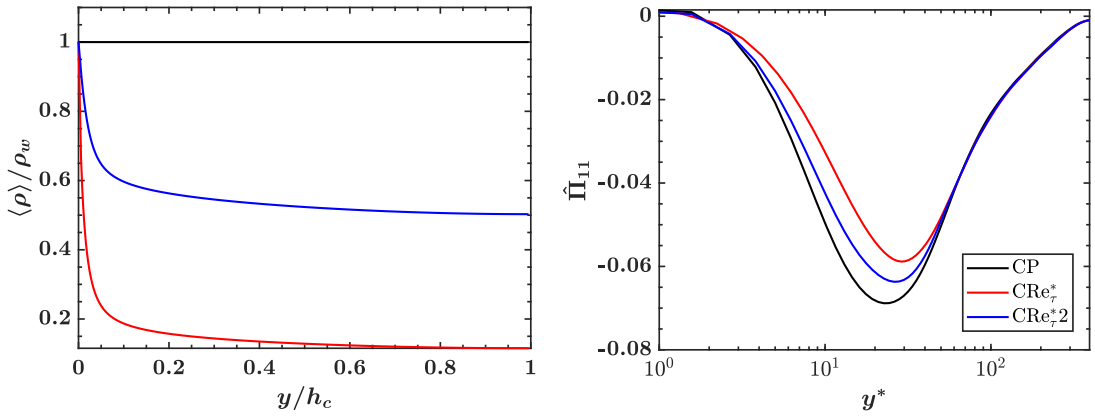

Figure 7-5: Mean density profile scaled by wall density (left) and streamwise component of pressure-strain correlation $\hat{\Pi}_{11}$ (right) for the cases CP, CRe$^*_\tau$ and CRe$^*_\tau$2. Values of $\hat{\Pi}_{11}$ are divided by Re^*_τ.

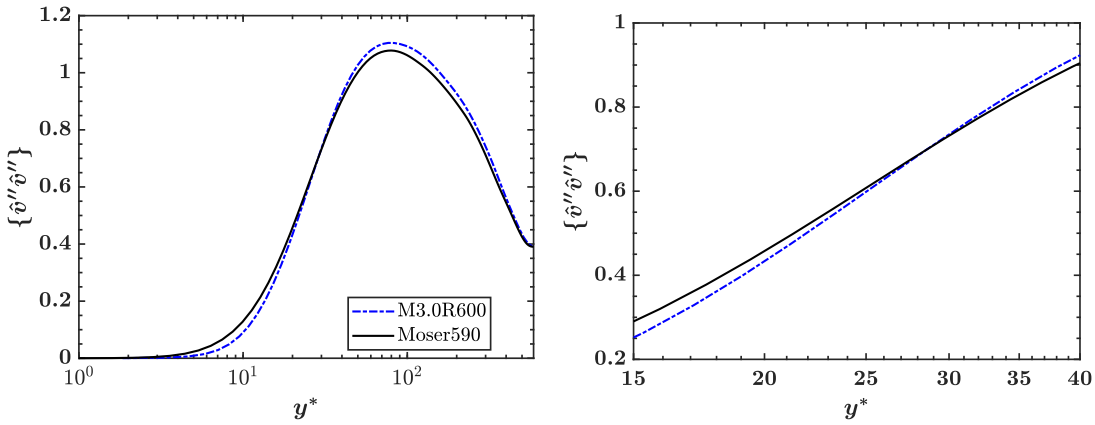

Figure 7-6: Semi-locally scaled wall-normal Reynolds stress ($\{\hat{v}''\hat{v}''\}$) for the cases M3.0R600 and Moser590 (incompressible case from Moser et al. (1999) with $Re_\tau = 590$).

the M3.0R600 case, however, the slope of the rise is much steeper for the M3.0R600 case and this is why around $y^* \approx 30$, its profile crosses the one of Moser590 (figure 7-6 (right)). This eliminates the offset that would have been created due to density gradients. The reason for the increased slope is unclear and is an interesting content for future research.

Chapter 8

Summary and Conclusions

In this thesis, we have rigorously characterized and modeled thermal turbulence in variable property channel flows. Particularly,

- The motivation behind solving RANS models in semi-local form is explained.
- The semi-local scaling framework (previous work of Patel et al. (2015, 2016); Pecnik and Patel (2017)) is presented and semi-local form of the instantaneous enthalpy, enthalpy variance, and turbulent heat flux transport equations are derived.
- DNS simulations are performed for four high-Mach number cases to obtain a database for validating the models, analysing governing parameters and studying the underlying physics of fluctuations in viscous heating. An existing in-house FORTRAN code is used, which has been extended with the implementation of Artificial Bulk Viscosity and Artificial Thermal Conductivity.
- **Low-Mach Number:** An existing DNS database is post-processed, by developing a FORTRAN code, to simplify the enthalpy variance transport equation and to analyse the governing parameters in thermal turbulence. With this knowledge, heat flux models are solved in conventional and semi-local scales.
- **High-Mach Number:** First, the cases with viscous heating are compared with the low-Mach number cases with uniform volumetric heating. Using the DNS simulations performed in-house, the physics of viscous heating and its fluctuations are studied using different correlation coefficients. Effects of viscous heating on the mean enthalpy, enthalpy variance and wall-normal turbulent heat flux is discussed and budgets of enthalpy variance and turbulent heat flux, obtained by post-processing the DNS data, are presented. Comments on the additional governing parameter (modified Eckert number) are made and then finally, RANS equations are solved for these cases using a 2-equation heat flux model.
- Having discussed about the success of semi-local scaling, we also present an important condition under which semi-local scaling can be compromised.

The findings of this thesis will help to improve heat flux modeling for various classes of variable property flows, like supercritical flows. The research outcomes can be further extended to develop robust heat flux models to capture the complex heat transfer characteristics in supercritical fluids. The development of 2-equation heat flux models for compressible flows will prove to be useful in scenarios where the existing tools like constant Pr_t model or Reynolds analogy theories fail. The findings of this thesis are:

Low-Mach Number Cases

1. The additional artifact terms in the enthalpy variance equation (equation (5-5)) are small compared to other budget terms and can be neglected.

2. The collapse in the enthalpy variance budget of the cases CP and CRe$^*_\tau$CPr* in semi-locally scaled form, is a sufficient proof to conclude that, up to a leading order, the variable property effects on thermal turbulence for low-Mach number cases are characterized by Re^*_τ and Pr^*. In other words, two cases with any combination of property profiles would have identical thermal turbulence behaviour provided their Re^*_τ and Pr^* profiles are similar.

3. The semi-locally scaled heat flux models seem to capture the variable inertia effects on thermal turbulence better than their conventionally scaled counterparts.

High-Mach Number Cases

4. The fundamental difference between the low-Mach number uniform heating cases and high-Mach number cases with viscous heating lies in the fact that viscous heating sources are highly non-uniform and are coupled with velocity turbulence. Due to this difference, the findings in Patel et al. (2017) pertaining to scalar transport in low-Mach number cases with uniform heating, does not necessarily hold true for the high-Mach number cases with viscous heating.

5. Fluctuations in the viscous heating source Φ can be caused due to two major reasons: (1) because of the fluctuations in streamwise velocity affecting the instantaneous velocity gradients near the wall, (2) because of passive mixing of TKE dissipation (ϵ), away from the wall.

6. Viscous heating contributes to a source term in the budget of enthalpy variance. This source term is as large as the conventional production term, but it is dominant very close to the wall ($y^* < 10$). The direct contribution of viscous heating to the budget of the wall-normal turbulent heat flux is negligible.

7. Thermal turbulence, unlike in low-Mach number cases, cannot be fully characterized by Re^*_τ and Pr^*. The modified Eckert number ($Ec^*_{\theta_\tau}$) also becomes important.

8. RANS modeling of thermal turbulence in high-Mach number cases cannot be done by simply using the heat flux model equations as for low-Mach number cases. Due to viscous heating, near the wall, the model equations of k_h and ϵ_{kh} are modified. One such modification is modeling of the Φ_{kh} term in the k_h model equation. The model proposed in this thesis for Φ_{kh} is based on physical understanding and hence proves to

be adequate over a range of Mach and Reynolds numbers. More work needs to be done to improve the ϵ_{kh} equation. An appropriate approach would be to derive the exact equation and check what terms, among the new terms arising due to viscous heating, are dominant and need modeling.

General

9. Very steep negative density gradients reduces the inter-component energy transfer from the streamwise fluctuations to the wall-normal and spanwise fluctuations, as was observed in Foysi et al. (2004). However, even in semi-local scales this effect is not characterized and hence two cases with the same Re_τ^* profiles can have different inter-component energy transfers and hence can have different anisotropies.

Appendix A

Derivation of Transport Equations

A-1 Instantaneous Form of the Semi-Local Energy Equation

In this section, detailed derivation of equation (3-15) is presented.

Starting with the dimensional form of the instantaneous energy equation,

$$\rho\frac{\partial h}{\partial t}+\rho u_j\frac{\partial h}{\partial x_j}=\frac{\partial p}{\partial t}+u_j\frac{\partial p}{\partial x_j}+\frac{\partial}{\partial x_j}\left(\alpha\frac{\partial h}{\partial x_j}\right)+\Phi. \tag{A-1}$$

Rewriting equation (A-1) using the continuity equation (2-1) as,

$$\frac{\partial \rho h}{\partial t}+\frac{\partial \rho u_j h}{\partial x_j}=\frac{\partial p}{\partial t}+u_j\frac{\partial p}{\partial x_j}+\frac{\partial}{\partial x_j}\left(\alpha\frac{\partial h}{\partial x_j}\right)+\Phi. \tag{A-2}$$

Introducing the characteristic scales presented in Table 3-2,

$$\begin{aligned}\frac{\partial \hat{\rho}\hat{h}\langle\rho\rangle c_p\theta_\tau^*}{\partial t}+\frac{1}{h_c}\frac{\partial \hat{\rho}\hat{u}_j\hat{h}\langle\rho\rangle u_\tau^* c_p\theta_\tau^*}{\partial \hat{x}_j}=&\frac{\partial \hat{p}\langle\rho\rangle u_\tau^{*^2}}{\partial t}+\hat{u}_j\frac{u_\tau^*}{h_c}\frac{\partial \hat{p}\langle\rho\rangle u_\tau^{*^2}}{\partial \hat{x}_j}\\&+\frac{1}{h_c^2}\frac{\partial}{\partial \hat{x}_j}\left(\hat{\alpha}\langle\alpha\rangle\frac{\partial \hat{h}c_p\theta_\tau^*}{\partial \hat{x}_j}\right)+\hat{\Phi}\frac{\langle\rho\rangle u_\tau^* c_p\theta_\tau^*}{h_c}.\end{aligned} \tag{A-3}$$

We then divide both the sides by $\langle\rho\rangle u_\tau^* c_p\theta_\tau^*/h_c$. Referring equation (3-5), $\langle\rho\rangle u_\tau^* c_p\theta_\tau^*$ represents q_w, which is a constant, and thus, can be moved inside/outside the derivatives. Similarly, $\langle\rho\rangle u_\tau^{*^2}$ represents τ_w and thus can be moved inside/outside derivatives. We get,

$$t_\tau^*\frac{\partial \hat{\rho}\hat{h}}{\partial t}+\frac{\partial \hat{\rho}\hat{u}_j\hat{h}}{\partial \hat{x}_j}=Ec_{\theta_\tau}^*\left(t_\tau^*\frac{\partial \hat{p}}{\partial t}+\hat{u}_j\frac{\partial \hat{p}}{\partial \hat{x}_j}\right)+\frac{\partial}{\partial \hat{x}_j}\left(\frac{\hat{\alpha}}{Re_\tau^* Pr^*\theta_\tau^*}\frac{\partial \hat{h}\theta_\tau^*}{\partial \hat{x}_j}\right)+\hat{\Phi}. \tag{A-4}$$

$Ec_{\theta_\tau}^*$ is defined as $u_\tau^{*^2}/(c_p\theta_\tau^*)$. Applying chain rule on the derivative, $\partial\hat{h}\theta_\tau^*/\partial\hat{x}_j$ we get,

$$t_\tau^*\frac{\partial \hat{\rho}\hat{h}}{\partial t}+\frac{\partial \hat{\rho}\hat{u}_j\hat{h}}{\partial \hat{x}_j}=Ec_{\theta_\tau}^*\left(t_\tau^*\frac{\partial \hat{p}}{\partial t}+\hat{u}_j\frac{\partial \hat{p}}{\partial \hat{x}_j}\right)+\frac{\partial}{\partial \hat{x}_j}\left(\frac{\hat{\alpha}}{Re_\tau^* Pr^*}\frac{\partial \hat{h}}{\partial \hat{x}_j}\right)+\frac{\partial}{\partial \hat{x}_j}\left(\frac{\hat{\alpha}\hat{h}}{Re_\tau^* Pr^*\theta_\tau^*}\frac{\partial \theta_\tau^*}{\partial \hat{x}_j}\right)+\hat{\Phi}. \tag{A-5}$$

Using equation (3-7), we can write,

$$\frac{\partial \theta_\tau^*}{\partial \hat{x}_j} = -\theta_\tau^* d_j, \tag{A-6}$$

where,

$$d_j = \frac{1}{2\langle\rho\rangle}\frac{\partial\langle\rho\rangle}{\partial \widehat{x}_j}. \tag{A-7}$$

Incorporating the continuity equation (3-8) in the left hand side of equation (A-5) we get,

$$t_\tau^*\hat{\rho}\frac{\partial \hat{h}}{\partial t} + \hat{\rho}\hat{u}_j\frac{\partial \hat{h}}{\partial \hat{x}_j} - \hat{\rho}\hat{u}_j\hat{h}d_j = Ec_{\theta_\tau}^*\left(t_\tau^*\frac{\partial \hat{p}}{\partial t} + \hat{u}_j\frac{\partial \hat{p}}{\partial \hat{x}_j}\right) + \frac{\partial \hat{q}_j}{\partial \hat{x}_j} - \frac{\partial \hat{D}_j}{\partial \hat{x}_j} + \hat{\Phi}, \tag{A-8}$$

where,

$$\hat{q}_j = \hat{\alpha}/(Re_\tau^* Pr^*)\partial\hat{h}/\partial\hat{x}_j, \tag{A-9}$$

and,

$$\hat{D}_j = \hat{\alpha}/(Re_\tau^* Pr^*)\hat{h}d_j. \tag{A-10}$$

A-2 Semi-Locally Scaled Enthalpy Variance Budget

In this section we will derive equation (3-34) in detail. The derivation steps of only the terms coming out of temporal, advection and density related terms in the enthalpy transport equation, will be shown. The other terms in the budget can be derived in a similar manner and their steps of derivation are quite straightforward.

The equations are derived using a recipe similar to what is used for constant property flows:

$$\overline{\hat{h}''\mathcal{H}(\hat{h})} = 0, \tag{A-11}$$

where $\mathcal{H}(\hat{h}) = 0$ is semi-locally scaled instantaneous energy equation (equation (3-15)).

Throughout the derivation, the following identities will be frequently used,

$$\overline{\hat{\rho}\hat{\gamma}} = \{\hat{\gamma}\},$$

and,

$$\overline{\hat{\rho}\hat{\gamma}''} = 0.$$

Temporal:

$$\overline{t_\tau^*\hat{h}''\hat{\rho}\frac{\partial \hat{h}}{\partial t}} = \overline{t_\tau^*\hat{h}''\hat{\rho}\frac{\partial \hat{h}''}{\partial t}},$$

$$= \overline{t_\tau^*\hat{\rho}\frac{\partial}{\partial t}\left(\hat{h}''\hat{h}''/2\right)},$$

$$= \underbrace{t_\tau^*\frac{\partial}{\partial t}\left\{\hat{k}_h\right\}}_{} - \underbrace{\overline{\hat{k}_h t_\tau^*\frac{\partial \hat{\rho}}{\partial t}}}_{\text{A}}.$$

Advection:

$$\overline{\hat{\rho}\hat{u}_j\hat{h}''\frac{\partial\hat{h}}{\partial\hat{x}_j}}.$$

Velocity and enthalpy are written using Favre decomposition. We get,

$$\underbrace{\overline{\hat{\rho}\left\{\hat{u}_j\right\}\hat{h}''\frac{\partial\{\hat{h}\}}{\partial\hat{x}_j}}}_{=0},\quad \underbrace{\overline{\hat{\rho}\hat{u}_j''\hat{h}''}\frac{\partial\{\hat{h}\}}{\partial\hat{x}_j}}_{\text{II}},\quad \underbrace{\overline{\hat{\rho}\left\{\hat{u}_j\right\}\hat{h}''\frac{\partial\hat{h}''}{\partial\hat{x}_j}}}_{\text{III}},\quad \underbrace{\overline{\hat{\rho}\hat{h}''\hat{u}_j''\frac{\partial\hat{h}''}{\partial\hat{x}_j}}}_{\text{IV}}.$$

Term III gives,

$$\underbrace{\frac{\partial}{\partial\hat{x}_j}\left(\left\{\hat{k}_h\right\}\left\{\hat{u}_j\right\}\right)}-\underbrace{\overline{\hat{k}_h\frac{\partial}{\partial\hat{x}_j}\left(\hat{\rho}\left\{\hat{u}_j\right\}\right)}}_{\text{B}}.$$

Term IV can be written as,

$$\overline{\hat{\rho}\hat{u}_j''\frac{\partial}{\partial\hat{x}_j}\left(\hat{k}_h\right)}=\underbrace{\frac{\partial}{\partial\hat{x}_j}\left\{\hat{k}_h\hat{u}_j''\right\}}-\underbrace{\overline{\hat{k}_h\frac{\partial}{\partial\hat{x}_j}\left(\hat{\rho}\hat{u}_j''\right)}}_{\text{C}}.$$

Term II can be written as,

$$\overline{\hat{\rho}\hat{u}_j''\hat{h}''}\frac{\partial\{\tilde{h}\}\sqrt{\overline{\rho}/\rho_w}}{\partial\hat{x}_j},$$

which can be expanded to give,

$$\overline{\hat{\rho}\hat{u}_j''\hat{h}''}\frac{\partial\left\{h^{vD}\right\}}{\partial\hat{x}_j}+\overline{\hat{\rho}\hat{u}_j''\hat{h}''}\frac{\left\{\tilde{h}\right\}}{\sqrt{\rho_w}}\frac{\partial\sqrt{\overline{\rho}}}{\partial\hat{x}_j}.$$

Using,

$$\frac{\partial\sqrt{\overline{\rho}}}{\partial\hat{x}_j}=\frac{1}{2\sqrt{\overline{\rho}}}\frac{\partial\overline{\rho}}{\partial\hat{x}_j}=\sqrt{\overline{\rho}}d_j,$$

we finally get,

$$\underbrace{\left\{\hat{u}_j''\hat{h}''\right\}\frac{\partial\left\{h^{vD}\right\}}{\partial\hat{x}_j}}+\underbrace{\left\{\hat{u}_j''\hat{h}''\right\}\{\hat{h}\}d_j}_{\text{P}}.$$

Terms A,B and C can be combined with the continuity equation (3-8) to give,

$$\underbrace{\overline{\hat{\rho}\hat{u}_j\hat{k}_h}d_j}_{\text{R}}.$$

Density Related Terms

$$\overline{-\hat{\rho}\hat{u}_j\hat{h}d_j\hat{h}''}.$$

The velocity and enthalpy are written using Favre decomposition. The terms obtained are,

$$\underbrace{\overline{-\hat{\rho}\left\{\hat{u}_j\right\}\left\{\hat{h}\right\}d_j\hat{h}''}}_{=0},\quad \underbrace{\overline{-\hat{\rho}\hat{u}_j''\{\hat{h}\}d_j\hat{h}''}}_{\text{P2}},\quad \underbrace{\overline{-\hat{\rho}\left\{\hat{u}_j\right\}\hat{h}''d_j\hat{h}''}}_{\text{J}},\quad \underbrace{\overline{-\hat{\rho}\hat{u}_j''\hat{h}''d_j\hat{h}''}}_{K}.$$

Term P2 is cancelled with P.

Terms J and K are combined to give,

$$\overline{-\hat{\rho}\hat{u}_j\hat{h}''\hat{h}''}d_j = \overline{-2\hat{\rho}\hat{u}_j\hat{k}_h}d_j.$$

Terms J,K and R when added, finally give,

$$\overline{-\hat{\rho}\hat{u}_j\hat{k}_h}d_j,$$

which is equal to,

$$\underbrace{-\left\{\hat{k}_h\right\}\left\{\hat{u}_j\right\}d_j - \left\{\hat{k}_h\hat{u}_j''\right\}d_j}.$$

The terms with red underbraces are the ones pending and show up in the final equation.

Likewise, if we repeat the steps for other terms, and by simple grouping as shown in table 3-4, we end up with the final equation (3-34).

A-3 Semi-Locally Scaled Turbulent Heat Flux Budget

In this section we will derive equation (3-40) in detail. The derivation steps of only the terms coming out of temporal, advection and density related terms in the enthalpy and momentum transport equation, will be shown. The other terms in the budget can be derived in a similar manner and the steps of derivation are quite straightforward.

The equations are derived using a recipe similar to what is used for constant property flows:

$$\overline{\hat{h}''\mathcal{N}(\hat{u}_i) + \hat{u_i}''\mathcal{H}(\hat{h})} = 0, \tag{A-12}$$

where $\mathcal{N}(\hat{u}_i) = 0$ and $\mathcal{H}(\hat{h}) = 0$ are semi-locally scaled instantaneous momentum and energy equations (3-9 and 3-15) respectively.

Throughout the derivation, the following identities will be frequently used,

$$\overline{\hat{\rho}\hat{\gamma}} = \{\hat{\gamma}\},$$

and,

$$\overline{\hat{\rho}\hat{\gamma}''} = 0.$$

Temporal:

$$\overline{t_\tau^*\left(\hat{u}_i''\hat{\rho}\frac{\partial\hat{h}}{\partial t}+\hat{h}''\hat{\rho}\frac{\partial\hat{u}_i}{\partial t}\right)}=\overline{t_\tau^*\left(\hat{u}_i''\hat{\rho}\frac{\partial\hat{h}''}{\partial t}+\hat{h}''\hat{\rho}\frac{\partial\hat{u}_i''}{\partial t}\right)},$$

$$=\overline{t_\tau^*\hat{\rho}\frac{\partial}{\partial t}\left(\hat{u}_i''\hat{h}''\right)},$$

$$=\underbrace{t_\tau^*\frac{\partial}{\partial t}\left\{\hat{u}_i''\hat{h}''\right\}}-\underbrace{\overline{\hat{u}_i''\hat{h}''t_\tau^*\frac{\partial\hat{\rho}}{\partial t}}}_{\text{A}}.$$

Advection:

$$\overline{\hat{\rho}\hat{u}_j\hat{u}_i''\frac{\partial\hat{h}}{\partial\hat{x}_j}+\hat{\rho}\hat{u}_j\hat{h}''\frac{\partial\hat{u}_i}{\partial\hat{x}_j}}.$$

Velocity and enthalpy are written using Favre decomposition. From first term above, we get,

$$\underbrace{\overline{\hat{\rho}\left\{\hat{u}_j\right\}\hat{u}_i''\frac{\partial\{\hat{h}\}}{\partial\hat{x}_j}}}_{=0},\quad\underbrace{\overline{\hat{\rho}\hat{u}_j''\hat{u}_i''\frac{\partial\{\hat{h}\}}{\partial\hat{x}_j}}}_{\text{II}},\quad\underbrace{\overline{\hat{\rho}\left\{\hat{u}_j\right\}\hat{u}_i''\frac{\partial\hat{h}''}{\partial\hat{x}_j}}}_{\text{III}},\quad\underbrace{\overline{\hat{\rho}\hat{u}_i''\hat{u}_j''\frac{\partial\hat{h}''}{\partial\hat{x}_j}}}_{\text{IV}},$$

and from the second term, we get,

$$\underbrace{\overline{\hat{\rho}\left\{\hat{u}_j\right\}\hat{h}''\frac{\partial\{\hat{u}_i\}}{\partial\hat{x}_j}}}_{=0},\quad\underbrace{\overline{\hat{\rho}\hat{u}_j''\hat{h}''\frac{\partial\left\{\hat{u}_i\right\}}{\partial\hat{x}_j}}}_{\text{VI}},\quad\underbrace{\overline{\hat{\rho}\left\{\hat{u}_j\right\}\hat{h}''\frac{\partial\hat{u}_i''}{\partial\hat{x}_j}}}_{\text{VII}},\quad\underbrace{\overline{\hat{\rho}\hat{u}_j''\hat{h}''\frac{\partial\hat{u}_i''}{\partial\hat{x}_j}}}_{\text{VIII}}.$$

Terms III and VII give,

$$\underbrace{\frac{\partial}{\partial\hat{x}_j}\left(\left\{\hat{h}''\hat{u}_i''\right\}\left\{\hat{u}_j\right\}\right)}-\underbrace{\overline{\hat{h}''\hat{u}_i''\frac{\partial}{\partial\hat{x}_j}\left(\hat{\rho}\left\{\hat{u}_j\right\}\right)}}_{\text{B}}.$$

Terms IV and VIII can be combined to give,

$$\overline{\hat{\rho}\hat{u}_j''\frac{\partial}{\partial\hat{x}_j}\left(\hat{h}''\hat{u}_i''\right)},$$

which can be written as,

$$\overline{\hat{\rho}\hat{u}_j''\frac{\partial}{\partial\hat{x}_j}\left(\hat{h}''\hat{u}_i''\right)}=\underbrace{\frac{\partial}{\partial\hat{x}_j}\left\{\hat{h}''\hat{u}_i''\hat{u}_j''\right\}}-\underbrace{\overline{\hat{h}''\hat{u}_i''\frac{\partial}{\partial\hat{x}_j}\left(\hat{\rho}\hat{u}_j''\right)}}_{\text{C}}.$$

Term II can be written as,

$$\overline{\hat{\rho}\hat{u}_j''\hat{u}_i''}\frac{\partial\{\tilde{h}\}\sqrt{\bar{\rho}/\rho_w}}{\partial\hat{x}_j},$$

which can be expanded to give,

$$\overline{\hat{\rho}\hat{u}_j''\hat{u}_i''}\frac{\partial\left\{h^{vD}\right\}}{\partial\hat{x}_j}+\overline{\hat{\rho}\hat{u}_j''\hat{u}_i''}\frac{\left\{\tilde{h}\right\}}{\sqrt{\rho_w}}\frac{\partial\sqrt{\bar{\rho}}}{\partial\hat{x}_j}.$$

Using,

$$\frac{\partial\sqrt{\bar{\rho}}}{\partial\hat{x}_j}=\frac{1}{2\sqrt{\bar{\rho}}}\frac{\partial\bar{\rho}}{\partial\hat{x}_j}=\sqrt{\bar{\rho}}d_j,$$

we finally get,

$$\underbrace{\left\{\hat{u}_i''\hat{u}_j''\right\}\frac{\partial\left\{h^{vD}\right\}}{\partial\hat{x}_j}}+\underbrace{\left\{\hat{u}_j''\hat{u}_i''\right\}\{\hat{h}\}d_j}_{\text{P}}.$$

Likewise doing the same for term VI, we get,

$$\underbrace{\left\{\hat{h}''\hat{u}_j''\right\}\frac{\partial\left\{u_i^{vD}\right\}}{\partial\hat{x}_j}}+\underbrace{\left\{\hat{u}_j''\hat{h}''\right\}\{\hat{u}_i\}d_j}_{\text{Q}}.$$

Terms A,B and C can be combined with the continuity equation (3-8) to give,

$$\underbrace{\overline{\hat{\rho}\hat{u}_j\hat{u}_i''\hat{h}''}d_j}_{\text{R}}.$$

Density Related Terms

$$\overline{-\hat{\rho}\hat{u}_j\hat{h}d_j\hat{u}_i''-\hat{\rho}\hat{u}_i\hat{u}_jd_j\hat{h}''}.$$

The velocity and enthalpy are written using Favre decomposition. The terms obtained from the first term above are,

$$\underbrace{\overline{-\hat{\rho}\{\hat{u}_j\}\{\hat{h}\}d_j\hat{u}_i''}}_{=0},\quad\underbrace{\overline{-\hat{\rho}\hat{u}_j''\{\hat{h}\}d_j\hat{u}_i''}}_{\text{P2}},\quad\underbrace{\overline{-\hat{\rho}\{\hat{u}_j\}\hat{h}''d_j\hat{u}_i''}}_{\text{J}},\quad\underbrace{\overline{-\hat{\rho}\hat{u}_j''\hat{h}''d_j\hat{u}_i''}}_{K},$$

and from the second term are,

$$\underbrace{\overline{-\hat{\rho}\{\hat{u}_j\}\{\hat{u}_i\}d_j\hat{h}''}}_{=0},\quad\underbrace{\overline{-\hat{\rho}\hat{u}_j''\{\hat{u}_i\}d_j\hat{h}''}}_{\text{Q2}},\quad\underbrace{\overline{-\hat{\rho}\{\hat{u}_j\}\hat{u}_i''d_j\hat{h}''}}_{\text{L}},\quad\underbrace{\overline{-\hat{\rho}\hat{u}_j''\hat{u}_i''d_j\hat{h}''}}_{\text{M}}.$$

Terms P2 and Q2 are cancelled with P and Q.

Terms J and K are combined to give,

$$\overline{-\hat{\rho}\hat{u}_j\hat{h}''\hat{u}_i''}d_j.$$

Also, terms L and M are combined to give,

$$\overline{-\hat{\rho}\hat{u}_j\hat{h}''\hat{u}_i''}d_j.$$

Terms J,K,L,M and R when added, finally give,

$$\overline{-\hat{\rho}\hat{u}_j\hat{h}''\hat{u}_i''}d_j,$$

which is equal to,

$$\underbrace{-\left\{\hat{h}''\hat{u}_i''\right\}\{\hat{u}_j\}\,d_j - \left\{\hat{h}''\hat{u}_i''\hat{u}_j''\right\}d_j}\,.$$

The terms with red underbraces are the ones pending and show up in the final equation.

Likewise, if we repeat the steps for other terms, and by simple grouping as shown in table 3-5, we end up with the final equation (3-40).

Appendix B

Description of the DNS code

The DNS code used in this thesis is developed in-house by the Fluid Dynamics of Energy Systems team headed by Dr. R. Pecnik . The equations solved in the code are,

$$\begin{aligned} \frac{\partial \rho}{\partial t} + \frac{\partial \rho u_i}{\partial x_i} &= 0, \\ \frac{\partial \rho u_i}{\partial t} + \frac{\partial \rho u_i u_j}{\partial x_j} &= -\frac{\partial p}{\partial x_i} + \frac{\partial \tau_{ij}}{\partial x_j} + f\delta_{i1}, \\ \frac{\partial \rho E}{\partial t} + \frac{\partial \rho u_j E}{\partial x_j} &= -\frac{\partial p u_j}{\partial x_j} - \frac{\partial q_j}{\partial x_j} + \frac{\partial \tau_{ij} u_i}{\partial x_j} + f u_1, \end{aligned} \tag{B-1}$$

where,

$$\begin{aligned} \tau_{ij} &= \mu \left(\frac{\partial u_i}{\partial x_j} + \frac{\partial u_j}{\partial x_i} - \frac{2}{3} \frac{\partial u_k}{\partial x_k} \delta_{ij} \right), \\ q_j &= -\lambda \frac{\partial T}{\partial x_j}. \end{aligned} \tag{B-2}$$

They are similar to the ones described in chapter 2, but in the energy equation, instead of solving for enthalpy, the code solves for total energy defined as,

$$E = i + \frac{1}{2} \left(u^2 + v^2 + w^2 \right), \tag{B-3}$$

where i is the internal energy per unit mass and the second term on right hand side represents total kinetic energy per unit mass. The equations in the code are non-dimensionalized using bulk velocity (U_b), bulk density (ρ_b), wall temperature (T_w) and channel half height (h_c). The energy equation is chosen to be non-dimensionalized using a scale of energy as U_b^2. This non-dimensionalization leads to viscosity as $(\mu/\mu_w)/Re_b$ and thermal conductivity as $(\lambda/\lambda_w)/(Re_b PrEc)$, where Re_b is defined as,

$$Re_b = \frac{\rho_b U_b h_c}{\mu_w}. \tag{B-4}$$

The Eckert number depends on the bulk Mach number (for ideal gases) as,

$$Ec_b = (\gamma - 1)Ma_b^2, \tag{B-5}$$

where γ is the ratio of specific heats. Ma_b is defined as,

$$Ma_b = \frac{U_b}{c_w}, \tag{B-6}$$

where c_w is the speed of sound computed at the wall.

The significant inputs required by the code are: Re_b, Ma_b, Pr, γ. Apart from these, the viscosity and thermal conductivity laws (as a function of temperature, for instance) also need to be provided. In equation (B-1), the term "f" is an external body force term which is required to maintain the flow in the channel (analogous to pressure gradient in the streamwise direction in pressure driven flows). The body force term is computed by an iterative algorithm, such that it ensures a desired mass flux in the channel. The power input to the domain associated with the body force term is added at the end of the energy equation.

For a fully developed channel flow, the spanwise and streamwise directions are periodic and hence they are discretized uniformly. The discretization in the wall-normal direction uses a hyperbolic tangent function to ensure clustering of cells near the walls. The code uses a Cartesian collocated grid arrangement, which implies that there exists a computational point at the wall. This simplifies the incorporation of boundary conditions. In a staggered grid arrangement, the wall coincides with intermediate nodes where fluxes are computed. Even though, this enables specification of a zero convective flux at the wall which in turn ensures strict mass conservation, it complicates the incorporation of boundary conditions.

At the walls, the code incorporates no-slip, no-penetration boundary conditions for velocities, isothermal boundary condition (Dirichlet) for temperature and a zero pressure-gradient (Neumann) boundary condition for pressure. A periodic boundary condition is used in the streamwise and spanwise directions.

The convective terms in equation (B-1) are discretized using the energy conserving split-formulation presented in Pirozzoli (2010). The code is based on a standard central finite differencing scheme of sixth-order for the convective terms. The viscous terms in the momentum equations are split into Laplacian form to avoid even-odd decoupling phenomena (Bernardini et al., 2021) and are discretized using a fourth-order standard central finite differencing scheme. Time advancement in the code uses an explicit third-order Runge-Kutta scheme (Gottlieb and Shu, 1998).

For the constant Re_τ^* cases, the same value of Re_τ^* was desired for two cases with different Mach numbers, but the DNS code takes the bulk Reynolds number as an input. The bulk Reynolds number entered in the code should be such that the semi-local Reynolds number obtained is of the desired value. There was a need to relate these two. This was done by using a MATLAB code which solves RANS equations using a 2-equation Nagano and Shimada (1996) turbulent stress model and a constant Pr_t model. The equations in the RANS code are non-dimensionalized using the friction velocity u_τ and ρ_w, and thus it takes Re_τ as an input. Providing the required Re_τ and property laws to maintain constant Re_τ^*, we get an approximate estimate of Re_b (bulk Reynolds number) which acts as an input to the DNS code. The bulk Reynolds number estimate from RANS is very close to the required value so as to

attain the desired Re_τ^*. Also, the temperature and velocity profiles obtained from RANS are used to build an initial condition for the DNS and this considerably reduces computational time.

B-1 Artificial Diffusivities for Shock Capturing

Artificial Diffusivities are those that do not carry a physical relevance but are added to make the code numerically stable in case of discontinuities in the domain (shock waves). A shock wave is a discontinuity encountered in compressible flows and it is so thin that one would need a very fine mesh to resolve it. Differentiation across such a discontinuity without sufficient resolution leads to spurious oscillations which might blow up the solution. Such discontinuities are artificially thickened using artificial diffusivities, such that the mesh resolution is sufficient to resolve it. Because they are unphysical, it is necessary to limit them only where required, for instance, very close to the discontinuities.

The implementation of the Artificial Bulk Viscosity (ABV) and the Artificial Thermal Conductivity (ATC) in the code was done as a part of this thesis. The code uses the formulation of Kawai et al. (2010), which is built upon the work of Cook and Cabot (2005) and Mani et al. (2009). ABV is computed in the code as,

$$\beta^* = C_\beta \rho f_{sw} \overline{\left| \sum_{l=1}^{3} \frac{\partial^4 \mathcal{F}_\beta}{\partial x_l^4} \Delta x_l^4 \Delta_{l,\beta}^2 \right|}, \tag{B-7}$$

where C_β is a constant taken as 1.0, ρ is fluid density, f_{sw} is a switching function (shock sensor) intended to remove ABV from places where it is not required (regions without shocks). It is defined as,

$$f_{sw} = H(-\nabla \cdot \boldsymbol{u}) \underbrace{\frac{(\nabla \cdot \boldsymbol{u})^2}{(\nabla \cdot \boldsymbol{u})^2 + |\nabla \times \boldsymbol{u}|^2 + \varepsilon}}_{D}, \tag{B-8}$$

where $H(-\nabla \cdot \boldsymbol{u})$ is the Heavyside function that ensures that ABV is not added in the regions with positive $\nabla \cdot \boldsymbol{u}$. This is because a shock can occur only in regions of $\nabla \cdot \boldsymbol{u} < 0$. The term D is a Ducros-type shock sensor so as to localize ABV only in the regions where there is a discontinuity (shock). ε is a small number to avoid division by zero in regions where both dilatation and vorticity are zero. $\mathcal{F}_\beta$ was chosen to be the magnitude of the strain rate tensor (S) by Cook and Cabot (2005). However, Mani et al. (2009) showed that using S as the function adds unnecessary ABV in the vortical regions of the flow, where S is non-zero, despite no sign of a shock there. This is why, Mani et al. (2009) proposed to replace S by $\nabla \cdot \boldsymbol{u}$ stating that near the shocks both the choices are equivalent, however, away from the shocks in the vortical regions, choosing $\nabla \cdot \boldsymbol{u}$ leads to very low ABV, as $\nabla \cdot \boldsymbol{u} << S$, which is desired. Δx_l is the grid spacing in the x, y and z ($l = 1, 2, 3$) directions. $\Delta_{l,\beta}$ is a suitable length scale so as to construct the dimensions of viscosity. $\Delta_{l,\beta}$ was approximated as $V^{0.33}$ by Cook and Cabot (2005) (where V is the volume of the cell). Such a length scale would work in the case of isotropic grids. For anisotropic grids, the formulation of Mani et al. (2009) is chosen in the code as,

$$\Delta_{l,\beta} = \left| \Delta \boldsymbol{x}_l \cdot \frac{\boldsymbol{\nabla \rho}}{|\boldsymbol{\nabla \rho}|} \right|, \tag{B-9}$$

which signifies that the suitable length scale is the grid spacing projected along the vector normal to the shock. $\overline{(.)}$ in equation (B-7) should not be confused with the usual Reynolds averaging operator. Here it signifies a gaussian filter, so as to obtain a smooth distribution of ABV.

The implementation of ATC is similar to that of ABV, however, the detail mathematical formulations can be referred in Kawai et al. (2010). The major difference lies in the fact that instead of using $\nabla \cdot \boldsymbol{u}$ as $\mathcal{F}_\beta$, internal energy per unit mass (i or e) is used.

Having presented the mathematics behind the formulation of ABV, one would like to know the reasoning that leads to the formulation. Mani et al. (2009) discusses that using ABV is better than using Artificial Viscosity (μ^*) because ABV acts on $\nabla \cdot \boldsymbol{u}$ in the momentum equation, and thus, it has little to no role to play in the vorticity equation. The vorticity equation (taken from Mani et al. (2009)) is,

$$\frac{d\omega}{dt} = RHS_1 - \underbrace{\frac{\nabla \rho}{\rho^2}}_{A} \times \underbrace{\nabla \left[\beta^* (\nabla \cdot \boldsymbol{u})\right]}_{B}. \tag{B-10}$$

Both the terms A and B are majorly oriented along the shock (because that is where one would have maximum variation in density and in dilatation), and hence are parallel. Thus, their cross product would be small. However, ABV contributes to an additional term in the dilation transport equation. Thus, away from the shock, if ABV is higher, then it would affect the physics associated with sound waves. This is why it is necessary to ensure that the ABV is small in the regions away from shock waves. This is ensured by using $\mathcal{F}_\beta$ as dilation and not S as discussed above. The order of the derivative of $\mathcal{F}_\beta$ in equation (B-7) would influence the distribution of ABV. Higher order implies that the ABV is localized in the region of discontinuity (Kawai et al., 2010).

Appendix C

Validation of the DNS and RANS Codes

The DNS code is validated against the data of Trettel and Larsson (2016) as shown in figures C-1 and C-2.

The implementation of the RANS model is validated with the fully developed channel flow results in Nagano and Shimada (1996). The validation is shown in figure C-3.

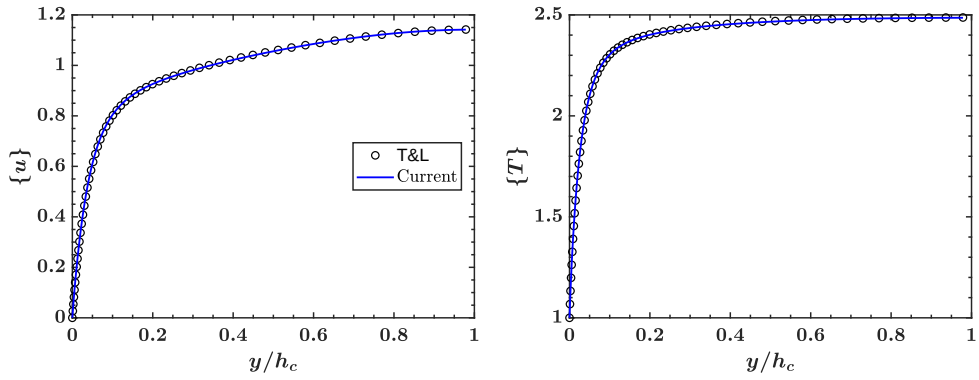

Figure C-1: Velocity (left) and temperature (right) profiles for the case M3.0R200, computed using the in-house code, and validated with the data of Trettel and Larsson (2016).

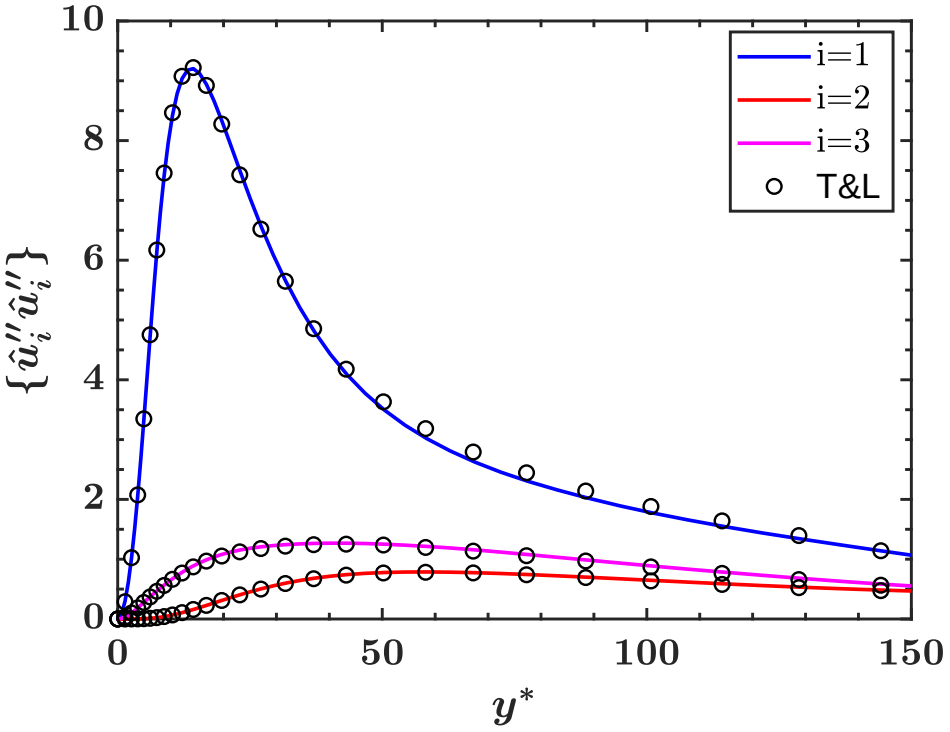

Figure C-2: Normal Reynolds stresses computed using the in-house code (lines) and validated with Trettel and Larsson (2016) for the case M3.0R200.

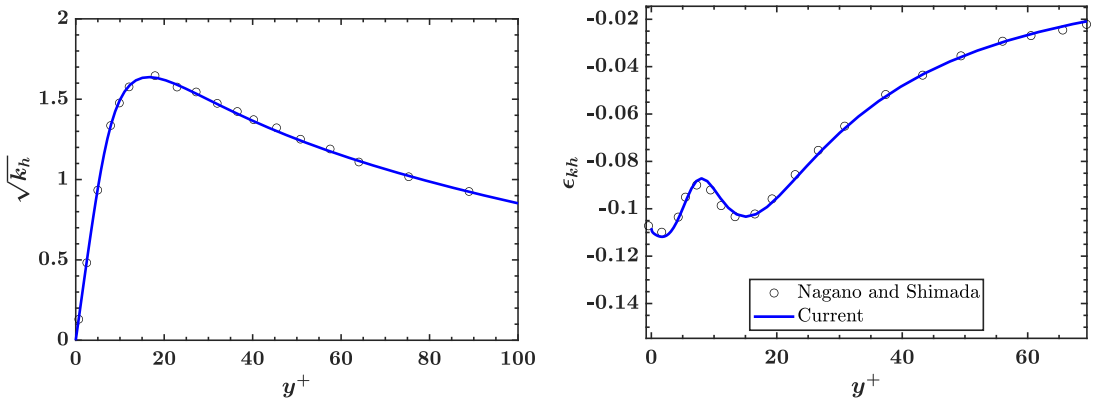

Figure C-3: Square-root of enthalpy variance (left) and its dissipation (right) for a fully developed channel flow with $Re_\tau = 180$ and $Pr = 0.71$.

Bibliography

K. Abe, T. Kondoh, and Y. Nagano. A new turbulence model for predicting fluid flow and heat transfer in separating and reattaching flows—ii. thermal field calculations. *International Journal of Heat and Mass Transfer*, 38(8):1467–1481, 1995.

R. Antonia, A. Chambers, and C. Friehe. Note on the viscous heating term in the temperature variance equation. *Boundary-Layer Meteorology*, 19(3):269–272, 1980.

C. Beguier, I. Dekeyser, and B. Launder. Ratio of scalar and velocity dissipation time scales in shear flow turbulence. *The Physics of Fluids*, 21(3):307–310, 1978.

M. Bernardini, D. Modesti, F. Salvadore, and S. Pirozzoli. Streams: A high-fidelity accelerated solver for direct numerical simulation of compressible turbulent flows. *Computer Physics Communications*, 263:107906, 2021.

R. D. Cess. A survey of the literature on heat transfer in turbulent tube flow. *Res. Rep*, pages 8–0529, 1958.

G. N. Coleman, J. Kim, and R. D. Moser. A numerical study of turbulent supersonic isothermal-wall channel flow. *Journal of Fluid Mechanics*, 305:159–183, 1995.

A. W. Cook and W. H. Cabot. Hyperviscosity for shock-turbulence interactions. *Journal of Computational Physics*, 203(2):379–385, 2005.

S. Corrsin. Heat transfer in isotropic turbulence. *Journal of Applied Physics*, 23(1):113–118, 1952.

B. Deng, W. Wu, and S. Xi. A near-wall two-equation heat transfer model for wall turbulent flows. *International journal of heat and mass transfer*, 44(4):691–698, 2001.

P. A. Durbin. Near-wall turbulence closure modeling without "damping functions". *Theoretical and computational fluid dynamics*, 3(1):1–13, 1991.

P. A. Durbin. Separated flow computations with the k-epsilon-v-squared model. *AIAA journal*, 33(4):659–664, 1995.

H. Foysi, S. Sarkar, and R. Friedrich. Compressibility effects and turbulence scalings in supersonic channel flow. *Journal of Fluid Mechanics*, 509:207–216, 2004.

S. Gottlieb and C.-W. Shu. Total variation diminishing runge-kutta schemes. *Mathematics of computation*, 67(221):73–85, 1998.

K. Hanjalić and B. E. Launder. Contribution towards a reynolds-stress closure for low-reynolds-number turbulence. *Journal of Fluid Mechanics*, 74(4):593–610, 1976.

S. Hoyas and J. Jiménez. Scaling of the velocity fluctuations in turbulent channels up to re τ= 2003. *Physics of fluids*, 18(1):011702, 2006.

P. G. Huang, G. N. Coleman, and P. Bradshaw. Compressible turbulent channel flows: Dns results and modelling. *Journal of Fluid Mechanics*, 305:185–218, 1995. doi: 10.1017/S0022112095004599.

W. Jones and B. Launder. The calculation of low-reynolds-number phenomena with a two-equation model of turbulence. *International Journal of Heat and Mass Transfer*, 16(6): 1119–1130, 1973.

B. A. Kader. Temperature and concentration profiles in fully turbulent boundary layers. *International journal of heat and mass transfer*, 24(9):1541–1544, 1981.

N. Kasagi and Y. Ohtsubo. Direct numerical simulation of low prandtl number thermal field in a turbulent channel flow. In *Turbulent Shear Flows 8*, pages 97–119. Springer, 1993.

N. Kasagi, Y. Tomita, and A. Kuroda. Direct numerical simulation of passive scalar field in a turbulent channel flow. *Journal of Heat Transfer (Transactions of the ASME (American Society of Mechanical Engineers), Series C);(United States)*, 114(3), 1992.

S. Kawai, S. K. Shankar, and S. K. Lele. Assessment of localized artificial diffusivity scheme for large-eddy simulation of compressible turbulent flows. *Journal of Computational Physics*, 229(5):1739–1762, 2010.

H. Kawamura, K. Ohsaka, H. Abe, and K. Yamamoto. Dns of turbulent heat transfer in channel flow with low to medium-high prandtl number fluid. *International Journal of Heat and Fluid Flow*, 19(5):482–491, 1998.

H. Kawamura, H. Abe, and Y. Matsuo. Dns of turbulent heat transfer in channel flow with respect to reynolds and prandtl number effects. *International Journal of Heat and Fluid Flow*, 20(3):196–207, 1999.

J. Kim. On the structure of pressure fluctuations in simulated turbulent channel flow. *Journal of Fluid Mechanics*, 205:421–451, 1989.

J. Kim and P. Moin. Transport of passive scalars in a turbulent channel flow. In *Turbulent Shear Flows 6*, pages 85–96. Springer, 1989.

B. Launder. Heat and mass transport. In *Turbulence*, pages 231–287. Springer, 1976.

J. Lee, S. Y. Jung, H. J. Sung, and T. A. Zaki. Turbulent thermal boundary layers with temperature-dependent viscosity. *International journal of heat and fluid flow*, 49:43–52, 2014.

S. K. Lele. Compressibility effects on turbulence. *Annual review of fluid mechanics*, 26(1): 211–254, 1994.

A. Mani, J. Larsson, and P. Moin. Suitability of artificial bulk viscosity for large-eddy simulation of turbulent flows with shocks. *Journal of Computational Physics*, 228(19):7368–7374, 2009.

F. Menter. Zonal two equation kw turbulence models for aerodynamic flows. In *23rd fluid dynamics, plasmadynamics, and lasers conference*, page 2906, 1993.

Y. Morinishi, S. Tamano, and K. Nakabayashi. Direct numerical simulation of compressible turbulent channel flow between adiabatic and isothermal walls. *Journal of Fluid Mechanics*, 502:273, 2004.

R. D. Moser, J. Kim, and N. N. Mansour. Direct numerical simulation of turbulent channel flow up to re τ= 590. *Physics of fluids*, 11(4):943–945, 1999.

H. K. Myong and N. Kasagi. A new approach to the improvement of k-ε turbulence model for wall-bounded shear flows. *JSME international journal. Ser. 2, Fluids engineering, heat transfer, power, combustion, thermophysical properties*, 33(1):63–72, 1990.

Y. Nagano and C. Kim. A Two-Equation Model for Heat Transport in Wall Turbulent Shear Flows. *Journal of Heat Transfer*, 110(3):583–589, 08 1988. ISSN 0022-1481. doi: 10.1115/1.3250532. URL https://doi.org/10.1115/1.3250532.

Y. Nagano and M. Shimada. Development of a two-equation heat transfer model based on direct simulations of turbulent flows with different prandtl numbers. *Physics of Fluids*, 8 (12):3379–3402, 1996. doi: 10.1063/1.869124. URL https://doi.org/10.1063/1.869124.

G. J. Otero Rodriguez, A. Patel, R. Diez Sanhueza, and R. Pecnik. Turbulence modelling for flows with strong variations in thermo-physical properties. *International Journal of Heat and Fluid Flow*, 73, 2018.

C. Pantano and S. Sarkar. A study of compressibility effects in the high-speed turbulent shear layer using direct simulation. *Journal of Fluid Mechanics*, 451:329, 2002.

A. Patel. Turbulence modeling for heat transfer to supercritical pipe flows. 2013.

A. Patel. *Universal characterization of wall turbulence for fluids with strong property variations*. PhD thesis, 2017.

A. Patel, J. W. R. Peeters, B. J. Boersma, and R. Pecnik. Semi-local scaling and turbulence modulation in variable property turbulent channel flows. *Physics of Fluids*, 27(9):095101, 2015.

A. Patel, B. J. Boersma, and R. Pecnik. The influence of near-wall density and viscosity gradients on turbulence in channel flows. *Journal of Fluid Mechanics*, 809:793–820, 2016.

A. Patel, B. J. Boersma, and R. Pecnik. Scalar statistics in variable property turbulent channel flows. *Physical Review Fluids*, 2(8):084604, 2017.

R. Pecnik and A. Patel. Scaling and modelling of turbulence in variable property channel flows. *Journal of Fluid Mechanics*, 823, 2017.

R. Pecnik, G. J. Otero Rodriguez, and A. Patel. RANS-models for fully developed turbulent channel flow with variable properties solved in MATLAB. 2018. URL https://github.com/Fluid-Dynamics-Of-Energy-Systems-Team/RANS_Channel.

S. Pirozzoli. Generalized conservative approximations of split convective derivative operators. *Journal of Computational Physics*, 229(19):7180–7190, 2010.

E. J. Plate. Aerodynamic characteristics of atmospheric boundary layers. Technical report, Argonne National Lab., Ill. Karlsruhe Univ.(West Germany), 1971.

S. B. Pope. Turbulent flows, 2001.

R. M. C. So and C. G. Speziale. A review of turbulent heat transfer modeling. *Annual Review of Heat Transfer*, 10, 1999.

T. Sommer, R. So, and H. Zhang. Heat transfer modeling and the assumption of zero wall temperature fluctuations. *Journal of heat transfer*, 116(4):855–863, 1994.

P. Spalart and S. Allmaras. A one-equation turbulence model for aerodynamic flows. In *30th aerospace sciences meeting and exhibit*, page 439, 1992.

S. Tamano. *Direct Numerical Simulation of Wall-Bounded Compressible Turbulent Flow*. PhD thesis, NagoyaInstitute, 2002.

H. Tennekes and J. L. Lumley. A first course in turbulence. 1972.

A. Trettel and J. Larsson. Mean velocity scaling for compressible wall turbulence with heat transfer. *Physics of Fluids*, 28(2):026102, 2016.

A. J. Trettel. *Transformations for variable-property turbulent boundary layers*. PhD thesis, UCLA, 2019.

Z. Warhaft and J. L. Lumley. An experimental study of the decay of temperature fluctuations in grid-generated turbulence. *Journal of Fluid Mechanics*, 88(4):659–684, 1978. doi: 10.1017/S0022112078002335.

F. M. White. *Viscous fluid flow*. New York: McGraw-Hill, 1974.

D. C. Wilcox et al. *Turbulence modeling for CFD*, volume 2. DCW industries La Canada, CA, 1998.

O. Zeman and J. L. Lumley. Modeling buoyancy driven mixed layers. *Journal of Atmospheric Sciences*, 33(10):1974–1988, 1976.

C. Zhang, L. Duan, and M. M. Choudhari. Direct numerical simulation database for supersonic and hypersonic turbulent boundary layers. *AIAA Journal*, 56(11):4297–4311, 2018.